To My Parents.

A NOVEL SQUID CALORIMETER AND ITS APPLICATION TO SOME INTERMETALLIC COBALT COMPOUNDS

A thesis submitted for the degree of Doctor of Philosophy of the University of London and for the Diploma of Membership of the Imperial College

by

ANIL KUMAR CHHABRA

Physics Department
The Blackett Laboratory
Imperial College of Science & Technology
London SW7 2BZ

September 1985

ABSTRACT

A novel SQUID calorimeter and its application to some intermetallic cobalt compounds

This thesis describes the use of a toroidal, soldered resistive SQUID as the basis of a calorimeter. We have made heat capacity measurements on some intermetallic cobalt compounds and the intermediate valence material $YbAl_3$.

We have confirmed that the properties of Y_9Co_7, believed to exhibit both superconductivity and ferromagnetism, are strongly quality dependent. The better the sample, i.e. the higher its resistance ratio, the less observable the magnetism and the higher the superconducting transition temperature. By the investigation of other intermetallic cobalt compounds we have developed a simple theory which indicates that the superconductivity in Y_9Co_7 arises from channels of yttrium known to exist in the structure of the compound. The model also suggests that the observed magnetism is associated with the separation of cobalt chains within these channels, a separation which we believe is not unique throughout the structure.

We have also measured the specific heat of $YbAl_3$ and, using prevailing theories to analyse our results, we have concluded that in this compound the behaviour cannot be described by the presence of a lorentzian feature at the fermi level alone. Our measurements on some pseudobinary alloys in which we have substituted Lu for Yb confirm this, and we propose that our results can be qualitatively understood by an eclectic interpretation of all the theories.

ACKNOWLEDGEMENTS

It gives me great pleasure to thank the following:

Dr. Gavin Park, my supervisor, who sadly passed away during this project.

Professor Bryan Coles and Dr. David Caplin, for taking over my supervision and their continued assistance in all aspects of this project.

Dr. C.N. Guy for his help in practical problems and his general enthusiasm.

Dr. A.P. Murani for introducing me to the intermediate valence problem and providing the samples.

Mr. Derek Podger for his technical assistance and Dr. H.E.N. Stone for help with the preparation of samples.

Deanne Eastwood for her efficient and helpful typing of this thesis.

To all my contemporaries who have not only been good friends, but also provided invaluable aid throughout this project.

And a special thanks to Brian and Pat Millicheap for proof-reading this thesis.

TABLE OF CONTENTS

	Page
Title page	2
Abstract	3
Acknowledgements	4
Table of contents	5
1. INTRODUCTION	8
2. HEAT CAPACITY OF METALS AT LOW TEMPERATURES	14
2.1 Introduction	14
2.2 Electronic heat capacity	15
2.3 The lattice heat capacity	16
2.4 Magnetic contributions	17
2.5 Schottky effect	18
2.6 The specific heat of a superconductor	19
3. SQUIDs	21
3.1 Introduction	21
3.2.1 Flux Quantisation in a superconducting loop	21
3.2.2 The Josephson effect	23
3.3.1 SQUIDs	24
3.3.2 The step pattern	27
3.3.3 The triangle pattern	30
3.4 The resistive SQUID	30
3.5 Noise in SQUID systems	34
4. METHOD	37
4.1 RSQUID calorimetry	37
4.2 The step method	38
4.3 Method of calibration	41

TABLE OF CONTENTS (continued)

		Page
5.	APPARATUS	45
	5.1 Introduction	45
	5.2 Sample chamber layout	49
	5.3 Electronics	51
	5.4.1 Construction of a soldered RSQUID	53
	5.4.2 Characterisation of the RSQUID	55
	5.5 Experimental procedure	58
	5.6 Calibrations	62
6.	INTERMETALLIC COBALT COMPOUNDS	67
	6.1 Introduction	67
	6.2 Yttrium-cobalt	72
	6.3 Superconductivity in $CeCo_2$	78
	6.4 Superconductivity in Zr_2Co	83
	6.5 Magnetism in Heusler alloys	87
	6.6 Magnetism in PdCo dilute solid solutions	91
	6.7 Heat capacity of Y_9Co_7	96
	6.8 Conclusion	100
7.	INTERMEDIATE VALENCE MATERIALS	104
	7.1 Introduction	104
	7.2 Valence fluctuations	105
	7.3 Results and discussions	111
	7.4 Conclusions	115

TABLE OF CONTENTS (continued)

	Page
Conclusion	124
References	128
Appendix A	136
Appendix B	147
Appendix C	158

CHAPTER 1

INTRODUCTION

We have investigated, using the RSQUID calorimeter, some intermetallic cobalt compounds and an intermediate valence system. The word SQUID is an acronym for Superconducting QUantum Interference Device, and is a device able to measure magnetic flux with a resolution of one flux quantum. Essentially, it is a superconducting loop interrupted by a Josephson junction. The term SQUID arises from loops with two junctions in which quantum interference can be observed. In Chapter 3 we discuss in more detail RF SQUIDs, in particular ones of toroidal geometry. The RSQUID is a Resistive SQUID, that is a SQUID which has had part of the superconducting loop replaced by a normal section.

The RSQUID was first applied to calorimetry by Park and Vaidya[1.1]. By using a normal metal with a known thermopower, and arranging the overall geometry of the RSQUID such that any heat current passing through it had to cross the normal region, they were able to produce a sensitive heat current meter. This formed the basis of the RSQUID calorimeter, in which the RSQUID constitutes a weak link to a constant temperature bath. A step method similar to ones conventionally used was applied successfully, and shown to have a relative accuracy $\sim$ 0.1%.

The major part of this project was spent in rebuilding and updating the RSQUID calorimeter. A complete revision of the room temperature electronics was undertaken and resulted in a semi-automated experiment. Complete automation was impossible due to the necessity of readjusting the RSQUID during the experiment. The rebuilding of the probe included the complete reconstruction of the RSQUID, as described in Chapter 5. No

attempt was made to change the sensitivity, since the limitations to the accuracy were due to other sources, such as fluctuations in the bath temperature and stray heat currents. Consequently, the dimensions of the Cu-Fe ring remain those reported by Vaidya[1.2].

The method and procedure used in running an experiment, although in principle the same as reported by Vaidya, is now in practice considerably different and is discussed in Chapter 4. The experimenter is now only required to ensure that the RSQUID is appropriately adjusted and set the temperature at which he wishes to take his specific heat measurement; from that point the system is completely automatic. The adjusting of the RSQUID during an experiment was found, once sufficient skill was obtained, to be necessary only a couple of times over the entire experimental range. Frequently the entire temperature range could be achieved without readjustment of the point contact.

In Chapter 6 we describe results on some intermetallic cobalt compounds. In particular we discuss the Y_9Co_7 compound, once considered to be Y_4Co_3 and first investigated by Pauthenet et al[1.3] in Grenoble. They showed that, while YCo_2 was an itinerant paramagnet, Y_4Co_3 exhibited ferromagnetic behaviour with a Curie temperature of 13K and a saturation moment of $0.1\mu_B$ per formula unit.

The structure of this compound proved to be complex and was identified as Ho_4Co_3 type structure, containing three atomic sites: a) h sites which formed a chain of triangular prisms parallel to the c axis and carried all the Y atoms and 2/3 of the Co atoms. b) d sites, closely associated with these prisms and containing 2/9 of the remaining cobalt atoms, and c) b sites, which lie along the c axis and contain the remaining cobalt atoms.

Magnetic and electrical measurements by Gratz et al[1.4], while confirming the ferromagnetic behaviour of the Y_4Co_3, found a Curie temperature of 8K and inferred that the magnetic moment was localised on the atomic b sites. Figiel et al[1.5], using NMR measurements, claimed the d sites carried the localised moments. Into this increasing controversy came Kolodziejczyk and Sarkissian[1.6]'s observation of magnetic ordering at 5K and the appearance of superconductivity at 1.5K. Whilst superconductivity and ferromagnetism has been reported in some ternary alloys such as RE Mo_6S_8[1.13,1.14] and RE Rh_4b_4[1.13, 1.15] (RE = rare earth) and the general subject of the coexistence of superconductivity and ferromagnetism reviewed by Ishikawa[1.13], these materials in fact exhibit superconductivity, which is then destroyed by re-entrant ferromagnetism. Sarkissian[1.11], through measurements of magnetoresistance and AC susceptibility, showed what seemed to be the mutual build up of magnetic ordering and superconductivity with the latter becoming dominant at lower temperatures. He concluded the existence of a hybrid state and that, in fact, no long range magnetic ordering took place in the system.

The conflicting results and the possibility of the coexistence of ferromagnetism and superconductivity led to a meeting to discuss the properties of Y_4Co_3 at Imperial College which was organized by B.R. Coles and E.P. Wohlfarth[1.7], where the information known to date was presented and discussed by all the workers in the field.

The general phase diagram of the yttrium-cobalt system was investigated by Grover et al[1.8], and this led to the establishing of Y_9Co_7 as the real phase, exhibiting the properties so far attributed to Y_4Co_3. They maintained that Y_4Co_3 was in

fact a defect structure of Y_9Co_7, with quantities of Y_8Co_5 present as second phase, and they further investigated the structure of Y_9Co_7. They found a hexagonal unit cell made up of triangular prisms of Y atoms parallel to the c axis, with four Co atoms at the centre of the prism and the remaining Co atoms arranged along the c axis.

B.R. Coles, at the Imperial College meeting, further claimed that the magnetism of the compound was $1\mu_B$ per 28 atoms, and the moments were localised on the so-called b sites. The possibility of growing a single crystal was discussed and thought to be prohibitively difficult.

Cheng et al[1.9] reported the measurement of specific heat, magnetoresistance, resistance and magnetovolume that confirmed the existence of local moments. They further confirmed the superconducting transition in their resistance data, and both this and the magnetic ordering in the specific heat. They further inferred that 20% of the electrons participate in superconductivity, while only 0.2% of the cobalt moments were involved in magnetic ordering, as opposed to 2%, the value predicted from the Curie-Weiss constant. They further concluded that Y_9Co_7 exhibited an exceptionally complicated fermi surface.

Yttrium, under pressure, becomes a superconductor, and this prompted the investigation of Y_9Co_7 at differing pressures. Huang et al[1.10] investigated the electrical resistance and magnetic susceptibility at pressures up to 20 Kbar in field up to 6T. They discovered that pressure strongly suppressed the magnetic ordering and increased the transition temperature for the onset of superconductivity. They also found that the magnetoresistance for pressures above 8 Kbar and temperatures above 5K was always positive. They concluded that the ferro-magnetism and superconductivity order parameters coexist around

the superconducting transition, but may vary strongly in space. Sarkissian[1.11] also maintained a spatial variation of the order parameter, inferred from depolarization of neutrons data.

Rastogi and Coles[1.12] have investigated the dependence of the observed phenomena in Y_9Co_7 on sample purity. They describe measurements on different samples of differing quality. (The quality of a sample taken to be such that the better samples have higher resistance ratios and higher superconducting transition temperatures). They showed that, with higher quality samples, the magnetic contribution was degraded, and in some samples no maxima associated with this ordering were seen at 4K. The Arrot plots for these samples proved to be non-linear, implying that no true long range ferromagnetism was present, and the maximum temperature at which hysteresis occurred was seen to decrease with improved quality of sample. They concluded that the magnetic ordering observed in this compound is of an itinerant, short range type, and the hysteresis seen above the ordering temperature is due to imperfections, as seen in some PdCo solid solutions.

Our approach has been to follow the work of Rastogi and Coles and measure the specific heat of a high quality sample. In addition, we have measured compounds whose properties we believe are related to the properties of Y_9Co_7. We have then attempted, using general and phenomenological arguments about 3d magnetism, to formulate a theory for superconductivity and magnetism in our samples.

In Chapter 7 we present specific heat data on $YbAl_3$. This compound is one of a group of rare earth alloys which seem to exhibit a valence that fluctuates about a non-integer value. These compounds are referred to as intermediate valence

materials. We have investigated the effect of dilution with Lu, and using the isomorphic $LuAl_3$ as a dummy sample we are able to present results on the variation of the electronic specific heat with temperature.

The fermi liquid theory of Newns and Hewson[1.16] has been applied successfully to some intermediate valence compounds. This suggests that the f level is in close proximity to the fermi energy and is hybridized with the conduction band. The treatment is along the lines of classical Friedel-Anderson impurity. The concentrated Kondo approach suggests that intermediate valence materials are in fact concentrated Kondo systems (CKS) with a high Kondo temperature. In this approach a many body resonance, referred to as the Abrikosov-Suhl resonance (ASR) appears at the fermi level and hence affects the physical properties of the material that are related to the density of states. The CKS approach has met with success in the field of heavy fermions.

We have attempted to apply these two approaches to our results, discussing the relative merits and failures of each theory. Finally, we have concluded with a brief summary of the thesis and a general discussion of our results and conclusions.

CHAPTER 2

THE HEAT CAPACITY OF METAL AT LOW TEMPERATURES

2.1 Introduction

The low temperature heat capacity of metals has been the subject of many reviews, and the monograph by Gopal[2.1] provides a good general introduction. The review article by Phillips[2.2] compares theoretical and experimental results, and contains references for the specific heats of all the elements. Heiniger et. al.[2.3] discuss in detail the heat capacities of the transition metals and their alloys, a subject omitted from the Phillips article. The extensive analysis of lattice vibrations and specific heat due to the lattice is presented by De Launay[2.4] in his review article.

We present here a brief introduction to the subject and recommend the above references for more detailed analysis and discussion.

The heat capacity of a simple metal at low temperatures can be expressed in the following form:

$$C_V = C_E + C_L + C_M + \ldots\ldots \qquad \text{Eq. 2.1}$$

where all the terms are assumed additive and C_E represents the electronic contribution, C_L the contribution due to the lattice and C_M that due to magnetic properties, etc. In section 2.2 we discuss in more detail the electronic contribution and propose an explicit form for its temperature dependence. In section 2.3 we similarly treat the lattice specific heat and in sections 2.4 through 2.6 we detail other possible contributions to the heat capacity that may arise due to phenomena such as magnetism and superconductivity.

2.2 Electronic Heat Capacity

The electronic heat capacity term in equation 2.1 can be derived assuming a simple Sommerfeld model in which the electrons are treated as a free Fermi gas obeying Fermi-Dirac statistics; this yields a term of the form

$$C_E = \frac{1}{3}\pi^2 k_B^2 N(\varepsilon_F)\ T = \gamma\ T \qquad \text{Eq. 2.2}$$

where k_B is the Boltzmann constant and $N(\varepsilon_F)$ is the density of electronic states at the Fermi level. In the free electron approach $N(\varepsilon_F)$ can be derived as

$$N_0(\varepsilon_F) = \frac{3mzN_0}{\hbar^2} \left(\frac{V}{3\pi^2 zN_0}\right)^{2/3} \qquad \text{Eq. 2.3}$$

where N_o is Avogadro's number, z is the valence of each atom, m the electron mass and V the volume of the sample. A detailed knowledge of the actual band structure within the metal enables the calculation of $N_{bs}(\varepsilon_F)$, an effective density of states at the Fermi level due to the more realistic picture of band formation during the condensation process. However, the observed γ is found to differ from this calculated value, and the interactions between the electrons themselves and between the electrons and the lattice have to be taken into consideration. Both these are included multiplicatively into the electronic specific heat, which can be expressed as

$$C_E \alpha (1+ \lambda_p + \lambda_e\ )\ N_{bs}\ T \qquad \text{Eq. 2.4}$$

where λ_p is the electron-phonon enhancement factor and λ_e the electron-electron enhancement factor, while N_{bs} is the density of states as calculated by a band structure calculation.

In general the electron-electron enhancement factor λ_e is believed to be $\sim 20\%$, while λ_p can be large, especially in superconductors. McMillan[2.5] has developed an equation relating the superconducting transition temperature, the phonon frequency spectrum and λ_p.

In transition metals the position of a d band in the vicinity of the Fermi level may enhance the density of states, as can also occur in dilute alloys where the solute forms a virtual bound state[2.6] (if the v.b.s. is near the Fermi level). A similar process is observed with the f level in the rare-earth alloys, where the level is hybridised with the conduction electron and takes on a line width. The group of alloy classed as intermediate valence materials are believed to obtain their properties due to the proximity of the f level to the Fermi energy. These are discussed in more detail in Chapter 7.

Of recent interest are heavy fermion materials[2.7]. These have greatly enhanced electronic specific heats, for example $CeCu_2Si_2$ has a $\gamma \sim 1100$ mJ deg^{-2}, as compared to 2 or 3 mJ deg^{-2}, the value for normal metals. It has recently been suggested that these are in fact concentrated Kondo systems with a low Kondo temperature ~ 10K[2.8], the high electronic specific heat being due to the appearance of a many body resonance at the Fermi level, which is part of theory. The interested reader is referred to the articles by Stewart[2.7] and Brandt and Moshchalkov[2.8].

2.3 The Lattice Heat Capacity

The low temperature heat capacity contribution due to the lattice can be expressed in the following form:

$$C_L = (12/5)\pi^4 R(T/\theta_D)^3 \qquad \text{Eq. 2.5}$$

where R is the gas constant and Θ_D is the so-called Debye temperature, a parameter that is related to the cut-off frequency of the acoustic spectrum of lattice vibrations. This expression is due to Debye and was derived by assuming the lattice was a continuous, dispersionless medium, with the discreteness of the lattice imposed to limit the number of modes. Experimental measurements of Θ_D using eq. 2.5 are found to be temperature dependent, and the expression is only truly valid for temperatures such that $T < \Theta_D/50$.

A more complex theory evolved by Born and von Karman, in which the lattice is treated as a collection of interacting, vibrating particles, predicts the experimentally observed temperature variation of Θ_D and also an optical branch to the frequency spectra of the lattice. The mathematical complexity of this theory makes the Debye model more attractive in the quantitative analysis of specific heat data below $\Theta_D/50$, a constraint which in most works, including the present project, is well above the experimentally achievable range.

2.4 Magnetic Contributions

The behaviour of an assembly of well defined interacting magnetic moments in the paramagnetic state can be described by the Curie-Weiss law

$$\chi \alpha C/(T - \Theta_p) \qquad \text{Eq. 2.6}$$

where C is the Curie constant. Below a temperature Θ_p the system undergoes a transition into a magnetically ordered state. If Θ_p is positive the system is ferromagnetic with a ground state in which all the spins are aligned, such as in Fe

with a θ_p of 1043K. If θ_p is negative, then the system is antiferromagnetic with the spins for example anti-parallel with respect to nearest neighbours and consequently no spontaneous magnetic moment below the temperature T_N ($\sim|\theta_p|$), that marks the onset of order.

Elementary excitations in simple magnetic systems take the form of spin waves, in which the spins precess with successive spins having a constant phase difference. These spin waves can be treated as virtual particles analogous to phonons in the lattice and are termed magnons. Assuming nearest neighbour interactions, the dispersion relations for these magnons can be obtained and from these the specific heat variation as a function of temperature, deduced. For cubic symmetry the magnetic contribution for ferromagnetic materials has the following form

$$C_m \alpha (T / |\theta_p|)^{3/2} \qquad \text{Eq. 2.7}$$

and for antiferromagnetic systems

$$C_m \alpha (T/ |\theta_p|)^3 \qquad \text{Eq. 2.8}$$

where θ_p in both equations is the respective ordering temperature.

2.5 Schottky Effect

In many magnetic materials, such as spin glasses, the ordering process is accompanied by an irregularity in the specific heat in the form of a Schottky anomaly, which was first investigated by Schottky in 1922. The Schottky effect can be visualised by considering a simple two level system with

an energy separation of ε. For temperature such that $T << \varepsilon/k_B$ (where k_B is the Boltzmann constant), only the lower level is occupied, while for temperature $T >> \varepsilon/k_B$, both levels are occupied. Between these two conditions one would expect a rapid change of internal energy with temperature and a corresponding bump in the specific heat. In this simple two level case, if the degeneracies are g_o and g_1 for the ground state and the excited state respectively, then we may predict

$$C_{sh} = (N\varepsilon^2 g_0 \exp(\varepsilon/k_BT))/k_BT^2 g_1(1+[(g_0/g_1)\exp(\varepsilon/k_BT)]^2) \qquad \text{Eq. 2.9.}$$

For a multi-level system the theory predicts a T^{-2} variation for the specific heat above the transition temperature.

2.6 The Specific Heat of a Superconductor

The transition to the superconducting state is accompanied by a λ -like anomaly in the specific heat. The BCS theory[2.9] gives some simple prediction for the specific heat at the transition temperature and in the superconducting state. The excess specific heat, due to the creation of Cooper pairs is related in the BCS theory to the electronic specific heat γ of the normal state:

$$\Delta C_E(T_c) = 1.43\gamma T_c \qquad \text{Eq. 2.10}$$

while the specific heat variation in the superconducting state is

$$(C_{Es}/\gamma T_c) = 8.5 \exp(-1.44T_c/T), \quad 2.5<T_c/T<6$$

$$(C_{Es}/\gamma T_c) = 26 \exp(-1.62T_c/T), \quad 7<T_c/T<12$$

Eq. 2.11

This behaviour is characteristic of an energy gap, an essential part of the theory in which the energy gap is related to T_c by

$$2\varepsilon_0 = 3.52k_BT_c \qquad \text{Eq. 2.12}$$

and can be considered as the energy required to break up a Cooper pair.

The effect of magnetic impurities in superconductors in general, is to reduce the transition temperature and compress the energy gap. As a function of impurity concentration the gap may vanish at a concentration for which the transition temperature is non-zero and a gapless superconductor results[2.10].

CHAPTER 3

SQUIDs

3.1 Introduction

This chapter deals with SQUIDs in general and the RSQUID in particular. All SQUIDs will be assumed to be of the toroidal point contact type, and particular emphasis is placed on RF SQUIDs since these are most commonly used today.

Section 3.2 gives derivations of flux quantisation in a closed superconducting loop and the A.C. and D.C. Josephson effects, since these play a major role in the operation of SQUIDs (both derivations are after Kittel[3.1]). Section 3.3 considers the function of a SQUID in detail. The general reviews by Giffard et al[3.2] and Silver and Zimmerman[3.3] are recommended for further reading. Also worth mentioning are the works of Park[3.4,3.5], which cover many of the more subtle concepts of SQUIDs.

Section 3.4 details the RSQUID, as discussed by Park[3.6] and Harding and Zimmerman[3.7]. Application of RSQUIDs to calorimetry is due to Park and Vaidya[3.8,3.9] and Vaidya[3.10], the originators of the RSQUID calorimeter.

Section 3.5 concludes with a short treatment of noise in SQUIDs and a discussion of how this affects the experimental behaviour of real systems.

3.2.1 Flux Quantisation in a Superconducting Loop

The Cooper pairs in a superconductor can be described by a single wavefunction. If we assume that $|\psi(r)|$ is the particle probability amplitude and that the concentration $n = \langle \psi(r)^+ \mid \psi(r) \rangle$ is constant, then we may write

$$\psi(r) = n^{\frac{1}{2}}e^{i\Theta}, \qquad \psi(r)^{+}=n^{\frac{1}{2}}e^{-i\Theta} \qquad \text{eq. 3.1}$$

The velocity of a particle can then be written as

$$\underline{v} = (\underline{p} - q\underline{A} /c)/m = (-i\hbar\underline{\nabla} - q\underline{A}/c)/m \qquad \text{eq. 3.2}$$

from which we can conclude an expression for the current density $\underline{J}$

$$\underline{J} = q\ \psi(r)^{+}\underline{v}\ \psi(r) = q(-\hbar\underline{\nabla}\Theta - q\underline{A}/c)/m \qquad \text{eq. 3.3}$$

If we now take the curl of both sides and note the identity curl $(\nabla)=\underline{0}$ we have

$$\text{curl } \underline{J} = - nq^{2}\underline{B}/mc \qquad \text{eq. 3.4}$$

Equation 3.4 is one of the London equations.

In a superconductor we are able to choose a path sufficiently deep inside the superconductor around which $\underline{B}$ and $\underline{J}$ are zero as a consequence of the Meissner effect. Then, for a closed loop along which $\underline{J} = \underline{0}$, from equations 3.4 and 3.2

$$\hbar c\underline{\nabla}\Theta = q\underline{A} \qquad \text{eq. 3.5}$$

where the integral $\int \underline{\nabla}\Theta.\underline{dl}$ once around the closed loop = $\Theta_2 - \Theta_1$, since ψ must be single valued. Then $\Theta_2 - \Theta_1 = 2\pi a$ where a is an integer.

Applying Stokes theorem:

$$\int_c \underline{A}.\underline{dl} = \int (\text{curl } \underline{A}).\ \underline{d\sigma} \qquad \text{eq. 3.6}$$

where the integral is taken over the area bounded by the closed path c. Since curl $\underline{A} = \underline{B}$ and $\int_c \underline{B}.\underline{d\sigma} = \varphi$ the flux passing

through the ring, we arrive at

$$(2\pi\hbar c/q)a = \varphi \quad \text{or} \quad \varphi = a\varphi_0 \qquad \text{eq. 3.7}$$

which shows that the flux through the ring is quantised in integral numbers of the flux quantum = $2.07.\ 10^{-15}$ Wb. A further consequence of this and the Meissner effect is, providing the superconducting ring is unbroken and superconductivity not lost, the flux through the ring will remain constant.

3.2.2 The Josephson Effect

Let us consider two superconductors separated by an insulator. As in equation 3.1 we can define a wave function for each superconductor of the form $\psi_1 = n_1^{\frac{1}{2}} e^{i\Theta(1)}$ and $\psi_2 = n_2^{\frac{1}{2}} e^{i\Theta(2)}$. For simplicity we assume the superconductors are identical and define a transfer interaction $\hbar T$ which is the probability of finding ψ_1 in region 2 and ψ_2 in region 1. Further, if we impose a voltage V across the insulator, the electron pairs experience a potential energy step of -2eV. We assume a pair on one side of the insulator experiences a potential difference -eV, and on the other side +eV. The Schrödinger equation then lets us write

$$i\hbar\,(\delta\psi_1/\delta t) = \hbar T\psi_2 - eV\psi_1 \qquad \text{eq. 3.8a}$$

$$i\hbar\,(\delta\psi_2/\delta t) = \hbar T\psi_1 + eV\psi_2 \qquad \text{eq. 3.8b}$$

by expanding eq. 3.8a and multiplying throughout by ψ_1^+

$$\tfrac{1}{2}\delta n_1/\delta t + in_1\,\delta\Theta_1/\delta t = ieVn_1/\hbar - iT(n_1n_2)^{\frac{1}{2}}e^{i\delta} \qquad \text{eq. 3.9a}$$

where $\delta = \Theta_2 - \Theta_1$; similarly equation 3.8b yields

$$\tfrac{1}{2}\delta n_2/\delta t + in_2\,\delta\Theta_2/\delta t = -ieVn_2/\hbar - iT(n_1n_2)^{\frac{1}{2}}e^{-i\delta} \qquad \text{eq. 3.9b}$$

equating real and imaginary parts

$$\delta n_1/\delta t = 2T\,(n_1 n_2)^{\frac{1}{2}} \sin\delta \qquad \text{eq. 3.10a}$$

$$\delta n_1/\delta t = -\,2T\,(n_1 n_2)^{\frac{1}{2}} \sin\delta \qquad \text{eq. 3.10b}$$

and

$$\delta\theta_1/\delta t = eV/\hbar - T(n_1/n_2)^{\frac{1}{2}} \cos\delta \qquad \text{eq. 3.11a}$$

$$\delta\theta_2/\delta t = -eV/\hbar - T(n_1/n_2)^{\frac{1}{2}} \cos\delta \qquad \text{eq. 3.11b}$$

From equations 3.10, equating $\delta n_1/\delta t = -\,\delta n_2/\delta t$ i.e. current flowing from region one is equal to current flowing into region two.

If V = 0 then equations 3.11 give the D.C. Josephson effect $\delta(\theta_2 - \theta_1)/\delta t = 0$ and the current j of superconducting pairs depends on the phase difference δ as

$$j = j_0 \sin(\theta_2 - \theta_1) \qquad \text{eq. 3.12}$$

i.e. with no applied voltage a D.C. current will flow across the junction with a value between j_0 and $-j_0$ according to the phase difference.

When V is non-zero equations 3.11 give $\delta(t) = \delta(0) - 2eVt/\hbar$, and equation 3.12 becomes

$$j = j_0 \sin(\delta(0) - 2eVt/\hbar) \qquad \text{eq. 3.13}$$

i.e. the current oscillates with frequency $\omega = 2eV/\hbar$ this is known as the A.C. Josephson effect.

3.3.1 SQUIDs

The word SQUID is an acronym for Superconducting QUantum Interference Device. The SQUIDs described here are RF SQUIDs, those driven at Radio Frequencies. A considerable amount of literature exists on the operation of these devices[3.2,3.3,3.4,3.13], and since an overall understanding

is necessary as the RSQUID forms an integral part of the apparatus, a brief review is presented here.

The standard method of operation of a SQUID system involves the SQUID (simply seen as a superconducting loop interrupted by a weak link) inductively coupled to a tank circuit driven near its resonant frequency. An audio bias can be used to modulate the RF amplitude or be placed directly into the coil. The system is shown schematically in Figure 3.1.

The weak link can be described[3.14] with a current phase relation of the form

$$I_s = \sum_i I_{c(i)} \sin (i\theta) \qquad \text{eq. 3.14}$$

where the $I_{c(i)}$ determine the critical current and θ is the phase difference between the two superconductors. Assuming only the first term in this expression is relevant, we recover the Josephson junction relation of equation 3.12 restated.

$$I_s = I_c \sin \theta \qquad \text{eq. 3.15}$$

From equation 3.5 we have for a weak link interrupting a closed superconducting loop, that the phase difference θ can be written as

$$\theta = 2\pi\varphi/\varphi_0 \qquad \text{eq. 3.16}$$

where φ_0 is the flux quantum and φ is the flux through the loop. We can further write for a ring with self inductance L and an applied external flux φ_{ext}, that the flux in the ring or SQUID is

$$\varphi = \varphi_{ext} - LI_c \sin (2\pi\varphi/\varphi_0) \qquad \text{eq. 3.17}$$

This defines the characteristics of the SQUID in the φ_{ext} - φ plane. By inspection there are two modes of operation,

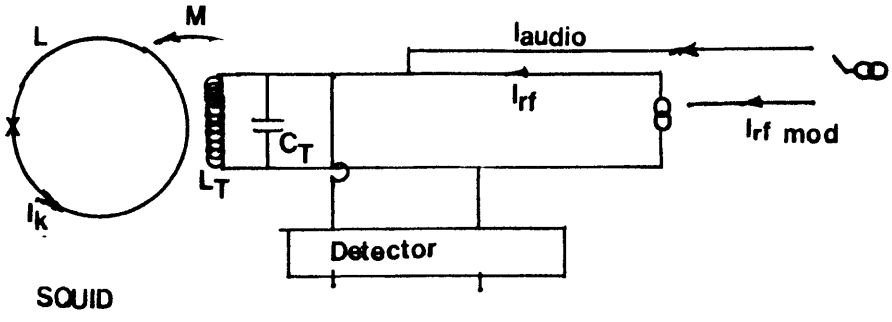


Figure 3.1: SQUID Electronics

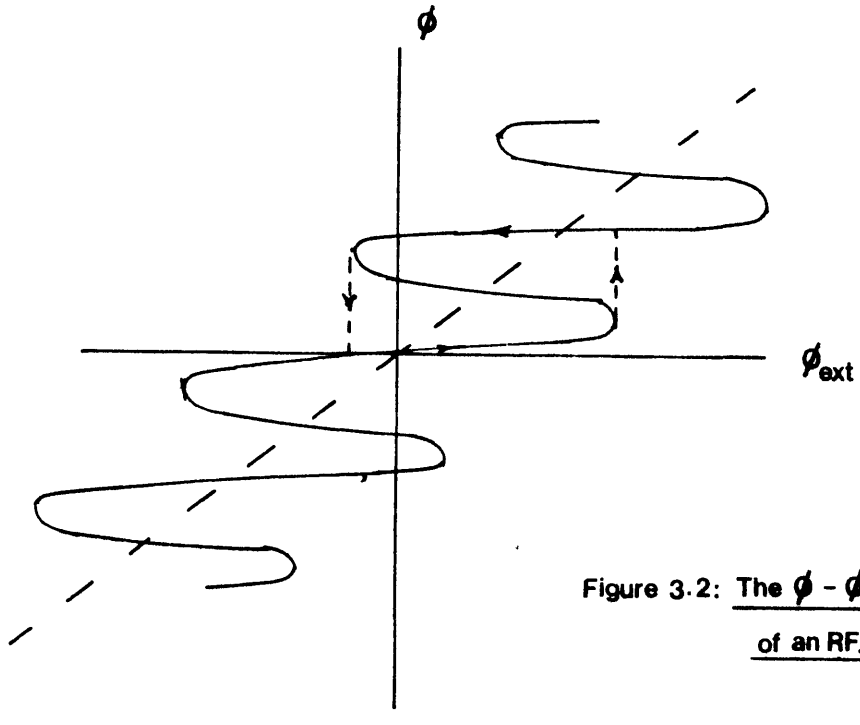


Figure 3.2: The $\phi - \phi_{ext}$ Charcteristics of an RF. SQUID.

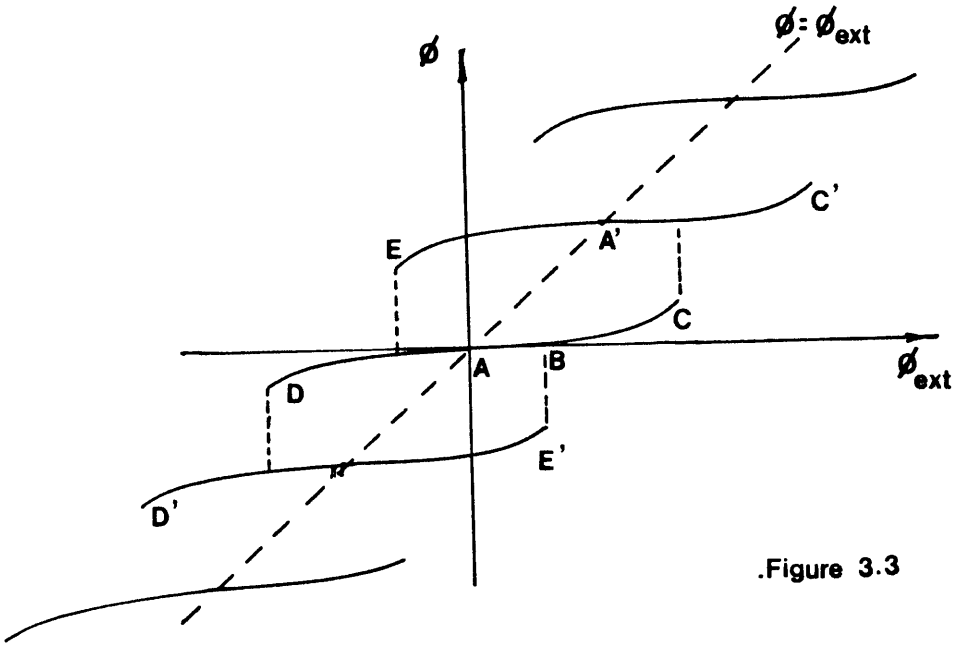
hysteretic and nonhysteretic. The hysteretic mode is employed in most systems and requires a parameter $\beta = 2\pi LI_c/\varphi_0$ to be less than 1, this ensures φ is a multivalued function of φ_{ext}. Figure 3.2 shows a typical φ, φ_{ext} characteristic.

Kurkijarvi[3.13] has shown that the positive slopes correspond to stable states that represent minima in the local potential energy, while the negatively sloped regions are unstable states, maxima in the local potential energy. Their picture concludes that at fixed φ_{ext} stable states on the positive slopes are separated by potential barriers - the negative slopes. By increasing φ_{ext} the system moves towards a barrier and at the point where the gradient on the φ_{ext} - φ plane becomes infinite the barrier vanishes (or alternatively the weak link goes normal) and the system, if it is correctly damped (I_c less than 0.5 φ_0/L), makes a transition to the next stable state. If this is not the case the system will traverse many states before it comes to equilibrium. If φ_{ext} is now decreased, the system will return in a similar fashion but along another path, as shown, to its original position, having executed a hysteretic cycle. This operation forms the basis of the SQUID measurement device.

3.3.2 The Step Pattern

Considered in more detail, the SQUID behaviour can be analysed to give the two most common modes of experimental operation in which one sees what are termed the step pattern and the triangle pattern.

As before, let us consider a SQUID ring of inductance L coupled to a tank circuit of inductance L_t, capacitance C_t and a load resistance of R_t. The circuit will have some quality factor Q and will be driven at ω_{rf}, a frequency near



.Figure 3.3

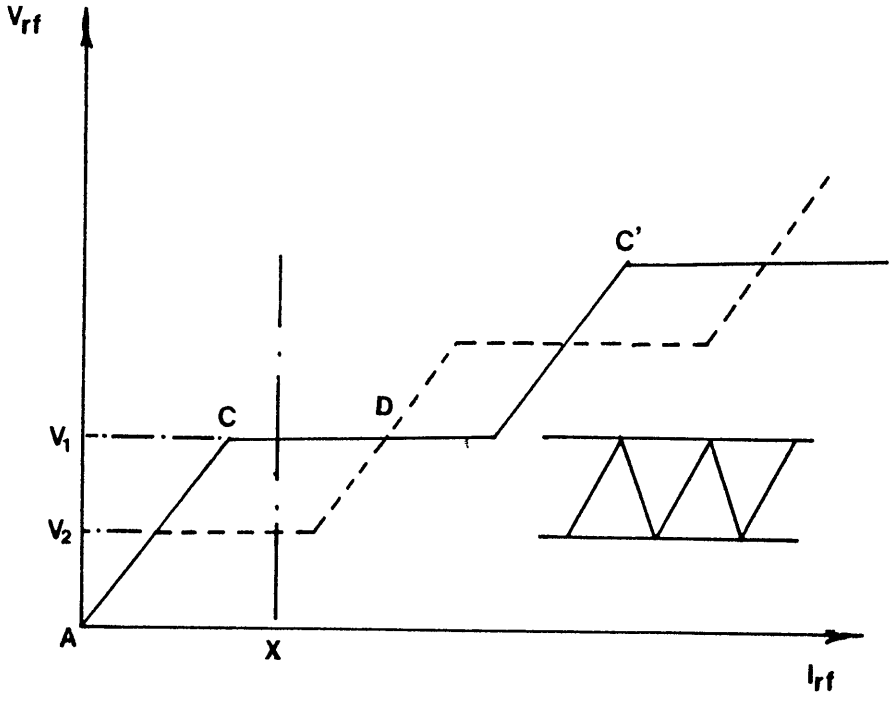


Figure 3.4: The Step Pattern.

its resonance point. We can define a coupling into the SQUID ring,

$$k = M/ (LL_t)^{\frac{1}{2}} \qquad \text{eq. 3.18}$$

where M is the mutual inductance between the SQUID ring and the tank circuit. An empirical optimisation is found to be $k^2Q \sim 1$ (3.2).

For simplicity we shall assume that the initial condition of the SQUID is such that the applied flux $\varphi_{ext}=0$ and the flux through the ring is also zero. This places us at the origin of the φ - φ_{ext} plane, as shown by the point A in figure 3.3. Here the SQUID characteristics are drawn with only the stable states shown. If we now increase I_{rf} the system will oscillate about the point A, the voltage V_{rf} (the detector output voltage) increasing linearly with I_{rf}. This corresponds to the linear section AC in figure 3.4 and represents the system oscillating about point A, and as I_{rf} is increased, its amplitude reaches towards points C and D.

At point C, φ_{ext} reaches a critical value φ_c and the system will make a transition to the next quantum state, then φ_{ext} decreases and the system returns to A via a path CA'EA having executed a hysteresis cycle and taken energy ΔE from the tank circuit. After this the tank circuit takes many cycles to recover sufficient energy for the system to execute another cycle, so any further increase in I_{rf} gives no corresponding increase in V_{rf} and the plateau CD is reached in figure 3.4. A further increase in I_{rf} causes the system to execute the symmetrically identical hysteresis loop of ADE'A, so the length of the plateau is doubled. Eventually, on further increase, I_{rf} is sufficient for the system to execute both hysteresis cycles per period of RF and any further

increase sends the system towards C' and D', causing a linear increase in the V_{rf} - I_{rf} plot. The process is repeated and a step pattern achieved.

If we now consider the initial point to be point B and $\varphi_{ext}=\frac{1}{2}\varphi_0$. The system will now reach point C much earlier than before and the first step will start as shown by the dotted line in figure 3.4. This step will only be half the length of the previously mentioned steps since only one hysteresis loop will be executed. If I_{rf} is now increased the pattern follows as before. The two step patterns shown trace out the envelope within which lie all other step patterns corresponding to all other initial conditions. This is intuitively obvious if one bears in mind that the point A' is identical to point A.

3.3.3 The Triangle Pattern

We consider any step pattern created by an initial condition of $\varphi = (n/m)\,\varphi_0$, where n and m are integers. It will lie between the two step patterns of figure 3.4, as stated previously. If the condition is now changed and $(n/m)\ \varphi_0$ becomes $(1+n/m)\ \varphi_0$ the step pattern is unchanged, due to the symmetry of the $\varphi_{ext} - \varphi$ characteristic.

It is this periodicity in φ_0 (actually $\varepsilon\varphi_0$ where ε is a number of the order unity > 1 : Park[3.4]) that is exploited to obtain the triangle pattern. I_{rf} is set to some value X, which places it in the middle of a step and changes in applied flux cause periodic variations of V_{rf} between V_2 and V_1 in the form of triangles. This forms the basis of measurements in SQUID systems.

3.4 The Resistive SQUID

A resistive SQUID can be viewed simply as a SQUID with a normal (resistive) section interrupting the superconducting

ring. Resistive SQUIDs have been known for many years, but until recently their use has been limited to Noise thermometry[3.16,3.17]. Park and Vaidya[3.8] reported the first use of an RSQUID as a sensitive heat current detector.

An RSQUID responds to magnetic flux in much the same way as the conventional SQUID; in addition, if a voltage is placed across the resistive section the detector voltage oscillates at the Josephson frequency $f=V/\varphi_0$. This voltage can be obtained if an electric current, I, is applied to the resistive section, or, alternatively, if the resistive section also has a thermal resistance w and a thermopower S, then a heat current applied across it will also produce a voltage. It is this behaviour that is exploited in this work.

It is not immediately obvious as to why the RSQUID should operate at all, if one considers that SQUID rings adhere to flux quantisation and the RSQUID has effectively a discontinuous superconducting loop - see section 3.2.1. If, however, we derive the equation of state for the RSQUID and compare it to that of the SQUID, we can show that both respond much the same under certain conditions. (After Park[3.6]).

The current passing through the weak link of a SQUID has two components, the current due to the R.F. drive that oscillates at a frequency ω_{rf}, and a second, more slowly varying current, i_k. If we assume that the flux through the ring is zero and setting i_k to zero, then if ω_{rf} is such that the skin depth $\delta \ll t$, the thickness of the resistive section, then the r.f. potential difference across the resistive region is negligible, as is $\underline{E}$ (Park[3.6]).

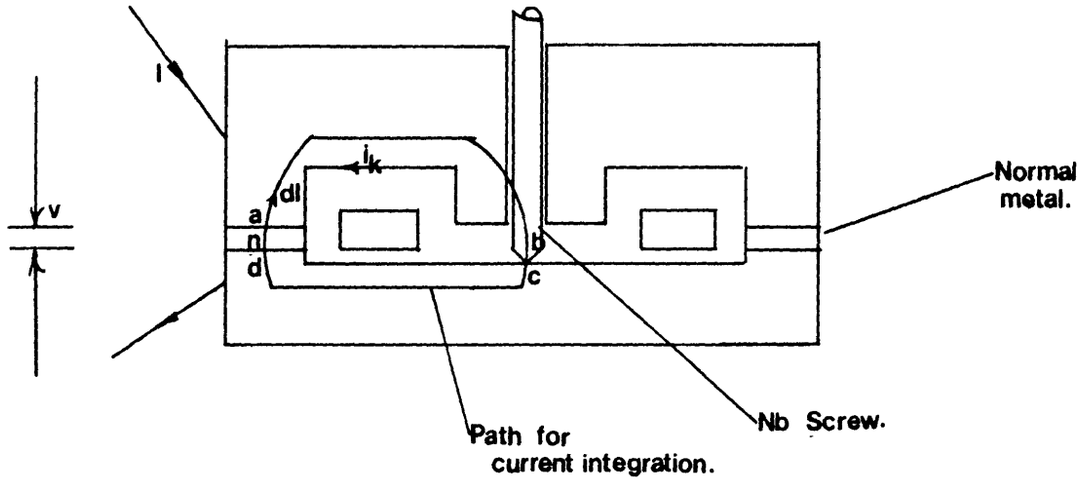


Figure 3.5: The Toroidal RSQUID.

From equation 3.5

$$\underline{A}/\varphi_0 + \underline{\nabla}\theta/2\pi = 0$$

Integrating around the loop shown in Figure 3.5, we obtain

$$\theta_n - \theta_j = 2\pi\varphi_s/\varphi_0 = 0 \qquad \text{eq. 3.19}$$

where $\varphi_s = \int_{abd} \underline{A}.\underline{dl}$, $\theta_n = \theta_d - \theta_a$ and $\theta_j = \theta_c - \theta_b$ since we have assumed that $i_k=0$ and that $\underline{E}=0$ on dna, then

$$V = -\int(\underline{E} + \underline{A}).\underline{dl} = -\int\underline{A}.\underline{dl} = -\delta\varphi_n/\delta t \qquad \text{eq. 3.20}$$

from the Josephson relation

$$\delta\theta_n/\delta t = (2\pi/\varphi_0) \delta\varphi_n/\delta t \qquad \text{eq. 3.21}$$

integrating

$$\theta_n = (2\pi/\varphi_0)(\varphi_n - \varphi_j) \qquad \text{eq. 3.22}$$

where φ_j is an integration constant, then

$$\theta_j = (2\pi/\varphi_0)(\varphi - \varphi_j) \qquad \text{eq. 3.23}$$

where $\varphi = \varphi_s + \varphi_n$. Now since $\varphi = \varphi_{ext} - LI_s$, we have for the RSQUID

$$\varphi = \varphi_{ext} - Li_c \sin ((2\pi/\varphi_0)(\varphi - \varphi_j)) \qquad \text{eq. 3.24}$$

which, if compared to eqn. 3.17, is the same apart from the constant φ_j. We conclude that the RSQUID behaves like the SQUID under the assumptions made.

In general, a current i_k flows through the weak link,

a current I is placed across the resistive region, and a heat current q passed through it. The above can now be generalised to give

$$\theta_j = (2\pi/\varphi_0)[(\varphi_{ext} - Li_k) - (i_k + I)r - (V_q + V_n)] \qquad \text{eq. 3.25}$$

where V_q is the voltage due to the heat current q and V_n is the voltage due to Johnson noise. This equation is only valid if φ_j varies quasistatically with respect to a fundamental time constant T_f. Park[3.6] has shown that T_f^{-1} varies between an upper limit, the RF frequency, f_{rf} and f_{rf}/Q; this limit was never approached in this work.

If we set φ_{ext} to zero and assume $i_k r$ is negligible, then eq. 3.25 yields that the detector frequency will vary as

$$f = (V_q + Ir)/\varphi_0 \qquad \text{eq. 3.26}$$

neglecting noise. It is this response that makes the RSQUID useful as the basis of a highly sensitive heat current meter.

3.5 Noise in SQUID systems

The presence of noise in SQUID systems has observable effects. Thermal fluctuations cause corresponding fluctuations in the SQUID characteristics, giving a variation in the transition probability and causing the steps to become rounded and tilted. Jackel and Buhman,[3.11] have analysed the noise contributions due to intrinsic, tank circuit and preamplifier noise. A quick summary will be presented here, with an additional piece on noise in RSQUID systems.

The intrinsic noise, as mentioned, is caused by thermal fluctuations of the states near the transition point C (figure 3.3) on the $\varphi_{ext} - \varphi$ plane; this manifests itself

in a probability of a transition occurring around this point (in a distribution that Kurkijarvi[3.12] characterised by a distribution width σ , he found that this was a direct cause of the experimentally seen tilt of the steps). Jackel et al introduced a parameter α which they define as the fractional step rise, which enables us to quantify the noise as an equivalent flux noise.

$$< \delta\varphi_I^2 > \sim 2\pi\alpha\varphi_0^2/(1-\alpha)^2\omega \qquad \text{eq. 3.27}$$

Similar treatment of the tank circuit noise, which arises due to Johnson noise in the resistance of the tank circuit, causing voltage fluctuations that give an equivalent flux noise of the form

$$< \delta\varphi_t^2 > \sim 4\pi\alpha^2 k_B T_t L / (1-\alpha)^2\omega \qquad \text{eq. 3.28}$$

where T_t is the effective noise temperature of the tank circuit distributed from room temperature to SQUID temperatures and k_B is the Boltzmann constant. Typically $T_t \sim$ 200 K.

Finally the preamplifier noise can be represented by a flux noise of the form

$$< \delta\varphi_A^2 > \sim 2\pi\alpha\ k_B T_n L /(1-\alpha)^2\omega \qquad \text{eq. 3.29}$$

where T_n is defined by

$$\langle \delta\varphi_V^2 \rangle = 4k_B T_n \ (\delta V_t/\delta I_{rf})_{step} \qquad \text{eq. 3.30}$$

and has a typical value 50 K.

We can therefore write the total noise $< \delta\varphi_N^2 >$ as

$$< \delta\varphi_N^2 > = < \delta\varphi_I^2 > + < \delta\varphi_t^2 > + < \delta\varphi_A^2 > \qquad \text{eq. 3.31}$$

which enables us to write

$$\langle \delta\varphi_N^2 \rangle_{2L} \sim (\alpha/(1-\alpha)^2)[(\pi\alpha\varphi_0/2\omega L)+(2\pi\alpha k_B T_t/\omega)+(\pi k_B T_n/\omega)] \quad \text{eq. 3.32}$$

Typically[3.10] in 20MHz systems $\delta\varphi_N/2L \sim 10^{-31}$ Joules. and is negligible with respect to φ_0, the resolution of a SQUID system.

Noise in the RSQUID has an additional contribution due to Johnson noise in the resistive section of the SQUID ring. It is more informative to treat this as a frequency noise, i.e. what frequency fluctuations will the Johnson noise cause in the RSQUID detector output. This frequency noise can be expressed as

$$\Delta f = 4\pi k_B T r/\varphi_0 \quad \text{eq. 3.33}$$

However, when a frequency is normally measured one counts a number of cycles over a period t_g. The variance σ_f^2 over a large number of measurements has been shown by Kamper[3.18] to be

$$\sigma_f^2 = \langle (f_0 - f) \rangle = (t_n t_g)^{-1} + (12 t_g^2)^{-1} \quad \text{eq. 3.34}$$

where $t_n = (2\pi/\Delta f)$, and the second term arises due to counters being unable to determine fractional counts.

The Johnson noise in an RSQUID manifests itself experimentally in the form of fluctuations in the frequency of the triangle pattern.

CHAPTER 4

METHOD

4.1 RSQUID Calorimetry

Any calorimetric measurement must determine two quantities, ΔQ, the heat input into the system, and ΔT, the resulting rise in temperature. The heat capacity is then $C_s = \lim_{\Delta T \to 0} \Delta Q/\Delta T$. Calorimeters are of two types: adiabatic and non-adiabatic. In adiabatic systems the sample is thermally isolated from its surroundings, and by inclusion of a heater and a thermometer on the sample, ΔQ and ΔT are measured directly. A general outline of the Nernst pulse method as commonly employed in these calorimeters is given by Joseph et al[4.1]. Martin et al[4.2] claim an absolute accuracy of 0.3% at the expense of a large sample, 100gm. In non-adiabatic systems the sample is linked to a constant temperature bath via a thermal resistance R. For example, by raising the temperature through the application of a heater pulse at the sample end, and observing the dynamic response, a time constant RC_s can be calculated and from this C_s, determined. Sullivan and Seidel[4.3] describe an A.C. method in which the heat capacity is measured by the application of an oscillatory heat current, and observation of the inverse amplitude of the resulting temperature oscillations. Many other non-adiabatic methods can be found in the literature[4.4,4.5].

The RSQUID heat current meter is well suited for calorimetry. Counting the cycles of the frequency output of the detector enables a direct measurement of ΔQ, while the difference between initial and final equilibrium frequencies determines ΔT.

In these experiments the RSQUID calorimeter is used as

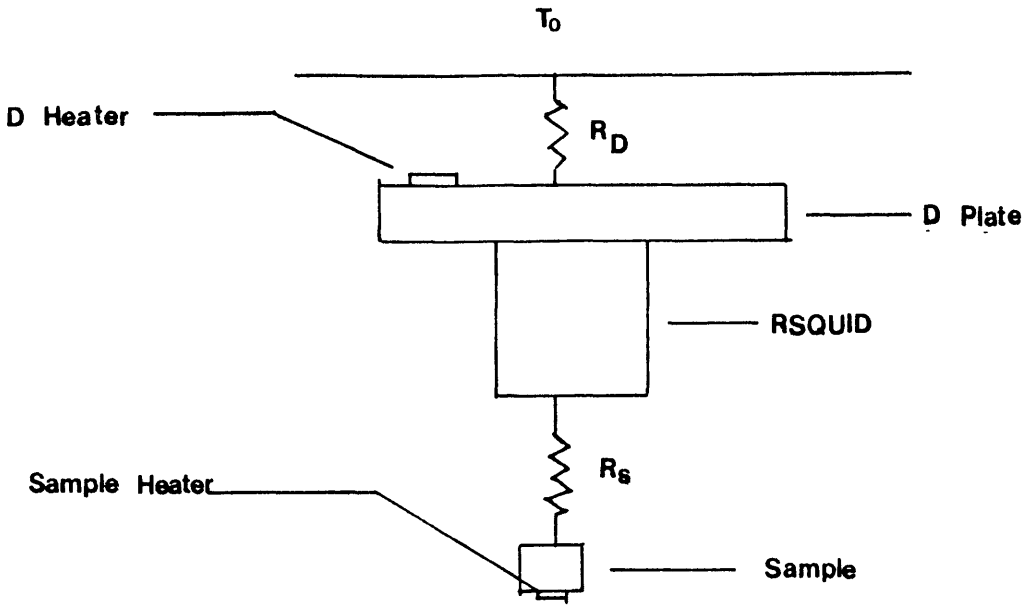
a non-adiabatic system, with the RSQUID forming part of the weak link to the bath. Any heat flowing in or out of the sample is then measured. Since the RSQUID measures the heat required to raise the temperature of the sample directly the profile of the dynamic response need not necessarily be a simple exponential, as is required by most methods of this form.

4.2 The Step Method

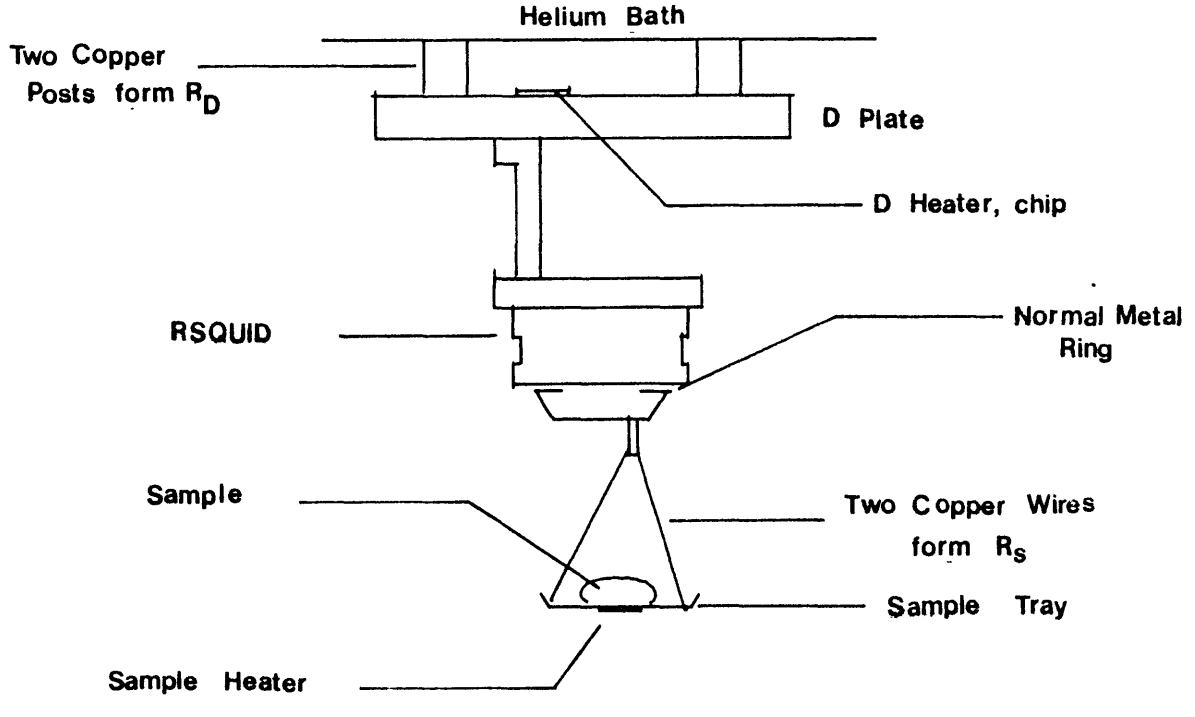
In conventional step methods the sample is connected to a constant temperature bath through a known thermal resistance R. A temperature step is applied through a heater pulse at the sample end of the system. From the response in time RC, the time constant is determined and C, the specific heat, calculated.

In the step method employed with the RSQUID the arrangement is as shown in figure 4.1. The D plate is connected to the helium bath at temperature T_0 through a thermal resistance R_D. A heater on this plate enables its temperature to be raised above that of the bath. Mounted on the D plate, through a single point of contact, is the RSQUID; from its bottom extend two copper wires which make up the thermal resistance R_S. These support the sample tray which has attached to it the sample heater.

At time t=0 the sample heater is turned on, as shown in figure 4.2. A gated up/down counter is made to count up. The temperature of the sample rises, as does the frequency output of the RSQUID. At time $t = t_g$ (t_g is the gate time) the counter is stopped, its value read and it is made to count down. At time $t = 2t_g$ the counter is stopped, the difference count it



Schematic view of experimental set up.



Diagramatic view of experimental set up.

Figure 4.1

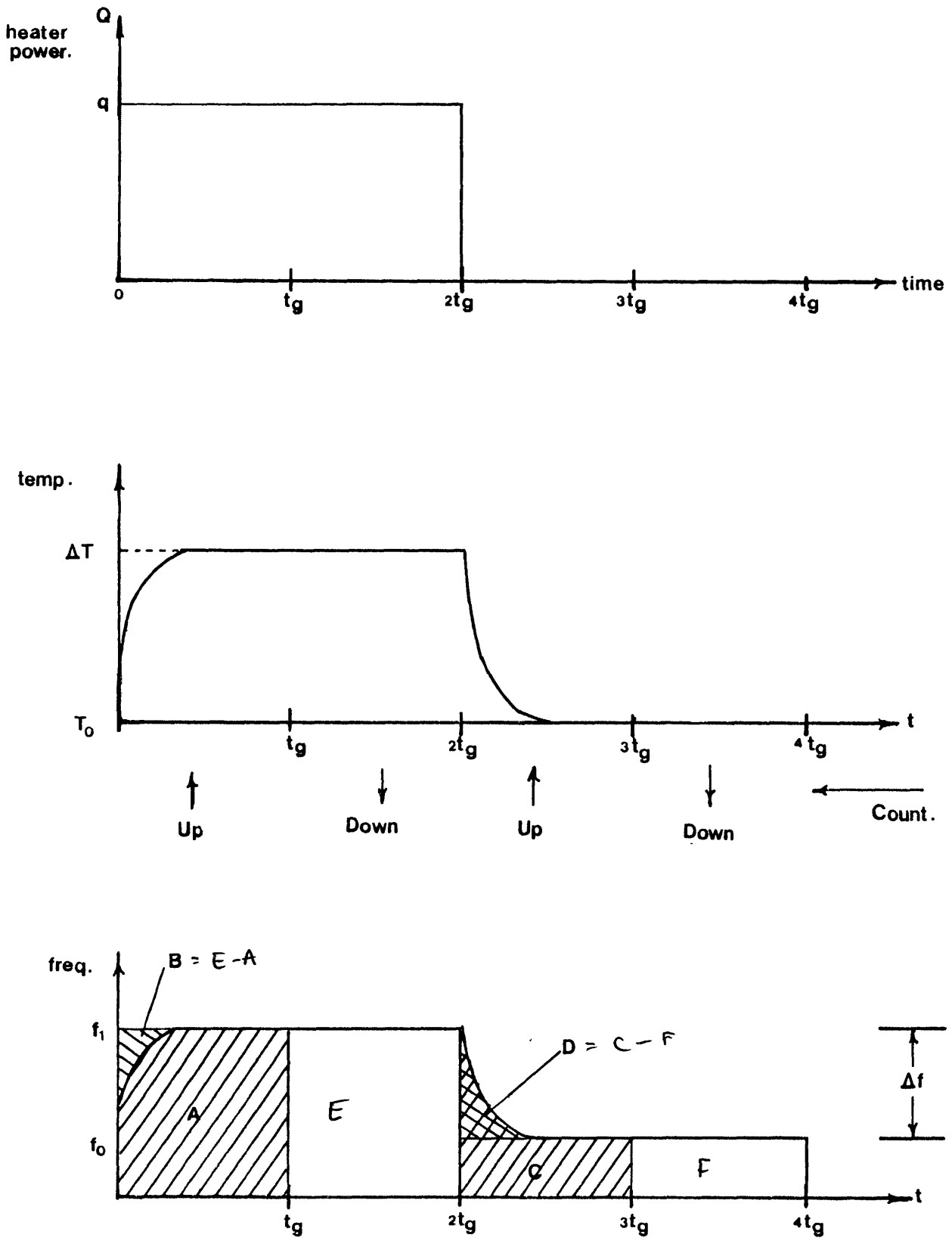


Figure 4.2: The 'Step Method' in practice.

now displays is read. It is then zeroed and made to count up as the heater power is switched off. At $t = 3t_g$ the counter is read and again made to count down. At $t = 4t_g$ the difference count is read and the whole cycle repeated.

For each cycle four numbers are produced: A, B, C and D. By inspection of figure 4.2, A and C are seen to be the areas under the relative sections of the frequency-time plot. B and D correspond to the amount of heat required to raise the sample and the sample tray by ΔT and the parts of the RSQUID below the normal metal ring by $\Delta T R_D/(R_D + R_S)$. If k is the sensitivity, then this amount of heat is $\Delta Q = kB$. Similarly, if, before the heater step, the frequency of the RSQUID was f_0, and after, when equilibrium had been reached, f_1, then $k(f_1-f_0) = R_s \Delta T$. By inspection $((A+B) - (C-D))/t_g$ is simply (f_1-f_0). We can therefore conclude that since $C_{sp} = \Delta Q/\Delta T$ that,

$$RC_{sp} = Bt_g / ((A + B) - (C - D)) \qquad \text{eq. 4.1}$$

where C_{sp} is the specific heat of the sample plus the tray and a contribution from the bottom of the RSQUID. During these experiments t_g was always chosen such that it was of the order of $10RC_{sp}$, giving an error of less than 0.1% if a simple exponential profile was assumed.

4.3 Method of Calibration

Before specific heat data could be measured the thermal resistance $R_s(T)$ and the addenda correction to the specific heat had to be known. The latter could easily be obtained by running the experiment without a sample, while the thermal resistance could be measured directly by placing a thermometer on the sample tray or by measuring a known sample, such as

copper.

In an attempt to analyse the dynamic response of the system to a heater pulse in the sample heater an electrical analogue such as in figure 4.1 was investigated and solved. However, on trying to obtain empirical parameters it was found that the system was somewhat more complex than at first imagined. Figure 4.3 shows a more realistic circuit. The dynamic response of this circuit showed that, provided R_R, the thermal resistance between the RSQUID and the D plate, was small, the major time constant of the response was $R_S C_{sample}$. This, although unimportant when using the RSQUID calorimeter, was desirable. Large R_R led to the problematic addition of a non-reproducible factor to the specific heat (presumably a large R_R would be due to a poor contact dominated by thermal contractions, hence non-reproducible). This was avoided by cold welding an In washer between RSQUID and D plate. During all these experiments R_R was a few K/W.

The actual calibrations were carried originally a number of times, and no noticeable deviation from calibration to calibration was observed.

The sample tray was measured by running the experiment without a sample and keeping a careful note of the temperature step caused by the sample heater pulse at each temperature. At 2K, ΔT was of the order of 15mK, and at 6K, 8mK. This constituted an addenda calibration.

Next, a 2gm sample of Cu, taken from a Johnson Matthey 99.9998% batch and annealed for a week at 800°C, was measured. Data points were taken at exactly the same temperature as the sample tray with exactly the same ΔT. The resulting measurements were compared to a known reference[4.6] for

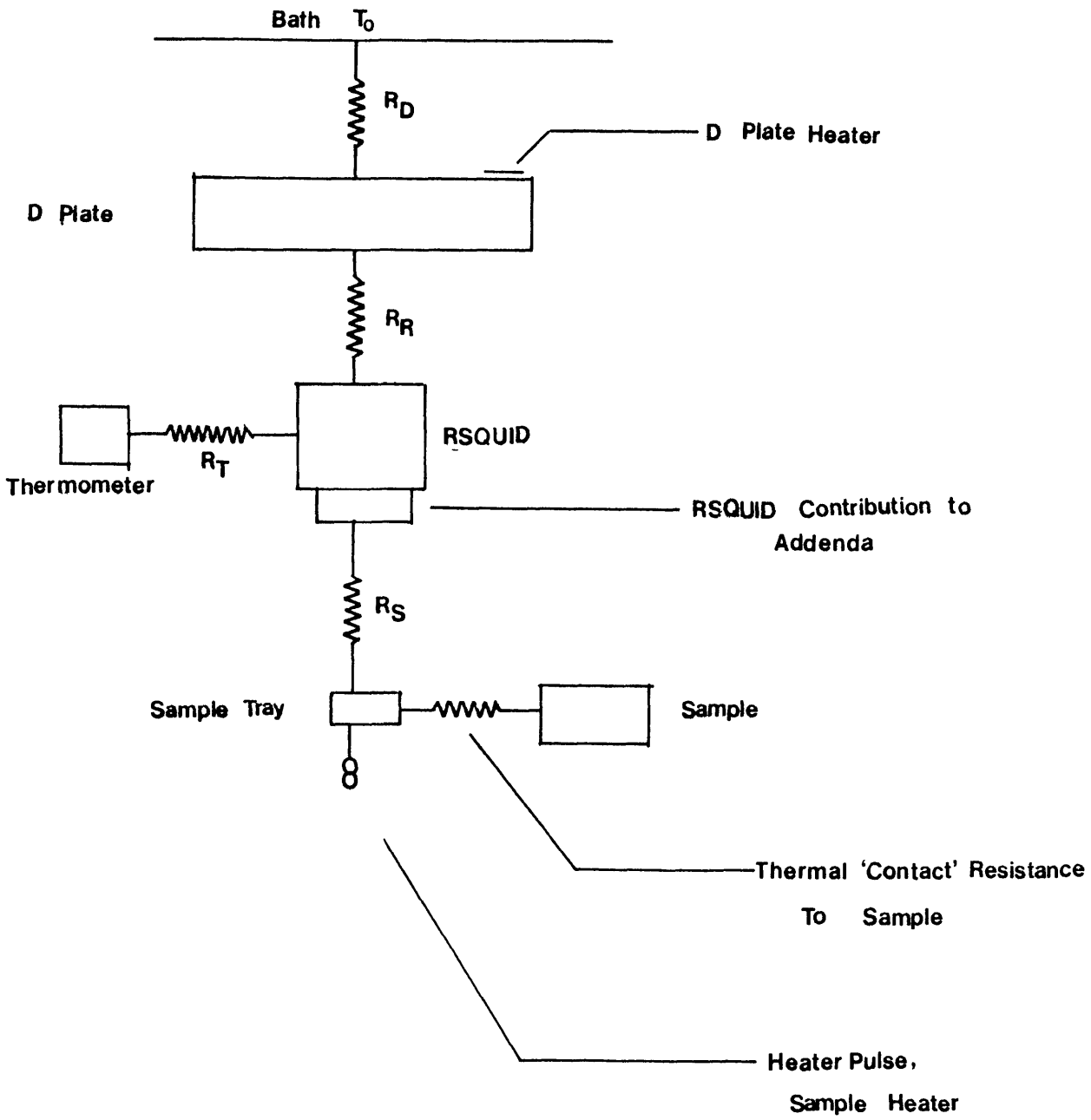


Figure 4.3: A More Realistic View of The System.

copper, and hence R(T) deduced. A further discussion of calibrations and diagrams of the actual calibration are to be found in Chapter 5.

CHAPTER 5

APPARATUS

5.1 Introduction

A large section of this research project was spent in overhauling and generally repairing the RSQUID calorimeter. This chapter details the changes made by the author in order to make the apparatus functional. Changes to combat the structural deficiencies, such as leaks, are omitted.

Section 5.2 concerns the major changes made at the low temperature end of the probe, and section 5.3 deals with the room temperature layout of the experiment. Much of the constructional technology for the RSQUID had to be rediscovered, and section 5.4 deals with the making of a toroidal soldered SQUID.

An adequate description of the probe is given by Vaidya[5.1] but, for completeness, a short description will be included here.

Figure 5.1 shows the probe used in these experiments. The top flange allows access to an enclosed (so that it may be pumped) helium dewar. Inside the dewar the probe ends in a vacuum can in which is mounted the RSQUID. The probe in more detail consists of six, thin walled stainless steel tubes, one of which is 12.7mm dia., and forms the pumping line, the remainder are of 4.8mm dia., and carry the R.F. line for the RSQUID, a screwdriver and an assortment of leads for the two heaters, the thermometer and the biasing current for the RSQUID. All are brazed to the vacuum can top.

Inside the vacuum can two D plates, so called because of their shape, are connected to the can top via four copper

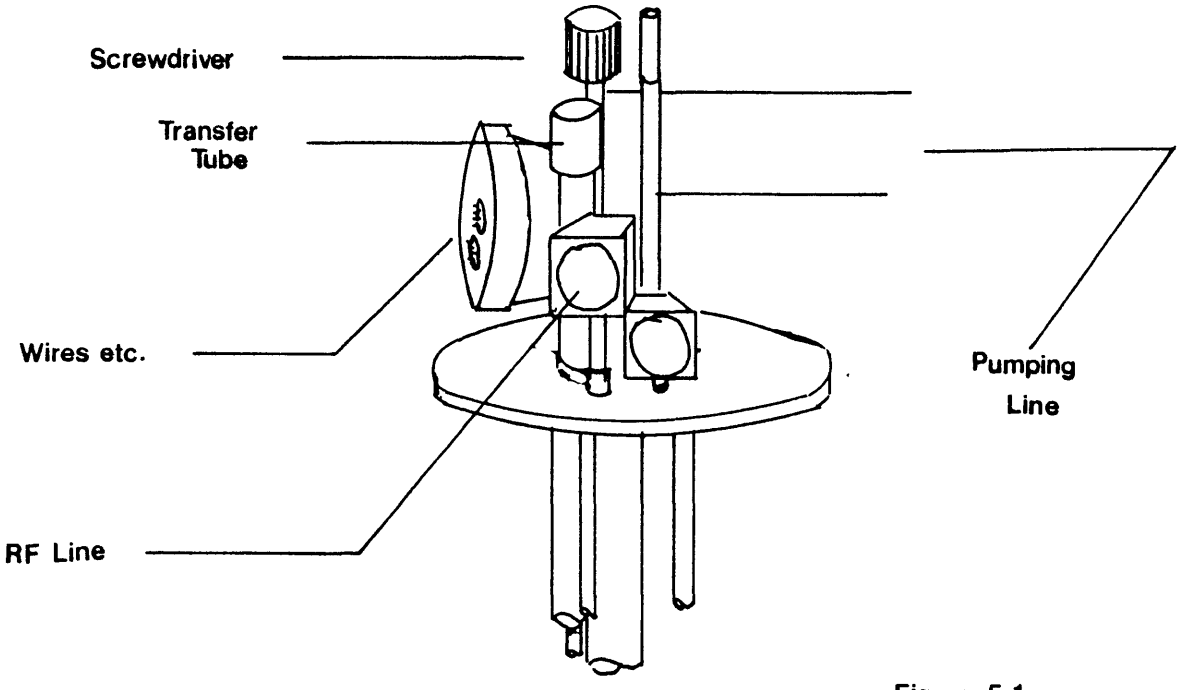
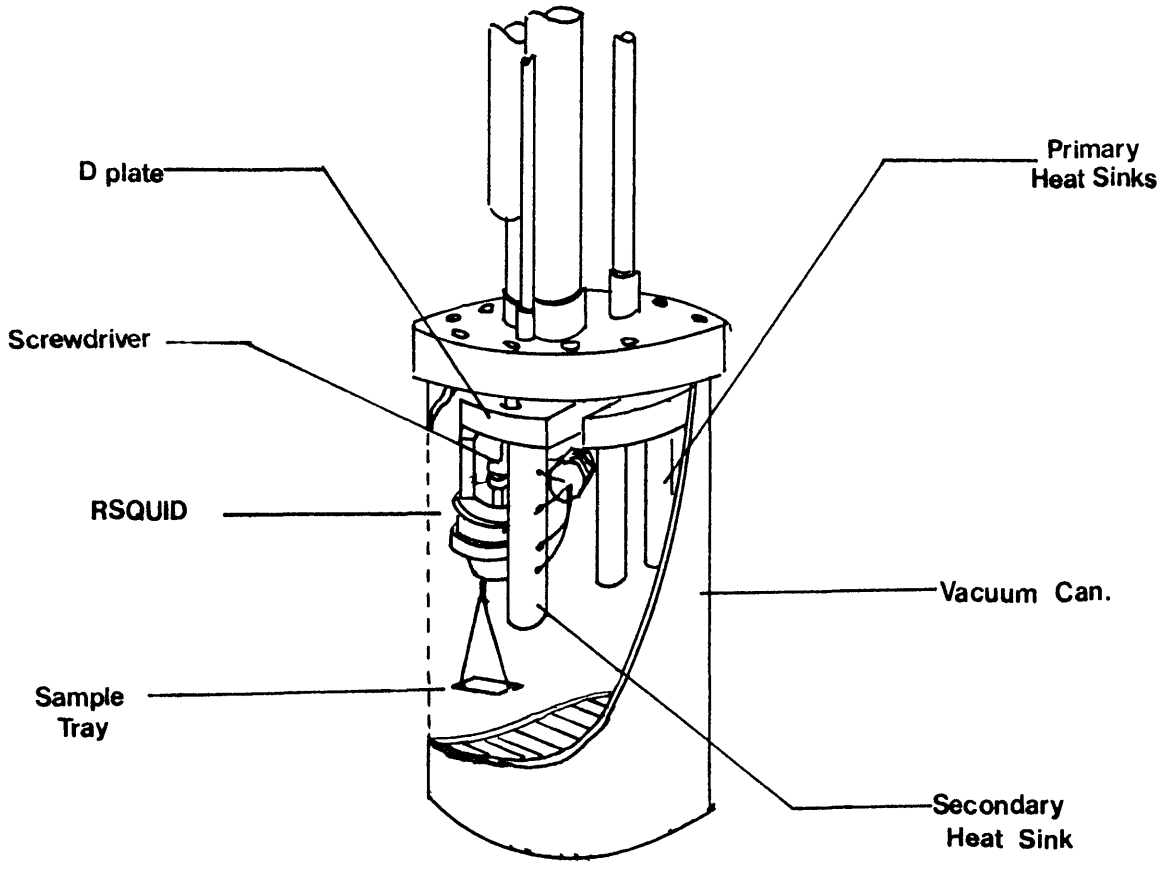


Figure 5.1:

The Basic Probe.



posts that form a thermal resistance to the bath. The wires coming from room temperature pass a radiation shield and then are heatsunk to the can for 20cm of their length. They then proceed to one of two heatsinks on the first D plate and then, passing through 5cm of 44 S.W.G. manganin wire, reach the secondary heatsink on the second D plate which supports the RSQUID. Also heatsunk to this D plate is the twisted pair that connects the RSQUID coil to the R.F. line. To reduce noise and interference the twisted pair is completely shielded.

The screwdriver entering the can immediately below the RSQUID is heatsunk to the bath and the D plate. Its blade, passing through a hole in the D plate, is in contact with the Nb screw which forms part of the weak link of the RSQUID.

The D heater is a 1KΩ chip resistor which is G.E. varnished to the underside of the D plate. A similar but physically smaller resistor is G.E. varnished to the sample tray, and forms the sample heater.

The thermometer is completely enclosed in a close fitting copper holder which is woods-metalled, since heating the RSQUID above the melting point of ordinary solder would be disastrous to the body of the RSQUID. Its four leads are G.E. varnished to the holder for 20cm of their length before they are connected to the secondary heatsink.

The RSQUID, shown in detail in figure 5.2, is screwed tightly into the D plate with an In washer between the two, which cold welds the joint, ensuring good, reproducible thermal contact to the D plate. The twisted pair run down this leg through a Pb shield into the Nb block, where they terminate as the excitation coil of the RSQUID.

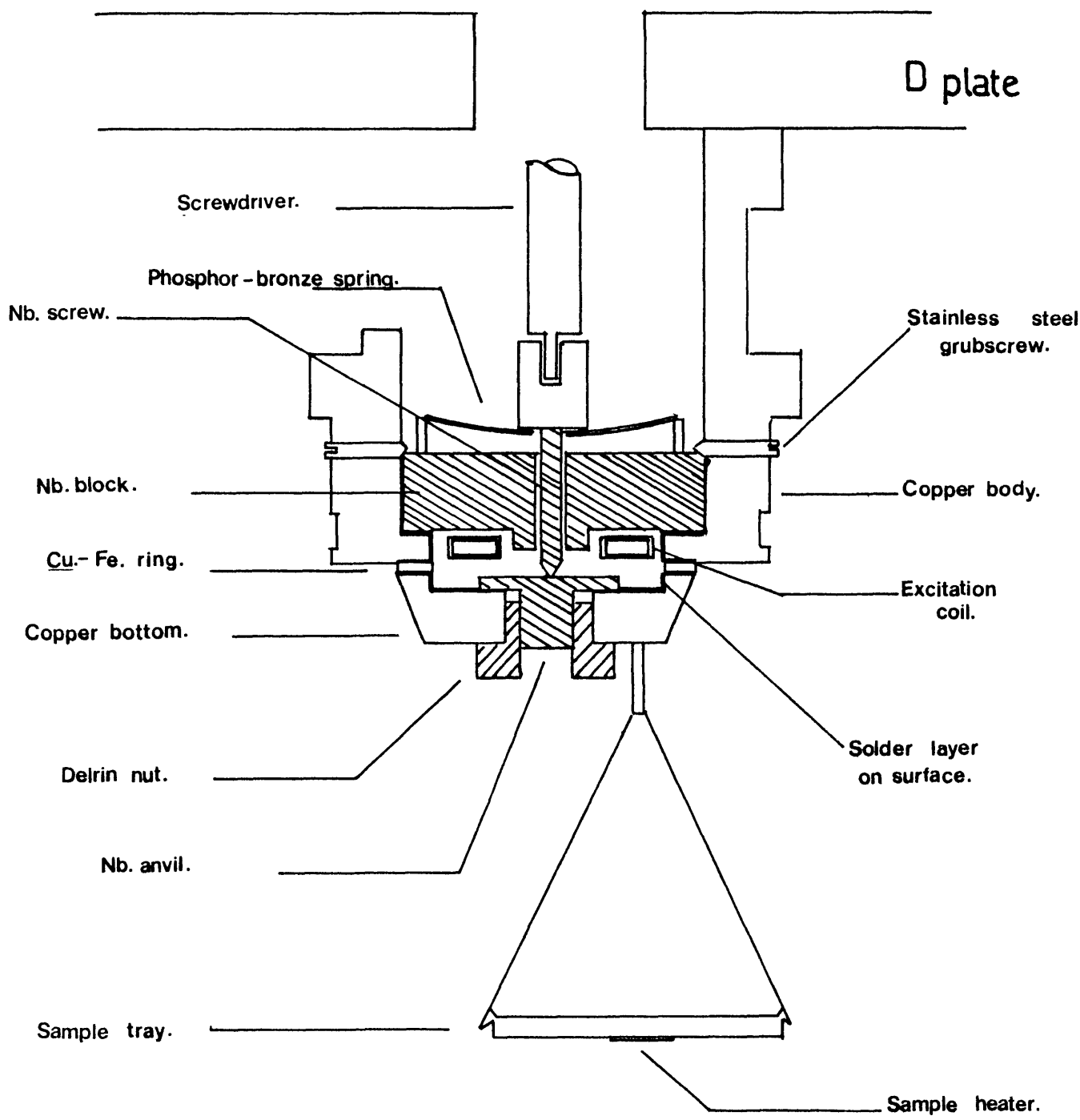


Figure 5.2 The soldered toroidal RSQUID.

5.2 Sample Chamber Layout

Many modifications have been made to the helium end of the probe, but the majority of the work has been in remaking what already existed. The RSQUID, as mentioned, was completely remade, as was the screwdriver, the co-axial cable and the tray. In addition, the thermometer mounting was completely changed.

The composite screwdriver, which is used for adjusting the RSQUID from room temperature, is made up of a stainless steel tube with a copper section, followed by a further stainless steel tube terminated in a brass blade. Originally this was thermally anchored by a washer-like piece of copper screwed to the copper section, from which a piece of braid linked it to the can top. In addition, a piece of braid also extended from the screwdriver blade to the D plate.

This, as described by Vaidya, was found to be adequate heatsinking. However, it was found that the heat current input to the D plate was a strong function of the thermal contact between the copper washer and the screwdriver. In its most extreme case the screwdriver was able to raise the D plate temperature to 8 K. To ensure a consistently good contact the braid was soldered to the copper section of the screwdriver. This not only enabled the base temperature to be reduced, but also represented a reproducible thermal contact from run to run.

The co-axial cable which made up the R.F. line to the RSQUID had to be completely remade, since the original leaked through a stycast seal. The method employed was similar to that described by Vaidya. A stainless steel tube formed the outer conductor, and a piece of 44 S.W.G. copper wire the

inner, with a polystyrene spacer every 4 cm. The ends were sealed with stycast (F.T. 1250, produced by Emerson and Cumming), the top being a vacuum seal, the bottom punctured so as to allow the cable to be pumped out with the rest of the probe. The resonant frequency of the co-axial cable by itself was 36 MHz, with a room temperature Q of 8, which improved upon cooling.

The major changes to the tray were prompted by two considerations - the samples used in this work were of considerably smaller mass than those used by Vaidya, and hence a reduction in the addenda contribution to the measurement is favourable. Secondly, an increase in the average data taking speed was necessary. To this end the sample tray size was reduced by 60%, and the total time constant further decreased by reducing the thermal resistance between the tray and the RSQUID. The latter having the advantage of additional structural strength, however, meant that the contribution to the addenda due to the bottom of the RSQUID would be greater. It was undesirable to have this contribution increased by any amount, so the copper ring from which the tray hung was replaced by a small copper post and the mass of the bottom of the RSQUID was reduced. Further, by decreasing the D plate thermal resistance to the bath, the fractional contribution to the heat capacity of the RSQUID was returned to the value achieved by Vaidya.

In the original apparatus the thermometer was mounted by simply varnishing it to the body of the RSQUID. Since a large fraction of the heat input to a thermometer is through its leads, this was considered unacceptable. A copper holder was made up and woods-metalled to the RSQUID body. Into this the thermometer fitted snugly, a thin layer of R.S. heatsinking

compound ensured a good thermal contact. The leads were then wrapped for 20cm of their length around the holder and G.E. varnished into place. This arrangement gave a good thermal contact between the body of the RSQUID and the thermometer case, and in addition to the leads of the thermometer.

5.3 Electronics

The room temperature layout of the system is as shown in Figure 5.3. This block diagram represents the required electronic layout of the experiment to employ the step method, as described in Chapter 4.

The temperature is now completely measured by a commercial P.C.B. conductance bridge manufactured by S.H.E. The output of this bridge is converted directly to temperature through a cubic spline fit by the P.E.T.

Both heaters are powered by stable power supplies and are monitored by the P.E.T. through IEEE D.V.M.'s.

A master oscillator is divided down by programmable dividers that output a symmetric 1:1 period; this provides the gate time, t_g, for the experiment. This is further divided by 2 and is then used as the control signal for the sample heater. An additional division by two then provides the signal for the Up-Down counter and the data ready signal for the computer, a Commodore P.E.T. The application of the counting system is detailed in Chapter 4.

The Phase Locked Loop (PLL) consists of a phase sensitive detector and a voltage controlled oscillator with a filter of 200μs. The output of the SQUID electronics is fed through a low noise amplifier to the PLL. This outputs a clean square wave, which is fed to the counting system.

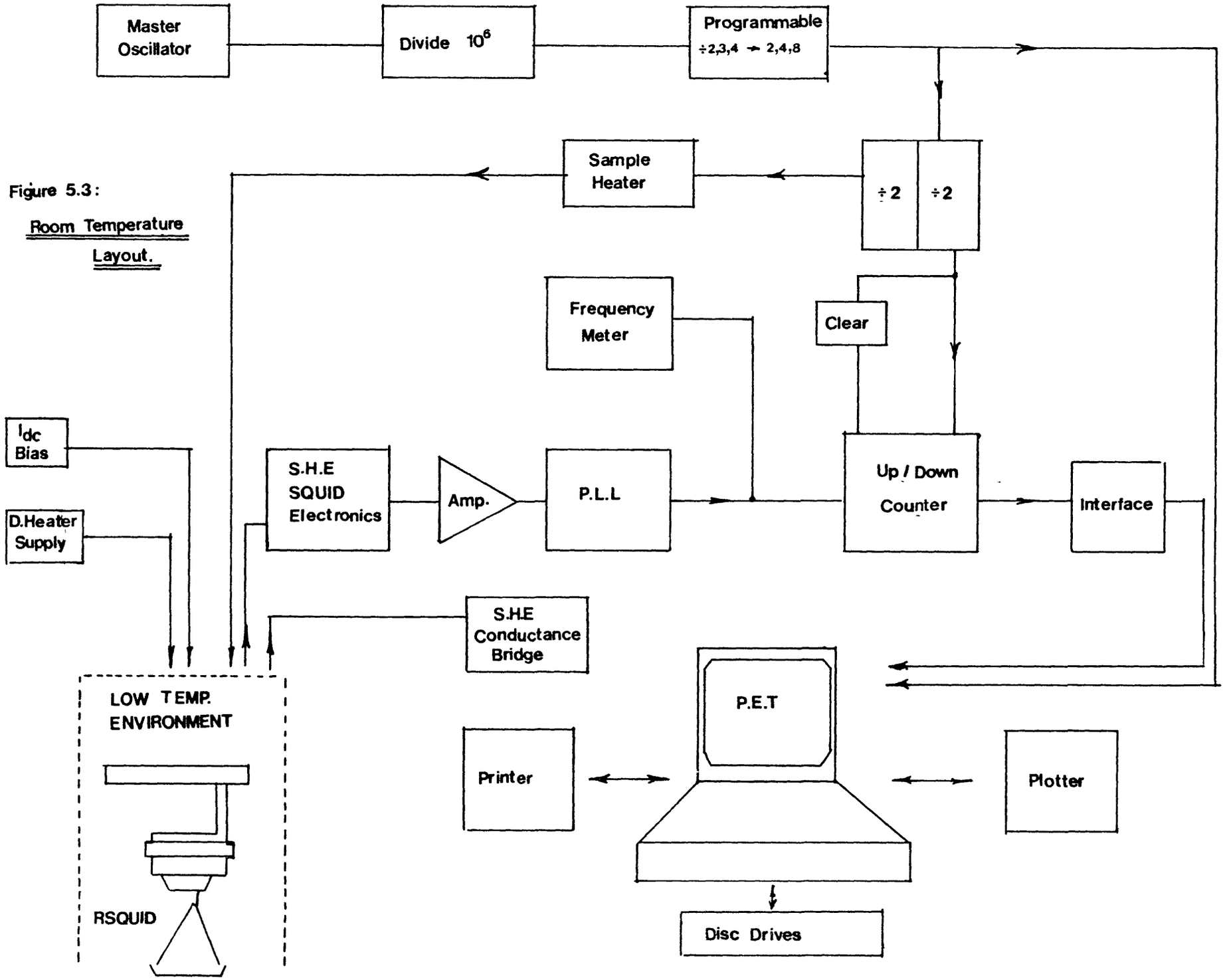


Figure 5.3:

Room Temperature Layout.

All data collection is now automated and the P.E.T. produces a printout of the raw data, a worked-out value for the specific heat and a list of the contributions due to the addenda and the grease used for thermal contact. The specific heat result is then stored on disc and plotted as the experiment proceeds.

The electrical circuits and programs enabling all this to be done are listed in Appendices C and B respectively.

5.4.1 Construction of a Soldered RSQUID

When first operated the existing RSQUID was found to respond only to changes in both thermal and electrical current. A constant application of either gave no constant frequency output as opposed to what would be expected. A possible explanation for this was thought to be that the RSQUID was "short circuited" by a superconducting bridge across its normal metal ring, causing it to behave like an RSQUID and a SQUID in parallel. In more detail, any constant voltage developed across the normal metal ring would cause a current in the superconducting short, but no voltage across the weak link, hence no shift of triangles. A change in voltage across the normal region would cause a current in the short, which in turn would attempt to modify the flux condition of the SQUID cavity. This would then cause a shift of the triangle pattern with a relaxation time thought to be related to the inductance of the cavity and the resistance of the weak link. Upon dismantling this was found to be the case, and a new RSQUID had to be constructed. Figure 5.2 shows a cross-sectional view of the RSQUID.

The description of how the original RSQUID was made, as

detailed by Vaidya[5.1], was found to be difficult to follow successfully, and a new approach was developed.

A piece of CuFe 0.1% was made up in the form of a thin foil of 75 μm thickness, both sides were then carefully tinned with PbSn solder, superconducting to 7.2 K. A hole of the same diameter as that in the bottom of the RSQUID was drilled through the centre of the foil.

Next, the bottom of the RSQUID was machined and, using a greased centering rod, was filled with solder. On to this was placed the tinned CuFe foil, and, by heating, it was soldered into place. Next, the main body of the RSQUID was placed on top, and the resulting assembly filled with solder.

The rod was then removed and the solder carefully machined away, leaving a thin layer on the copper walls, but with the edge of the CuFe foil showing. Similarly, the outside was machined to size. A close inspection was made to ensure the CuFe ring appeared sandwiched between two thin layers of solder, with no whiskers of solder across its length.

Into the bottom was inserted the Nb anvil, which made up one side of the weak link. This was secured into position by a delrin nut so constructed that upon cooling, due to the differential contractions of delrin, Nb and Cu, the anvil would be pulled into the solder so as to ensure a good superconducting contact. If this was not the case the poor contact would introduce a capacitative section to the superconducting ring of the RSQUID. Experimentally this would mean that one would observe stationary steps but would be unable to achieve the triangle mode of operation.

A block of Nb was secured through the main body of the RSQUID onto the ledges formed by the sides (see figure 5.2), by four stainless steel grub screws. This formed the top of

the RSQUID cavity and had varnished to it a toroidal coil of 55 turns of 44 S.W.G. Cu wire, which was the excitation coil of the RSQUID. The twisted pair that effectively terminated in this coil, passed through a hole in the Nb block and were soldered to the R.F. line on the D plate. Through the centre of the block was a 14 Ba tapped hole, through which came the Nb screw, which made up the point contact with the Nb anvil. A phosphor-bronze strip attached to the top of the block so as to form a spring for the screw ensured a good contact between the screw and the block.

The fully constructed, soldered RSQUID was a self-supporting SQUID with a low resistance thermal path along its length that included a normal metal ring, which also formed the resistive ring of a toroidal RSQUID.

5.4.2 Characterisation of the RSQUID

After construction and assembly of the RSQUID it was necessary to check two important characteristics:

1) That at any fixed temperature the frequency output of the detector as a function of the heat current was linear.

2) Similarly, that at any fixed temperature the frequency-biasing current (electrical current through normal metal ring) plot was linear.

This was done at a range of temperatures, and Figure 5.4 shows a typical plot of frequency against sample heater power, in this case at 2 K. Figure 5.5 shows a similar plot of biasing current vs. frequency. Both exhibit the desired linear behaviour. It must be noted that for low frequency, i.e. small heater power and small biasing current, one would not expect linear behaviour. For an RSQUID, if $i_k r$ (see section 3.4) is not negligible, the results of section 3.4 do not hold. In these experiments $i_k r$ was always negligible.

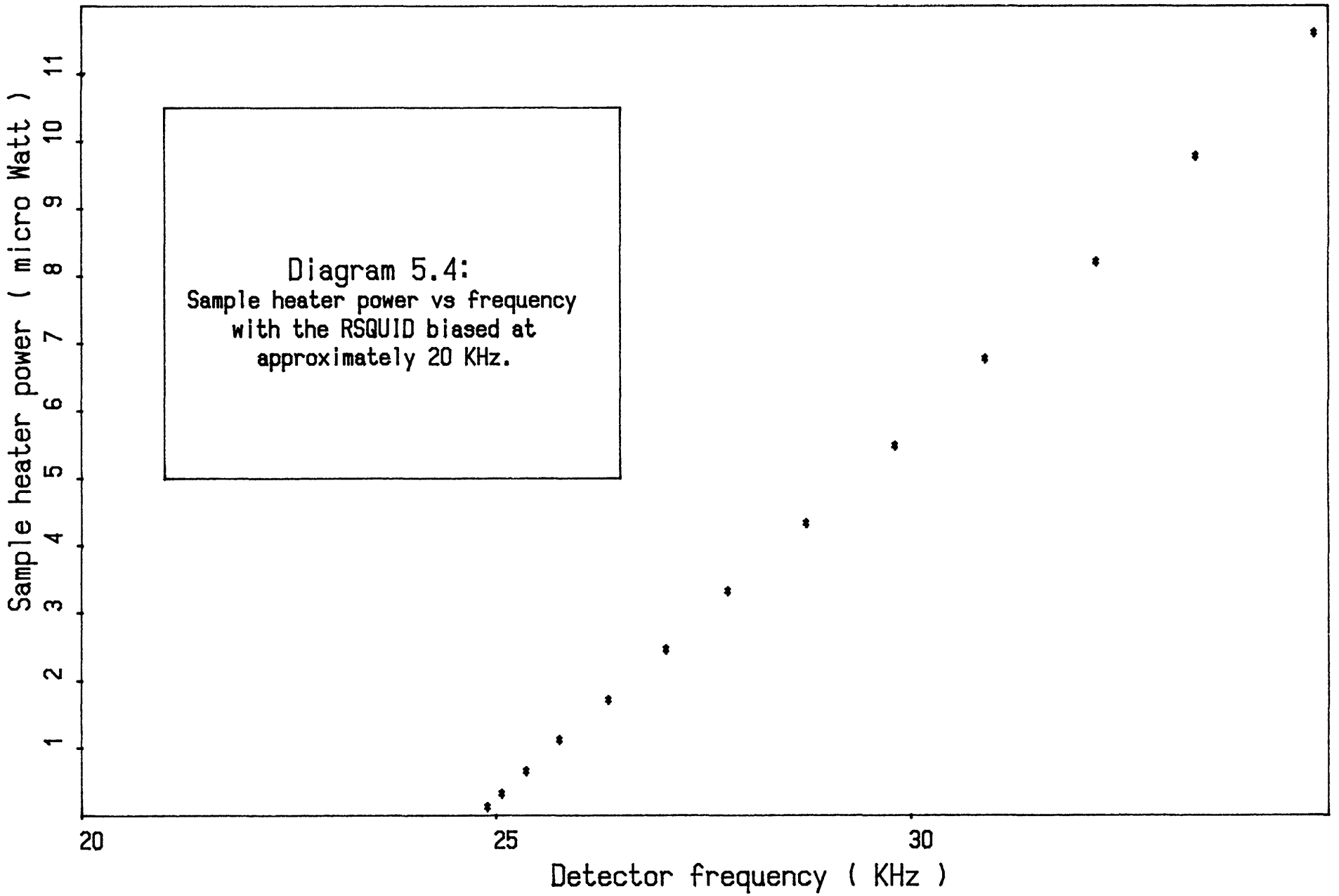


Diagram 5.4:
Sample heater power vs frequency with the RSQUID biased at approximately 20 KHz.

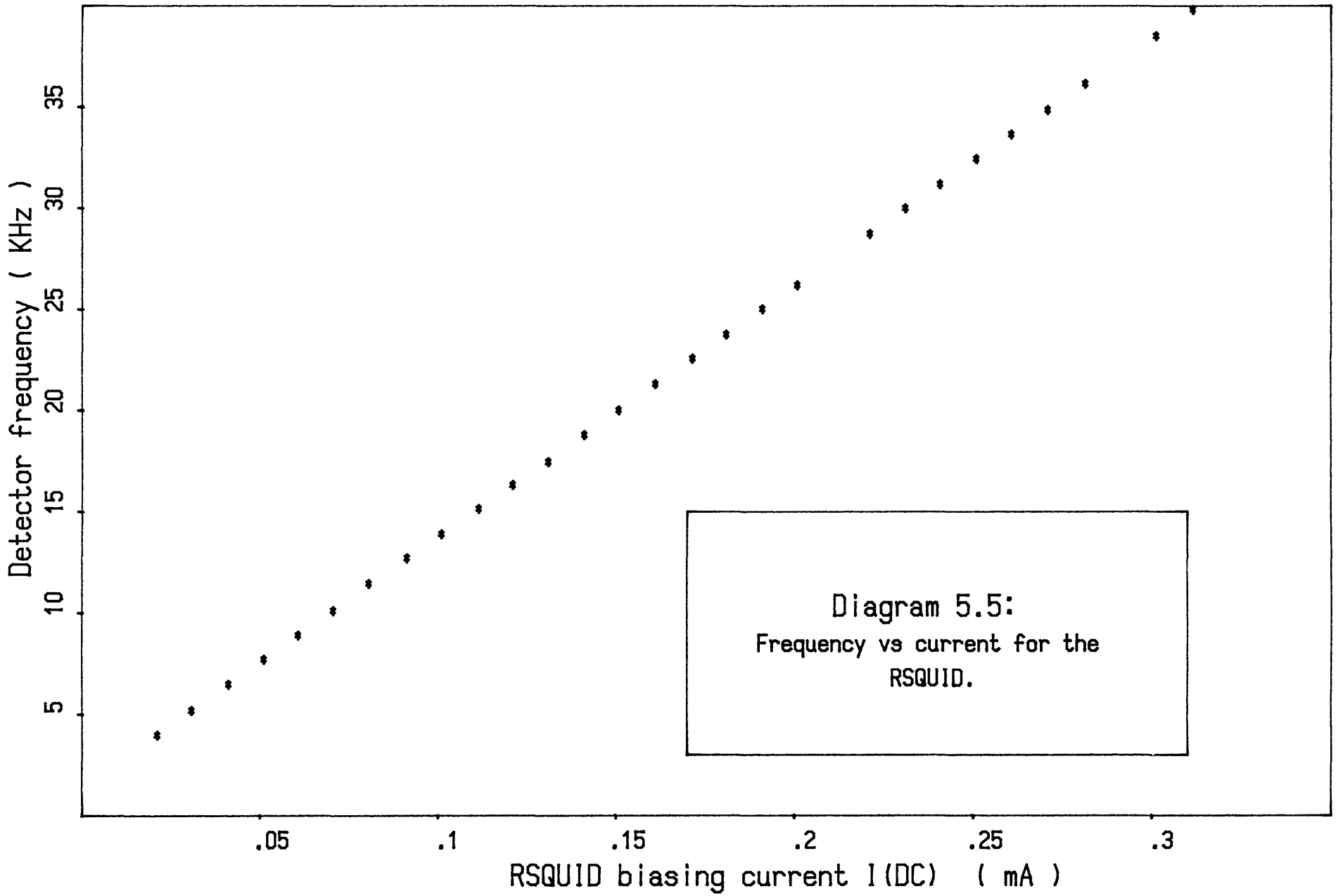


Diagram 5.5:
Frequency vs current for the RSQUID.

The sensitivity as a function of temperature, although not critical, is useful to know. Figure 5.6 shows the behaviour obtained; it varies between 1 nW Hz^{-1} to 2 nW Hz^{-1} and compares well with that reported by Vaidya.

The ohmic resistance as a function of temperature is shown in Figure 5.7. This actually shows a complex behaviour, but can be considered constant over the temperature range with which we are concerned (up to 6.5K). The sharp rise around 7K is attributed to an additional contribution to the resistance from the normal-superconducting interfaces of the ring as the transition temperature of the RSQUID is approached. A similar effect was reported by Vaidya.

The characteristics observed and presented here for the new RSQUID qualify our assertion that it may be used in the calorimetry probe, as was its predecessor.

5.5 Experimental Procedure

The sample to be measured is weighed and placed on the sample tray. A known amount of Apiezon 'N' grease is used to ensure a good thermal contact. Wun and Phillips[5.2] have published a polynomial fit, enabling the specific heat contribution due to the grease to be subtracted; this contribution was invariably less than 0.5% of the measured heat capacity of the sample. The vacuum can is sealed with an Indium O ring seal and the probe placed in the cryostat.

The cryostat consists of a standard twin walled helium dewar, its interspace accessible in order that it may be evacuated, surrounded by a nitrogen dewar. The interspace of the helium dewar is flushed with nitrogen gas and then pumped with a rotary pump. This leaves a small amount of

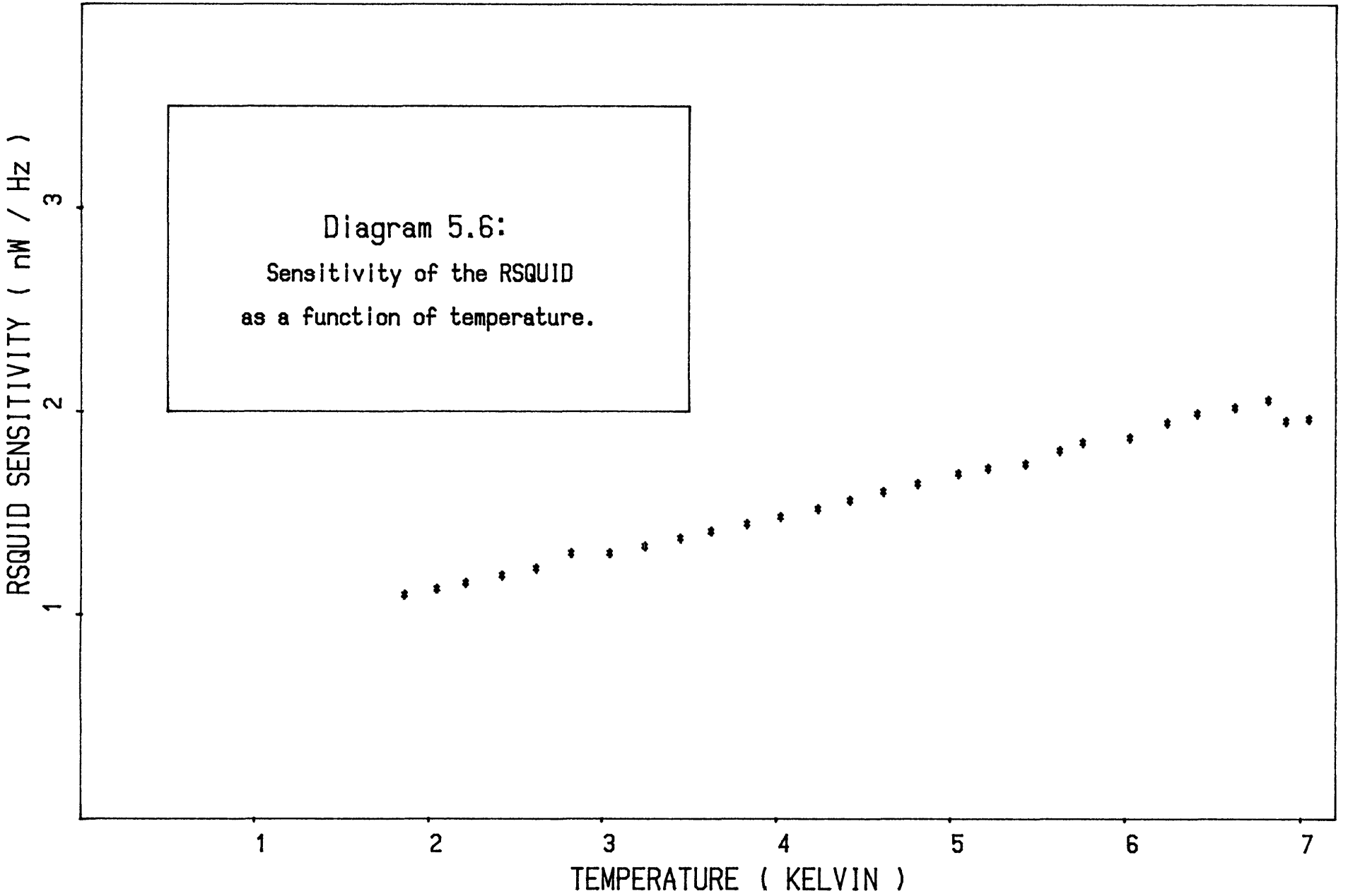


Diagram 5.6:
Sensitivity of the RSQUID
as a function of temperature.

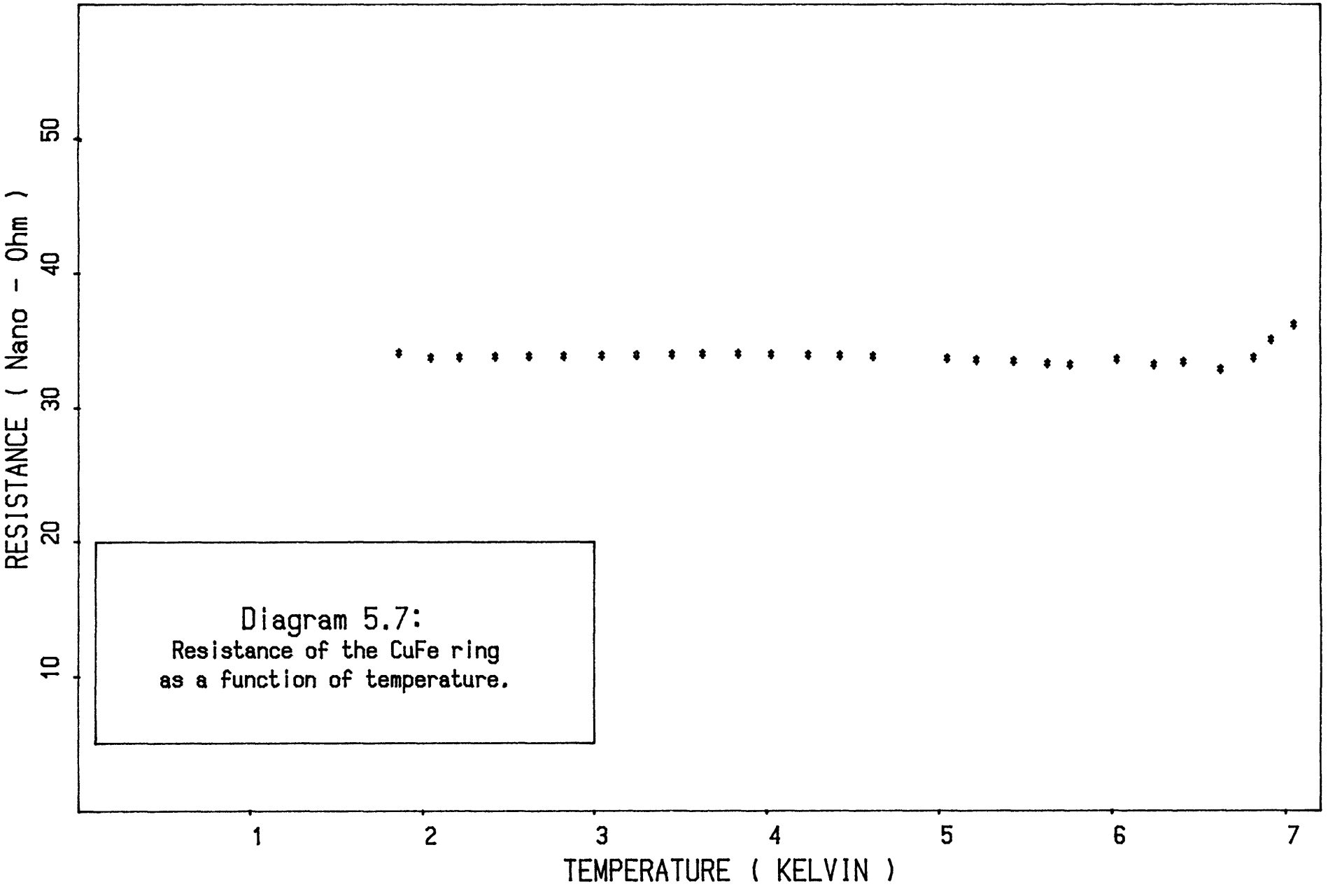


Diagram 5.7:
Resistance of the CuFe ring
as a function of temperature.

exchange gas that will freeze out at helium temperatures. The probe is pumped to 10^{-4} torr and a few cubic centimetres of dry nitrogen gas is introduced into the vacuum space to act as exchange gas. The helium dewar is flushed and filled with helium. The nitrogen dewar is filled with liquid nitrogen and the cryostat allowed to cool. On average it took two hours for the RSQUID to reach nitrogen temperatures.

Before helium was transferred into the helium dewar the vacuum can was pumped. Typically 5 litres of helium were required to completely fill the dewar. After transferring, the helium bath was pumped to a base temperature of 1.2 K and maintained there by continuous pumping throughout the experiment. A further hour was required for the RSQUID to reach equilibrium and experimentation to begin.

Once the RSQUID had been adjusted by using the screw driver, running the experiment required the temperature of each measurement to be set by changing the heater power to the D heater. Once the desired temperature had been set the 'Data point' option on the control program of the computer was selected, the number of step up- step-down cycles required, the gate time and the conductance of the thermometer entered. The system from here on was completely automatic.

The number of cycles selected was executed, and the resulting counts printed with RC worked out for each set of four cycles. At the end of a set of cycles a mean value for RC is worked out as well as a standard deviation. From this the specific heat of the sample is calculated with corrections made for the addenda contribution. By utilising the known sensitivity as a function of temperature the computer can further determine the temperature step from the counts taken and make a correction to the temperature. The final specific

heat result is printed, stored on disc and plotted.

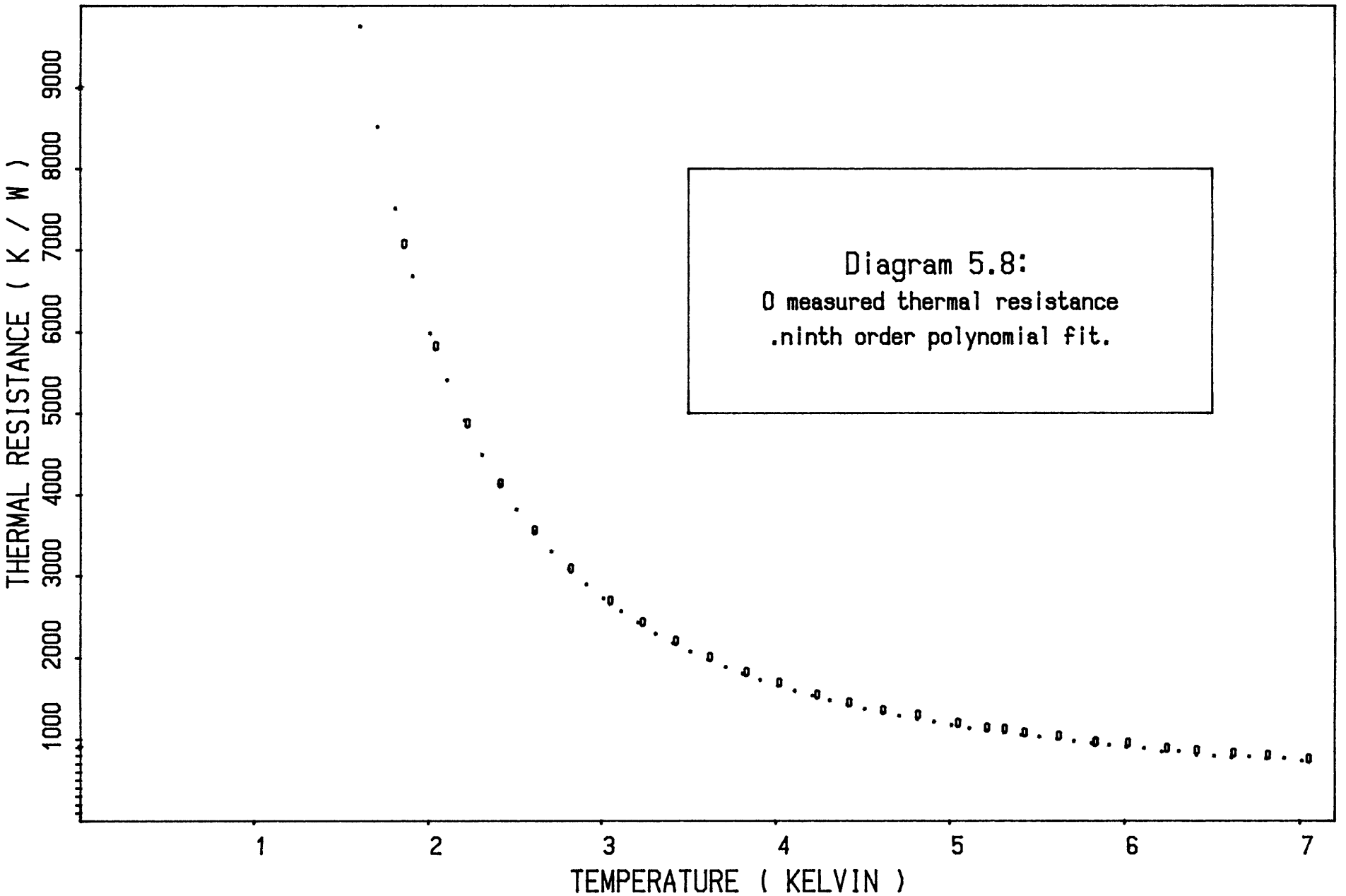
On average, after 20 runs the Nb screw becomes blunted, making it difficult to adjust the RSQUID. The system is then disassembled and the screw sharpened by placing it in a lathe and running a grinding stone over the surface of the screw until a sharp 90° angle point is achieved. The RSQUID is then adjusted at room temperature, taken half a turn off adjustment and replaced in the probe. This is necessary because otherwise differential thermal contractions would cause the screw to become blunted. Unfortunately, the rig has now to be recalibrated; due to the relatively long time between point sharpening this procedure was not changed.

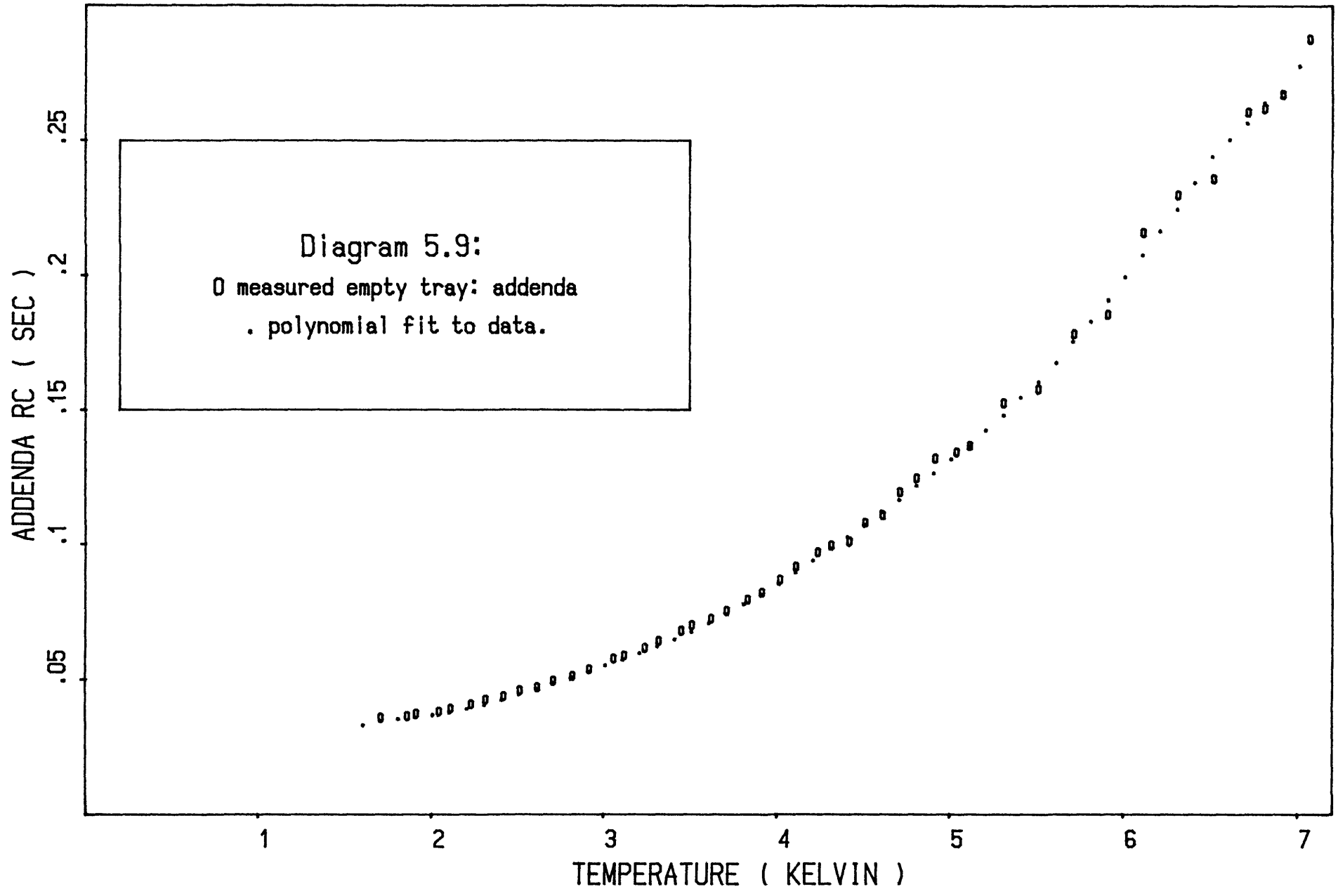
5.6 Calibrations

As mentioned in Chapter 4, two calibrations were essential in order for the calorimeter to be used. One was the addenda correction and was simply done with a 'no sample' run. The other was the R(T) calibration and was, in this case, done by measuring a copper sample of known heat capacity.

The measured R(T) and $RC(T)_{addenda}$ were fitted to ninth order polynomials by a least squares fitting program written by the author. (Program reproduced in Appendix B). This enabled the computer that controls the experiment to produce a value for the heat capacity of any sample as the data was taken. Both fits and the original data are shown in figures 5.8 and 5.9.

The thermometry which used a pre-calibrated germanium thermometer (calibrated by Cryogenic Calibrations Ltd.) was fitted to a cubic spline fit (program courtesy of Dr. C.N. Guy).


THERMAL RESISTANCE (K / W)
1000
2000
3000
4000
5000
6000
7000
8000
9000
1
2
3
4
5
6
7
TEMPERATURE (KELVIN)
Diagram 5.8:
0 measured thermal resistance
.ninth order polynomial fit.

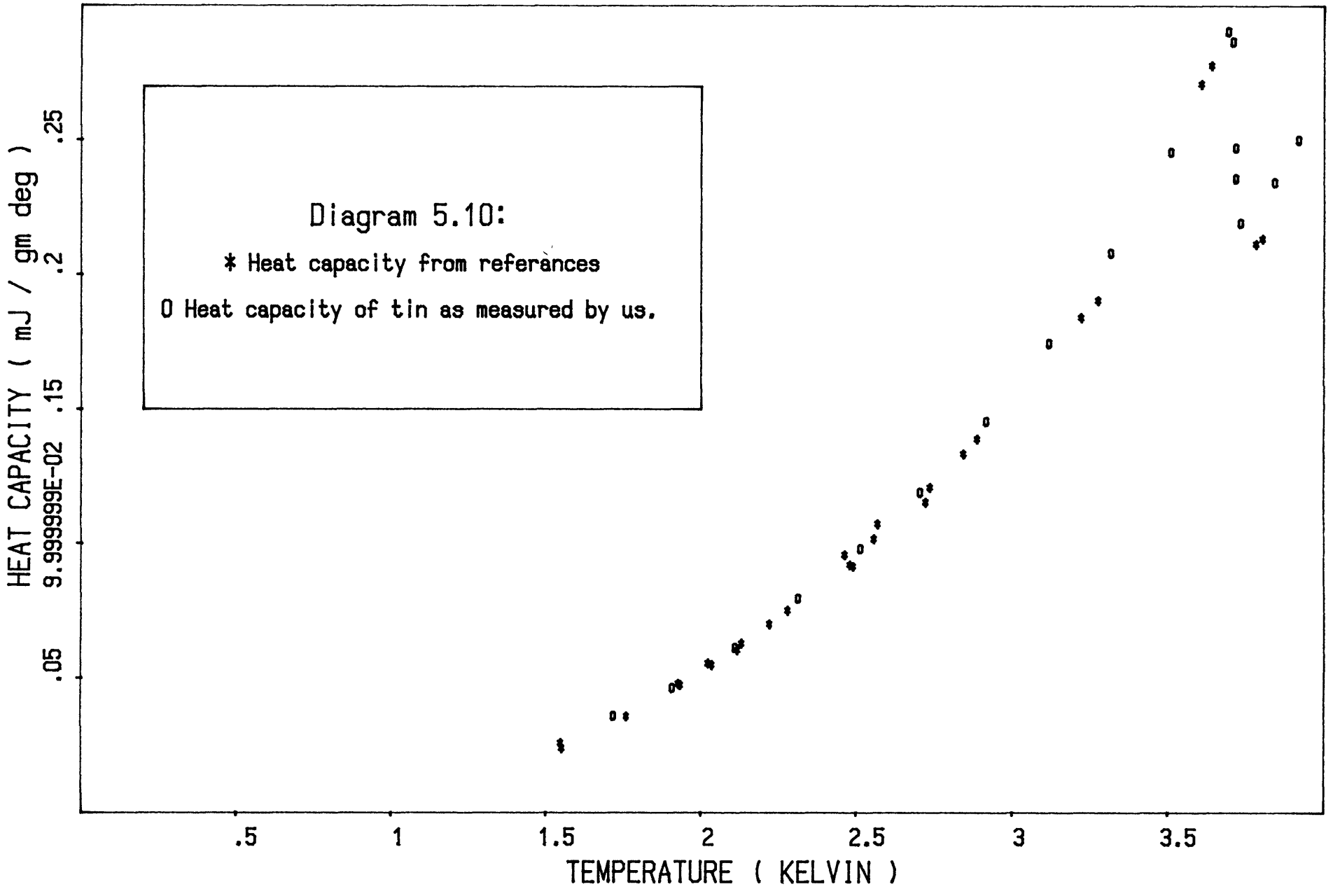

Diagram 5.9:
0 measured empty tray: addenda
. polynomial fit to data.
ADDENDA RC (SEC)
.05
.1
.15
.2
.25
1
2
3
4
5
6
7
TEMPERATURE (KELVIN)

The resulting fit was stored on disc, from where the computer could load it into memory to be used during an experiment.

5.7 Accuracy and Limitations

The temperature range of the RSQUID calorimeter is limited by the superconducting transition of the RSQUID, which is 7.2 K. This gives a comparatively limited specific heat window. However, across the range the scatter due to Johnson noise in the RSQUID resistive region and fluctuations in the bath temperature was found to be constant from experiment to experiment, varying with gate time. Typically, for any given value of RC and at gate time of 4.8 seconds, the scatter at 2 K was 4×10^{-4}, which implies an optimum scatter in the data of 0.1%. At 6 K the scatter had risen to 10^{-3}, implying a spread of 0.25%.

During all experiments the scatter was always kept to below 0.5%, except with the empty tray and with very small samples, in which case, due to the much smaller value, the scatter occasionally exceeded 0.7%; however, it was always maintained below 1%. We therefore would claim an absolute accuracy of 1.5%. This is well exhibited by a sample of Sn(1gm) which was measured and compared to published data[5.3], which is shown in figure 5.10.


Diagram 5.10:
* Heat capacity from referances
O Heat capacity of tin as measured by us.
HEAT CAPACITY (mJ / gm deg)
9.999999E-02
.05
.15
.2
.25
.5
1
1.5
2
2.5
3
3.5
TEMPERATURE (KELVIN)

CHAPTER 6

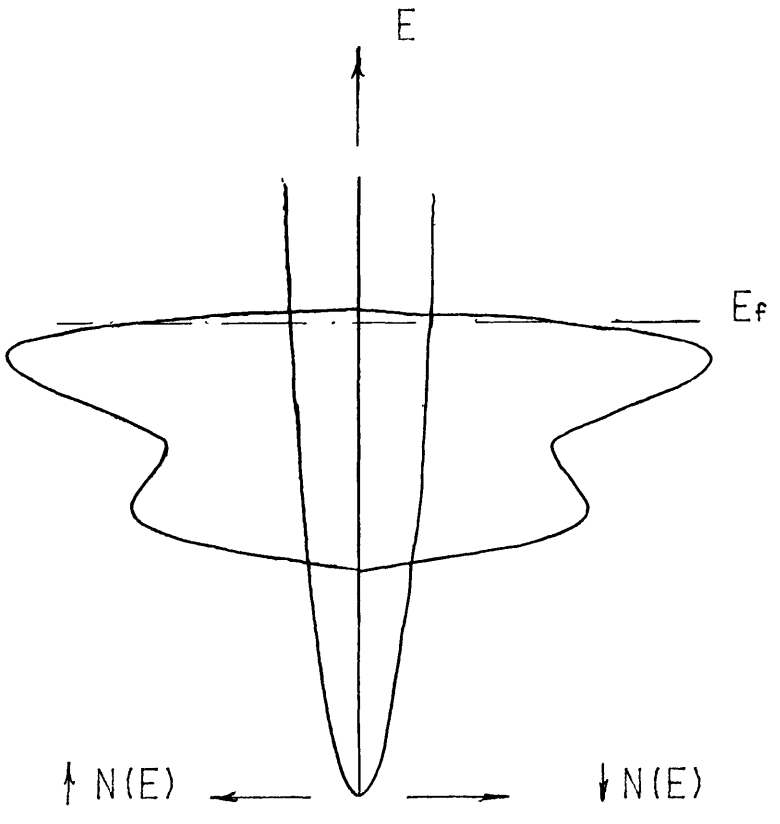
INTERMETALLIC COBALT COMPOUNDS

6.1 Introduction

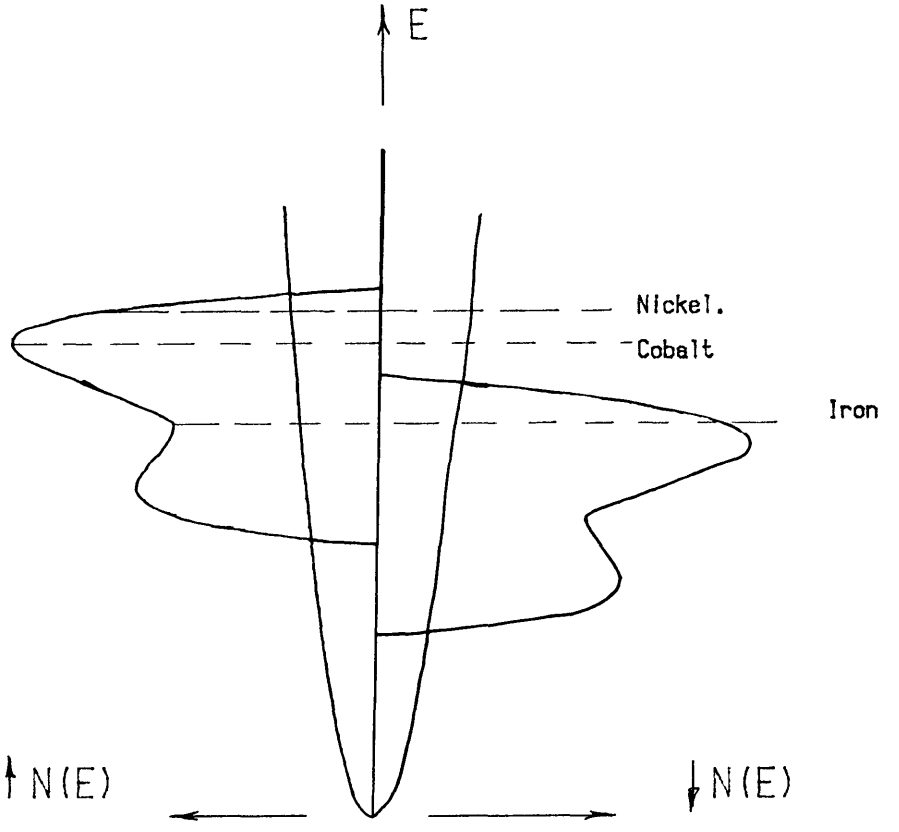
Yttrium has provided useful candidates for the investigation of 3d magnetism in alloys of the type Y_nM_m, where M=Fe, Co or Ni. Buschow[6.1], with a rudimentary band model, explains the observed magnetic moment and Curie temperature variations with composition quite successfully.

The band structures shown in diagram 6.1 are applied with the Stoner criterion: a form of competition between the exchange interaction and kinetic energy. If I is the average Coulomb interaction and $n(\varepsilon_f)$ is the density of states at the Fermi level, then the Stoner criterion can be expressed as $I\ n\ (\varepsilon_f) > 1$ and, if satisfied, the band splits into spin up and spin down sub-bands and the system is magnetic. With the addition of the Wohlfarth-Stoner[6.2] relationships, which relate the Curie temperature to the degeneracy temperature, a function of slope and change of slope at the Fermi surface, we can arrive at a qualitative explanation of the results as depicted in diagram 6.2.

Pure Ni has a 3d band that is Stoner split into spin up and spin down sub bands. The Fermi level is believed to lie below the top of one band, but above the other. With the addition of yttrium, the band slowly fills and since the magnetic moment is related to the number of holes it falls with composition, as observed. The Curie temperature decreases since the density of states is becoming smaller, until before the band is full the Stoner criterion is no longer satisfied and at a composition of YNi_5 the sub-bands are no longer split, but are yet unfilled, resulting in a high density of states and



Band structure for a system in which the Stoner criterion is not satisfied.



Band structure for a system in which the Stoner criterion is satisfied.

Figure 6.1: Simple Band Structures.

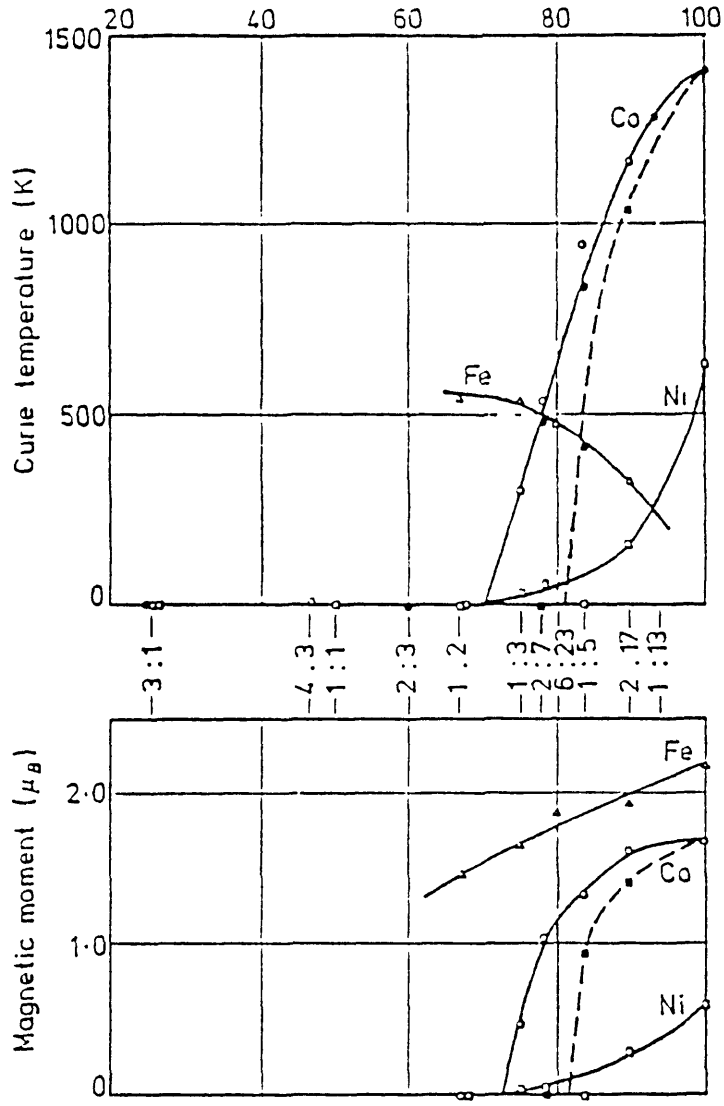


Diagram 6.2: Magnetic moment and Curie temperature as a function of composition for Y - Ni, Y - Co and Y - Fe after Buschow.[6.1]

an enhanced Pauli paramagnet.

The situation in cobalt is similar. The Fermi level is above one band and in the other; however, it is lower relative to that in Ni, and the number of holes is greater. The process of alloying with Y has a similar effect, with the composition of YCo_2 being an exchange enhanced paramagnet.

In Fe, the situation is more complex. The Fermi level is below the top of both split sub-bands and lies in a local minimum of one of them. Alloying with Y raises the Fermi level, causing the bands to fill and consequently the magnetic moment to fall. However, since $n(\varepsilon_f)$ must first increase, an initial increase in the Curie temperature is expected and observed.

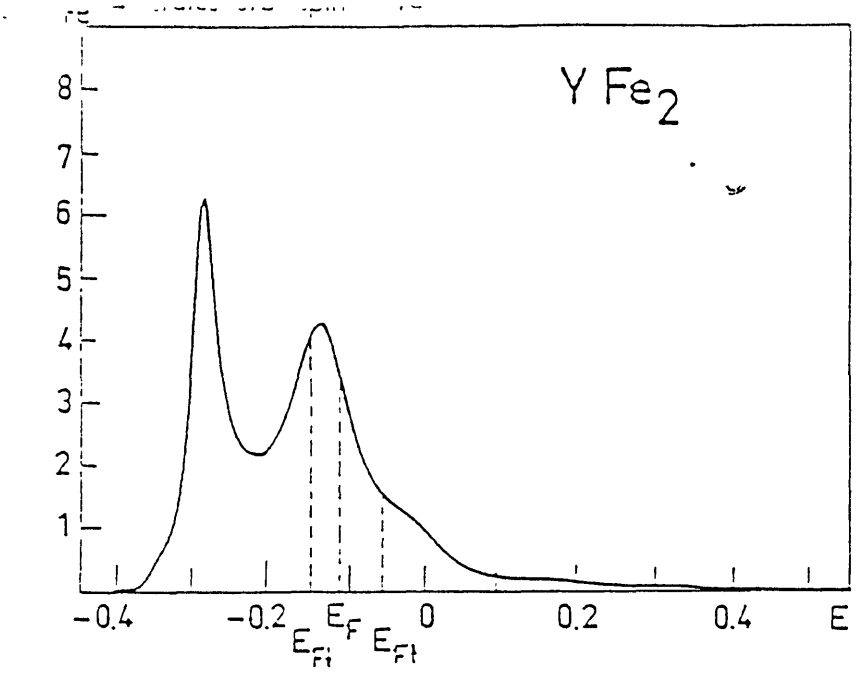
More detailed band calculations such as those by Cyrot et al[6.3] compare well with those assumed in diagram 6.1. They calculated an electron transfer of 1/3 electrons per 3d atom from yttrium for the stoichiometric compositions YNi_2, YFe_2 and YCo_2. The band structures they obtained are shown in diagram 6.3.

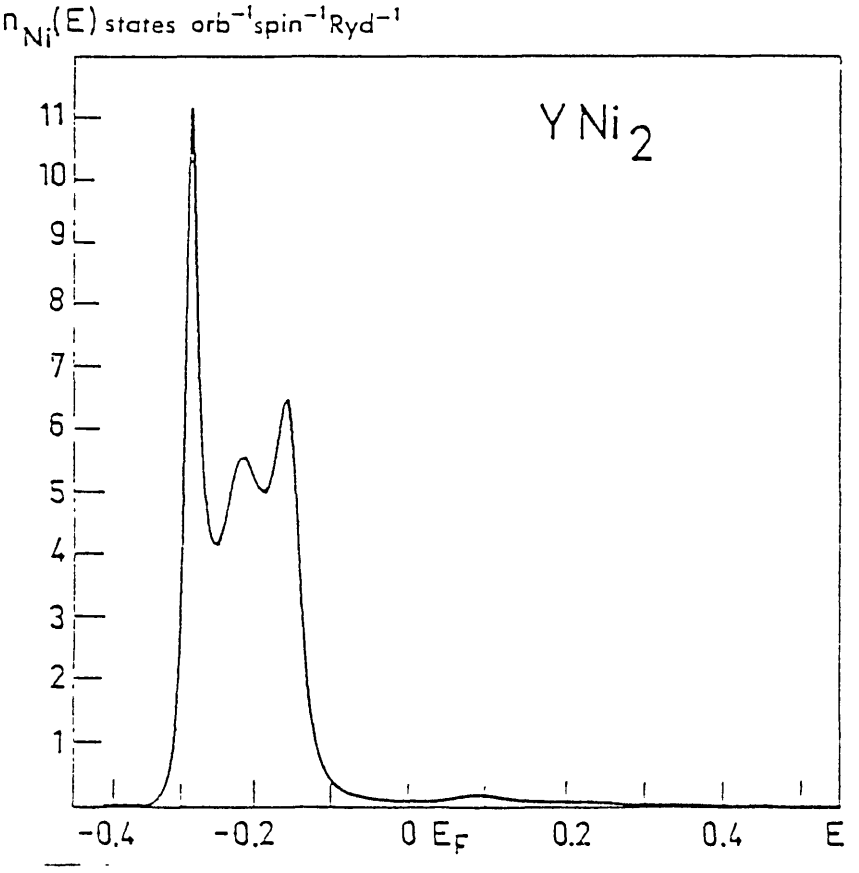
This chapter presents results and discussions on the yttrium rich end of the yttrium-cobalt phase diagram. The above argument ignores all forms of structure and band variations and yet is relatively successful. By measuring the heat capacity and susceptibility of the yttrium-rich phases we hope, by similar arguments, to explain the anomalous behaviour of Y_9Co_7. In addition, we have investigated compounds such as Zr_2Co, known to be superconducting $\sim$ 5K and $CeCo_2$ also superconducting with a $T_c \sim 1.4K$ in the hope that the appearance and enhancement of superconductivity in these compounds may explain or help formulate arguments for the properties of Y_9Co_7.

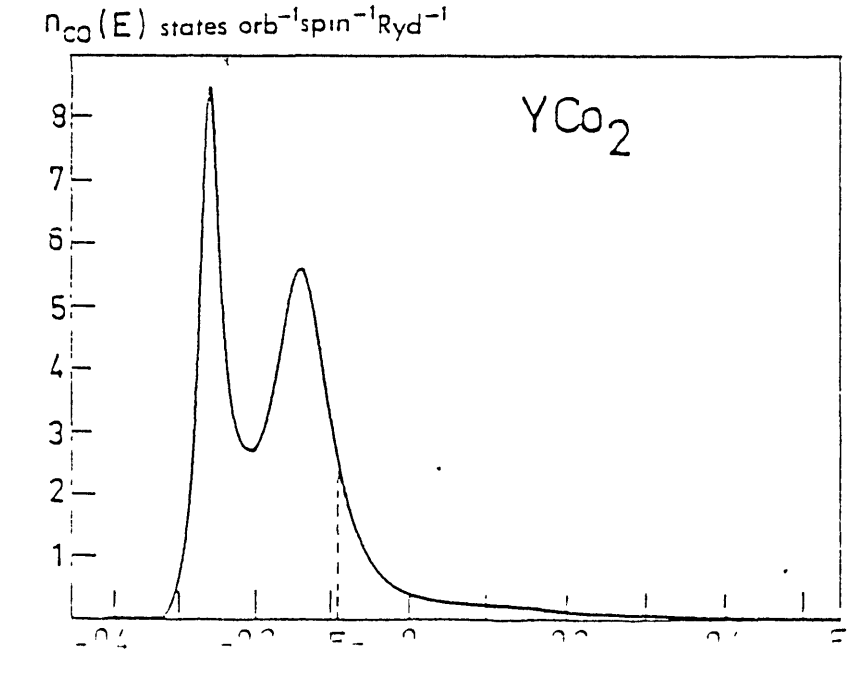
The disorder effects exhibited in Y_9Co_7 and the presence of magnetic remanence above the ordering temperature have led

Diagram 6.3:

Band structures as calcualted for YFe_2, YNi_2 and YCo_2 by Cyrot et. al.[6.3]







us to note that a similar effect exists in dilute PdCo solid solutions. We have undertaken an investigation of the disorder effects on the specific heat of Pd 0.2 at% Co to observe what would be expected if this analogy were plausible.

Finally, the peculiar structure of Y_9Co_7 leads us to the possible structure dependence of magnetic behaviour. We have investigated a Co_2TiAl compound, a weakly ferromagnetic Heusler alloy, noting its specific heat and discussing briefly the applicability of any conclusions we have reached.

The basic approach of this chapter is to form a simple working model on the basis of empirical observation and general features of 3d magnetism. By considering our own data in the light of this, we suggest possible modifications of the model, and in the concluding section we summarize our overall conclusions.

6.2 Yttrium-Cobalt

A complete phase diagram for the yttrium rich end of the Yttrium-Cobalt system was produced by Grover et al[6.4] and is reproduced in diagram 6.4. We have fabricated all the phases up to YCo, the method of sample production was generally similar and based on the phase diagram. Appropriate amounts of yttrium and cobalt were arc melted in an argon atmosphere and suction cast to produce a button, for specific heat measurements, and a rod for susceptibility. The samples were then closed in evacuated quartz capsules and annealed for the appropriate times at the temperatures suggested by the phase diagram. (For more numerical details see table 6.1). An exception to this latter stage of sample preparation was the Y_3Co_2 phase. This compound is known to be metastable, and consequently on production of an as-cast sample no further treatment such as annealing was attempted.

Sample	(A_xB_y) A	B	% loss in cost	Heat treatment
PdCo(0.2%)	JM3N	JMSP	0.17%	
as cast				
annealed	"	"	"	800°C for 8 days
$CeCo_2$ (1)	R3N	JMSP	0.2%	-
$CeCo_2$ (2)	R3N	JMSP	0.17%	800°C for 7 days
$Ce_{24}Co_{11}$	R3N	JMSP	0.2%	-
Co_2TiAl	JMSP	KL3N/JMSP	0.2%	800°C for 24 hours quenched in water
Y_1Co_1	550	JMSP	.16%	600°C for 7 days
Y_3Co	550	JMSP	0.075%	600°C for 7 days
Y_3Co_2	550	JMSP	0.17%	-
Y_8Co_5	550	JMSP	0.15%	600°C for 11 days
Zr_2Co	JMSP	JMSP	0.2%	-

JMSP, JM3N } Johnson Matthey Chemicals Ltd.

KL3N Koch Light Laboratories

550 Koch Light Laboratories: batch 550

R3N REacton: Rare earth metals & compounds Ltd.

Table 6.1 Details of Sample Preparation

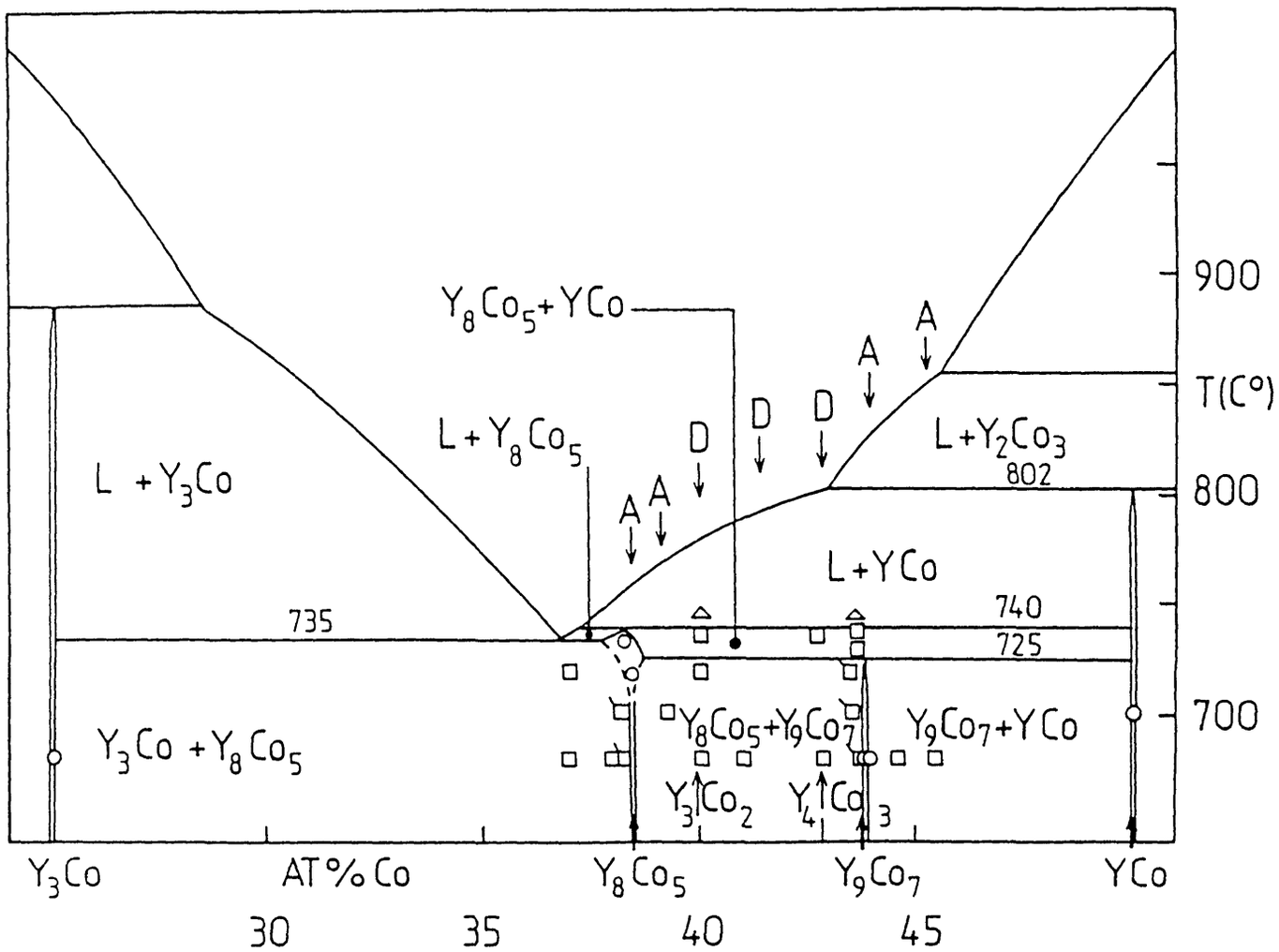


Diagram 6.4: The Y - Co phase diagram as investigated by Grover et. al.[6.4]

Assuming an electronic specific heat of the form:

$$\gamma T = (1/3)\pi^2 k_B^2\, n(\varepsilon_f)\, T \qquad \text{Eq. 6.1}$$

where k_B is the Boltzmann constant and $n(\varepsilon_f)$ the density of electronic states at the Fermi level, we have deduced from our specific heat measurements γ, Θ_D the Debye temperature and $n(\varepsilon_f)^\gamma$ the density of states from the specific heat.

Similarly, the Pauli paramagnetic susceptibility of a material may be expressed as

$$\chi_p = 2\mu_B^2 n(\varepsilon_f) \qquad \text{Eq. 6.2}$$

where μ_B is the Bohr magnetisation. We have measured, using an extraction and integration type magnetometer, the susceptibility of our samples at 4.2K. We have further calculated $n(\varepsilon_f)^\chi$.

These expressions apply to simple metals and a more general approach yields

$$\gamma = (1/3)(\, 1 + \lambda_p + \lambda_e \,)\pi^2 k_B^2\, n(\varepsilon_f) \qquad \text{Eq. 6.3}$$

where λ_p and λ_e are the electron-phonon and electron-electron enhancement factors. Also in many materials the observed paramagnetic susceptibility is Stoner enhanced, and a more appropriate expression would be

$$\chi_p = 2\mu_B^2\, n(\varepsilon_f) \,/\, (\, 1 - J_{eff} 2\mu_B^2\, n(\varepsilon_f) \,) \qquad \text{Eq. 6.4}$$

where the denominator is the Stoner enhancement factor and a statement of the Stoner criterion for magnetism.

In table 6.2 we present results for all our samples, the table includes values for $n(\varepsilon_f)^\chi / n(\varepsilon_f)^\gamma$ as evaluated from

equations 6.1 and 6.2, also included are results for YCo_2, an exchange enhanced paramagnet.

Our overall conclusion can only confirm the uniqueness of the Y_9Co_7 phase. More detailed discussion of the specific heat is presented in section 6.7, but as can be seen from the table it has a low γ compared with the paramagnetic YCo_2 and the superconducting Zr_2Co, yet exhibits the properties of both. Further, the ratio $n(\varepsilon_f)^{\chi}/n(\varepsilon_f)^{\gamma}$ bears little comparison to either of the two mentioned materials.

A sample containing both the Y_8Co_5 and Y_3Co_1 phases has been investigated by A.C. Mota (Zurich) and has exhibited superconductivity at 117 mK. We suggest from our $n(\varepsilon_f)^{\chi}/n(\varepsilon_f)^{\gamma}$ results that, due to the similar value for Zr_2Co, the phase responsible for superconductivity is in fact Y_3Co_1. Our results further suggest that the investigation of Y_3Co_2 to lower temperature may well prove fruitful in showing a superconducting transition since the $n(\varepsilon_f)^{\chi}/n(\varepsilon_f)^{\gamma}$ ratio in this compound is also close to the observed value for Zr_2Co. However, the metastable nature of this phase may well have an influence in any such search.

From our results we can only really conclude that no consistent pattern emerges from the density of states, or the susceptibilities from which we can obtain clues as to the nature of the properties of Y_9Co_7. A simple model for the magnetism of cobalt may prove useful. Pure cobalt with a band structure as described in section 6.1 and shown in diagram 6.1 is ferromagnetic and has a hexagonal close packed structure with an almost ideal axial ratio (c/a) of $\sqrt{8}/3$ or 1.635. Therefore, each cobalt atom has twelve nearest neighbours at a distance of 2.502 Å. Compression of the cobalt lattice would cause a

Phase	γ (mJ/mol deg^2)	Θ_D (K)	$\chi_{4.2}$ ($\times 10^{-4}$) emu. mol^{-1}	$n(\varepsilon_f)^\chi/n(\varepsilon_f)^\gamma$
Y*	10.2	280	2	0.713
Y_3Co	5.0	205	2.7	1.966
Y_8Co_5	4.6	221	6.7	5.3
Y_9Co_7	3.4(5.6)	220	3.18$^+$	2.06
Y_3Co_2	5.1	221	2.4	1.7
YCo	7.4	297	12	5.90
$YCo_2$$^{++}$	12.0	240	37	11.22
Zr_2Co	10.5	265	5.19	1.799

* Ref. (6.39, 6.40)

$^+$ Ref. 6.37

$^{++}$ Ref. 6.38

Table 6.2 Comparison of our results for some intermetallic cobalt compounds

all results in average atomic mole

broadening of the band and consequently a reduction of $n(\varepsilon_f)$ the density of electronic states at the Fermi level. If the Stoner criterion parameter I is purely intra-atomic, then at some separation, the cobalt lattice would cease to be ferromagnetic and become paramagnetic. In YCo_2 the 3d band is paramagnetic, in Buschow's description this is attributed to the electron transfer from yttrium and the loss of the Stoner criterion, we suggest that compression of the Co-Co separation may also play a role, since the 3d bands are certainly not full. YCo_2 is a cubic Laves phase, and the Cobalt-Cobalt separation is 2.44 Å. Ignoring the electron transfer from Yttrium, we will in an over-simplification assume this is close to a critical separation below which the cobalt atoms are no longer magnetic.

If we now expand the lattice the 3d band will become narrower and, above some Co-Co distance, the 3d band's width will be s-d hybridization dominated, as opposed to d-d-overlap dependent. The spatial spread of the 3d wavefunction is such in cobalt that at a distance of about 4 Å this would occur[6.5]. Thus, for our purposes, which are essentially qualitative, we suggest a 4 Å separation from nearest neighbour cobalt atoms would cause a more local moment character. We now have a rudimentary model for cobalt ferromagnetism based on cobalt-cobalt separation.

6.3 Superconductivity in $CeCo_2$

Luo et al[6.6] have investigated the $CeCo_2$ stochiometric phase for a range of samples around this composition, in all of which the alloy is believed to have a C15 cubic Laves phase structure. Their results are shown in diagram 6.5, in which they have plotted lattice parameter vs superconducting transition

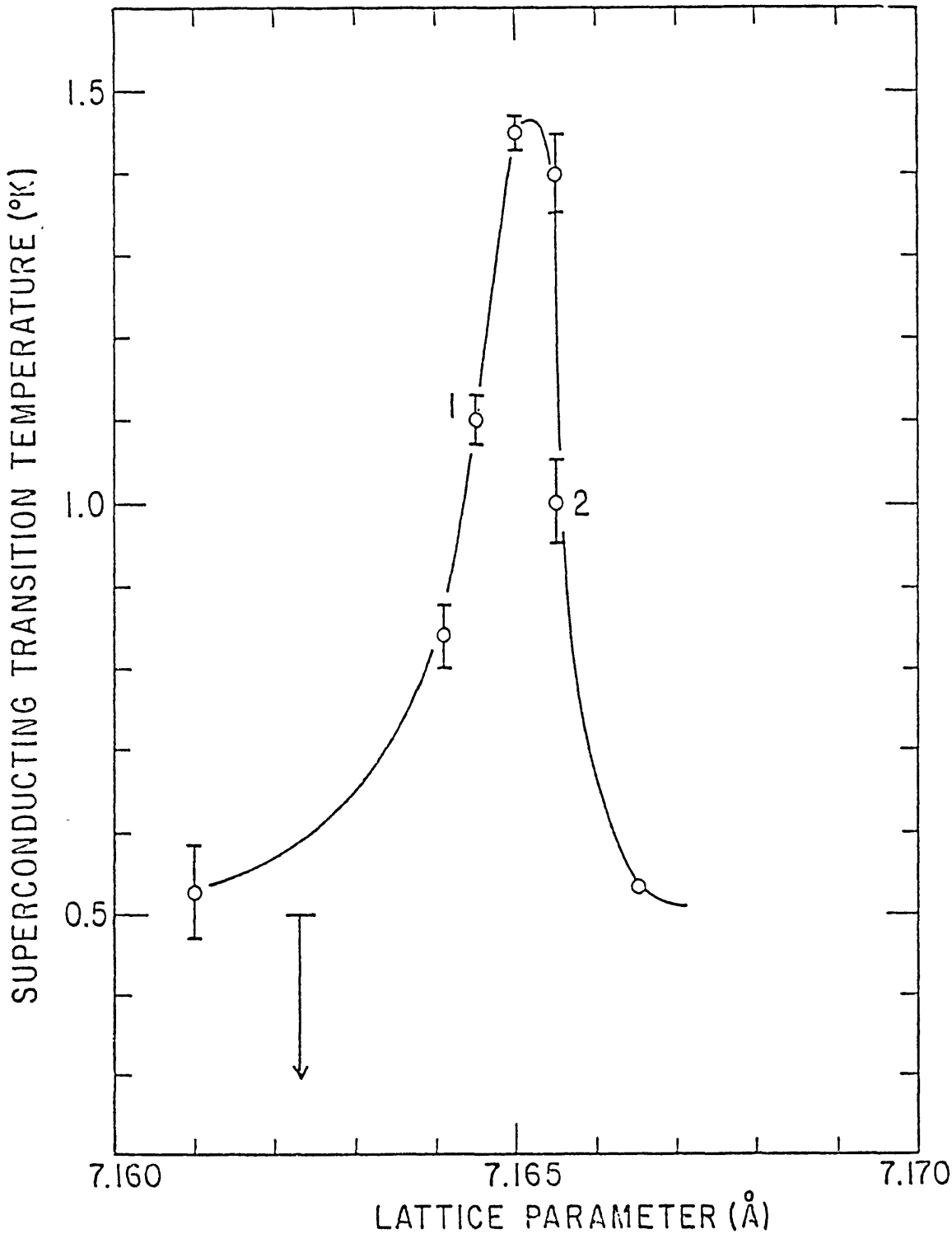


Diagram 6.5: Results for $CeCo_2$ as reported by Luo et. al.[6.6]

temperature. They report no consistent behaviour of T_c with composition. The samples marked one and two were further investigated at pressures up to 20 Kbar, they assumed a value for the compressibility of 3×10^{-7} bar^{-1} and expected a decrease ~1°K for alloy 2 at 20 kbar. They observed only a 0.04°K decrease, while sample 1 appeared to have a pressure-independent T_c up to 14 Kbar.

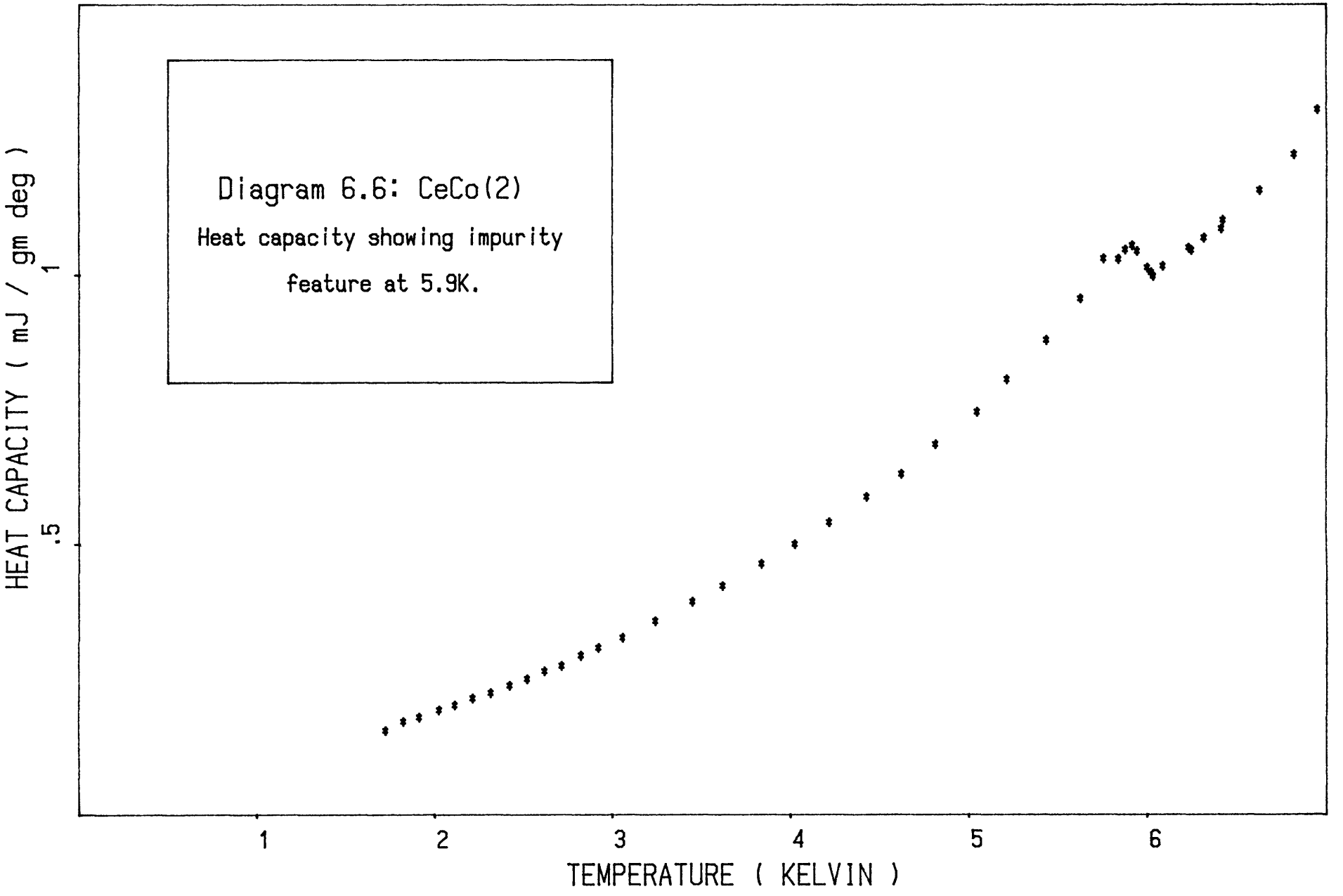
We suggest that our rudimentary model, with a few modifications, may well explain this behaviour. The C15 cubic Laves phase such as observed in $MgCu_2$ is a cubic structure with 24 atoms per unit cell, which can be visualised as two interpenetrating lattices, upon which lie the two types of atoms. If in general our compound is AB_2, then the B atoms lie at the corners of tetrahedra which are joined point to point throughout space. This arrangement leaves holes into which the A atoms are accommodated in a diamond structure. (For more detail see for instance Hume-Rothery and Raynor[6.7]). The A-A distance can be shown to be a $\sqrt{3}/4$, where a is the length of the cubic unit cell and the B-B separation as a $\sqrt{2}/4$.

α Cerium is the high pressure, low volume phase of Cerium which is known to be superconducting at 50 Kbar with a T_c of 1.7 K. Upon further compression, the superconducting transition temperature decreases rapidly with pressure[6.8]. Gschneidner[6.9], in his article on the physical properties of metals, gives an analytical expression for the pressure-dependence of the volume of α-Cerium.

$$\Delta V/V = - 0.1706 - 37.4 \times 10^{-7} (P-P_o) + 22.8 \times 10^{-12} (P-P_o)^2$$

Eq. 6.5

where P_o = 7.7 Kbar and the expression is valid up to 100 Kbar. He further quotes the compressibility of α-Ce at 7.7 Kbar to


Diagram 6.6: CeCo(2)
Heat capacity showing impurity
feature at 5.9K.
HEAT CAPACITY (mJ / gm deg)
.5
1
1
2
3
4
5
6
TEMPERATURE (KELVIN)

be 5.122×10^{-6} bar^{-1}.

For the lattice parameter quoted by Luo et al the Co-Co separation is seen to be of the order necessary, by our simple model, for magnetism to occur. On further increase of the lattice parameter the Co atoms become more magnetic, tending toward full long range ferromagnetism. For a lattice parameter of 7.160 Å the calculated Ce-Ce separation implies that the Cerium is under compression. Use of the Gschneidner equation further suggests that the Ce-atoms are in the α -Cerium phase experiencing a pressure of 50.6 Kbar. As the lattice parameter increases, the chemical pressure decreases and, as reported by Pobst and Witting[6.8], one would expect an increase in the superconducting temperature, the maximum value being at 50 Kbar and corresponding to 1.7 K. However, in competition with this is the increasing tendency of the Cobalt atoms to become magnetic as the lattice parameter increases. Therefore, at some critical separation the increasing T_c should pass through a maximum, less than 1.7 K, and fall with further increase in lattice parameter. This is exactly what has been observed by Luo et al.

The pressure variation of T_c, as observed by these workers in this model, may well be expected. The compression of alloy 2 would cause a reduction of the Cobalt tendency towards magnetism. This would imply an increase in T_c, but the pressure would lead to a decrease of T_c due to compression of the Ce-atoms. Again, the interplay between these processes, and the recognition of the fact that the compressibility of such a close-packed structure may be small, suggests that the results obtained by Luo et al are not due to disorder.

We decided to measure the specific heat of $CeCo_2$, and in our model expected some form of correlation between this and that of α -Ce at 50 Kbar, which has been reported to be

12.8 mJ mol deg^{-2} [6.41]. A sample was prepared by arc-melting the appropriate amounts of Ce and Co in an argon atmosphere; table 6.1 shows the appropriate numerical and quality details for sample 1. No annealing was initially attempting and the speficic heat showed an unexpected λ like anomaly at 6K. AC susceptibility measurements show a corresponding cusp. This mysterious behaviour led us to produce a second sample (sample 2 in table 6.1), which was annealed for eight days at 800°C, and was found to exhibit the same behaviour; diagram 6.6 shows the specific heat as measured by us. A microscopic analysis of the surface showed a quantity of lighter Cobalt rich phase in sample 1, while sample 2 showed an even larger presence of this second phase.

The Cerium-Cobalt phase diagram is as of yet still controversial. No cobalt rich phase could be responsible for the magnetic behaviour; however, a Ce rich phase $Ce_{24}Co_{11}$, was thought to be a possible candidate. This was prepared by a similar process to the $CeCo_2$ samples (see table 6.1) and its A.C. susceptibility measured. No anomaly was observed in the relevant temperature range.

At present a sample of $CeCo_2$ is being prepared and measured independently at Birmingham. We expect the observed anomaly to be an impurity effect.

A value for the specific heat γ does exist in literature [6.11] and, for completion, we quote it here: 12mJ mol^{-1} deg^{-1}, but one must note that the error in this is $\pm$ 1.5mJ.

6.4 Superconductivity in Zr_2Co

Zr_2Co constitutes an interesting comparison to Y_9Co_7. Pure Zr with a superconducting transition temperature T_c of 0.55K would seem to suffer (T_c-wise) with the addition of a 3d magnetic

material such as cobalt. On the contrary, the superconducting transition temperature of Zr_2Co has been reported to lie between 5 and 6K, depending on composition and heat treatment[6.12].

Table 6.1 contains the basic information on the production of our Zr_2Co samples. As with most of our samples, appropriate amounts of high purity Zr and Co were arc-melted together in a low pressure argon atmosphere. Since heat treatment is believed to decrease the superconducting T_c[6.12], no annealing was attempted and the specific heat of the as-cast sample was measured. The basic results are shown in table 6.2. The observed superconducting transition temperature was 5.2K, in reasonable agreement with the above quoted reference.

McMillan [6.13] derives an equation which relates the phonon-frequency spectrum, the superconducting transition temperature and the electron-phonon enhancement factor. This has frequently been used to determine a value for λ_p, the phonon-electron enhancement factor, with the information about the phonon acoustic spectra approximated by the Debye temperature, Θ_D and a measured T_c giving a form.

$$T_c = (\Theta_D/1.45) \exp [-((1.04(1+\lambda_p))/(\lambda_p-\mu^*(1+0.62\lambda_p)))] \qquad \text{Eq. 6.6}$$

where μ^* is a parameter that is approximately 0.1 for metals and 0.13 for transition metals.

In table 6.3 we present the electronic specific heat, γ, the Debye temperature Θ_D and the electron-phonon enhancement factor λ_p, for pure Zr, the high Tc Zr_2Co and the non-superconducting, paramagnet $ZrCo_2$. The structure of pure Zr is close packed hexagonal, while Zr_2Co is $CuAl_2$ type structure

Sample	γ mJ/(mol deg^2)	Θ_D (K)	λ_p	T_c (K)	T_F (K)
Co_2TiAl	5.22	449	-	-	130
Zr	2.78	290	0.41	0.55	-
Zr_2Co	10.5	265	0.67	5.2	-
$ZrCo_2$ *	8.8	181	0.18	-	-
$CeCo_2$ +	12	-	-	1.4	-

* Ref. 6.14

\+ Ref. 6.11

Table 6.3 Comparison of our results for the superconducting samples and Co_2TiAl

and $ZrCo_2$ is a C15 cubic Laves phase. In the former two we have used T_c and Θ_D in the Mcmillan equation to obtain λ_p while in $ZrCo_2$ the λ_p value is as calculated by Klein et al[6.14]. Substituting this value into the Mcmillan equation implies a superconducting transition temperature that is below the millikelvin region.

We can now apply our simple model to this system to see if we may interpret the properties from Zr to $ZrCo_2$. In Zr the atomic distances are 3.225 Å; taking this as a basis we note that dT_c/dP for Zr is positive with an approximate value of 14×10^{-6} $Kbar^{-1}$ [6.15]. We can now predict that the required pressure on a Zr lattice to raise the superconducting transition temperature from 0.55K to 5.2K is 332 Kbar.

Zr_2Co is known to have a tetragonal $CuAl_2$ type structure[6.16] with a lattice parameter of 6.366 Å[6.12]. The Co-Co separation in this structure is $a/\sqrt{2}$ = 4.301 Å, a separation in our model that allows little 3d wavefunction overlap. If we consider this inhibits long range ferromagnetism and localised moment formation due to sufficient electron transfer to the cobalt atoms from the Zr atoms, we can treat the Co atoms as 'non-magnetic', such as in Co_2Al_9[6.17]. However, the smaller Zr-Zr distance of 2.812 Å implies considerable compression of the Zr lattice. Gschneidner[6.9] gives a compressibility for pure Zr of the form

$$\Delta V/V = -11.77 \times 10^{-7} P + 4.484 \times 10^{-12} P^2 \qquad \text{Eq. 6.7}$$

In using this we must note that the validity of this expression is only guaranteed for pressures up to 40 Kbar. However, in our first order simple calculations we will assume a wider range of applicability. Solving this equation for a compression from 3.225 Å to 2.8117 Å we obtain a value for the

required pressure of 345 Kbar, which agrees well, considering the approximations, with our value calculated from dT_c/dP.

Extending similar ideas to the Laves phase $ZrCo_2$ with a lattice parameter of 6.957 Å[6.14], we obtain a Zr-Zr distance ~ 3.0125 Å, which, using equation 6.7, implies the Zr atoms are suffering a compression of 47.4 Kbar and hence should be superconducting at T_c = 1.2K. However, in competition with this, the Co-Co distance is 2.460 Å, very close to the 2.302 Å required in our model for long range ferromagnetism to be possible. The Co-Co separation is in fact greater than YCo_2, which implies that the compound should be an enhanced paramagnet and analogous to pure Pd, where the paramagnetic nature and the d-d interaction inhibits the formation of Cooper pairs and hence no superconductivity is observed. This agrees with our analysis and experiments, but the calculated λ_p[6.14] is too small for a T_c of the magnitude we have predicted. We suggest that the process of electron transfer to the cobalt atom from the Zr atoms is responsible for the comparatively small Stoner enhancement factor, i.e. in $ZrCo_2$ S~ 2, while in Pd S~ 10; this may also reduce the number of electrons available to participate in superconductivity, adding an additional factor to the inhibiting of Cooper pair formation.

6.5 Magnetism in Heusler Alloys

Heusler alloys are described as ternary intermetallic compounds X_2YZ with an $L2_1$ type structure. Generally X is a transition metal, Y is normally Mn, and Z is a B sub group metal. The structure can be visualised as a system of four interpenetrating face-centered-cubic lattices: A, B, C and D, as shown in figure 6.7. The occupation is such that X is on the A and C sites, with Y on the B sites and Z on the D sites.

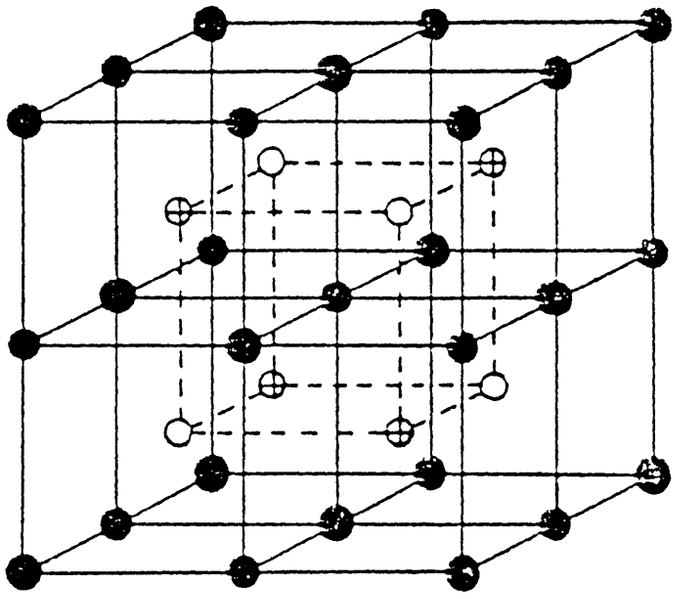


Diagram 6.7: The Heusler, $L2_1$, structure.

These were the first materials to exhibit ferromagnetism while not containing one of the ferromagnetic transition metals, iron, cobalt or nickel. For instance, Cu_2MnAl is a Heusler alloy with a ferromagnetic ordering temperature of 600°K. Interest persists in these alloys, since they are ternary compounds in which the magnetic properties can be altered by changing the degree or type of chemical disorder, implying that the observed ferromagnetic ordering is structure dependent.

Antiferromagnetic Heusler alloys have also been discovered in Pd_2MnIn_2 and a review by Webster,[6.18] discusses more generally the effect of disorder and the use of X-rays and neutrons as probes in these alloys.

Generally Heusler alloys of the form X_2MnZ have the observed magnetic moment associated with the Mn atoms, and since the lattice parameter is ~ 6 Å, this implies a Mn-Mn distance ~ 4.2Å, a separation which, according to our model, precludes any 3d overlap and hence any co-operative magnetism. In Cu_2MnAl the Mn atom carries 3.8 μ_B moment, but magnetic behaviour has been observed in CuMn alloys, where the d-d interaction is mediated by processes such as the RKKY interaction, and magnetic ordering is also present in dilute solid solutions such as PdCo, where the solute-solute distances are large, yet co-operative magnetic behaviour is observed and is due to the nature of the host matrix (see section 6.6). In Heusler alloys that contain cobalt, i.e. Co_2MnAl and Co_2MnSi, the magnetic moment is now shared with both the Co and the Mn sites, and due to the 3d atom separation 3d overlap is certainly now possible.

This poses a possible modification of our model in the Co-Co large separation scheme. We now have the possibility of

collective magnetism due to either structure effects or to a mediator of the 3d-3d interaction, a not unpredictable modification.

To investigate further the magnetism in Heusler alloys we proposed the calorimetric study of an alloy in which only cobalt is the 3d magnetic constituent. Gladysevskij et al[6.19] have shown that Co_2TiAl has an $L2_1$ structure with a lattice parameter of 5.847 Å. Webster and Ziebeck[6.19] investigated it further and have shown that the Co sites carry a magnetic moment of 0.35 μ_B per cobalt atom and the ferromagnetic ordering temperature is 138 K.

The cobalt-cobalt separation in Co_2TiAl is 2.92 Å and in our simple model the alloy should be magnetic. If, however, as expected in Heusler alloys, the magnetism is also associated with the structure and the valence of the other two constituents [6.20], we would expect to see this reflected in the electronic specific heat, i.e. if compared to YCo_2 we would expect a similar density of states if the 3d bands are playing a dominating role in the magnetic behaviour.

The required amounts of cobalt, titanium and aluminium were melted together in a low pressure argon atmosphere using an arc-furnace. The resulting button was annealed at 800°C for 24 hours and then quenched into water at room temperature. A small section was spark-machined off and its AC susceptibility checked for a ferromagnetic transition around 130°K. The remainder was used for specific heat data and the results are shown in table 6.2.

The measured electronic specific heat for Co_2TiAl is of the same order numerically as the Y_9Co_7, Y_8Co_5 and Y_3Co_2 phases. We might well consider this as evidence for the structure dependence of the observed ferromagnetism. Although the argument would be tentative, since a sharpening of the 3d bands due to expansion of the cobalt lattice is also a plausible argument, i.e.

the electronic specific heat of pure cobalt is 4.73 mJ mol^{-1} deg^{-2} [6.21] and any increase in the height of the 3d band would increase the density of states at the Fermi level and hence γ .

6.6 Magnetism in PdCo dilute solid solutions

Palladium has a paramagnetic susceptibility that is strongly exchange enhanced with a Stoner factor s$\sim$10. This is believed to be due to a high density of d states at the Fermi level and an attractive exchange interaction between d electrons with parallel spins. The electron phonon enhancement factor is 0.41[6.22] and is sufficiently strong for Pd to have a superconducting transition temperature of 0.2K, where Cooper pairing is not inhibited by the exchange interaction between the parallel spins. In a 'nearly' ferromagnetic material such as Pd, long-lived spin fluctuations are predicted[6.23] with a characteristic temperature of 320K. Chen et al[6.24] claim the first experimental observation of these spin fluctuations as a paramagnon contribution to the specific heat which they have measured using a unique differential calorimetric technique[6.25].

With the addition of elements from the first transition group in dilute form Pd exhibits marked and varied characteristics. With the addition of Cr, Kondo-like behaviour is observed, and although Co, Fe and Ni maintain their magnetic properties when dissolved in Pd they exhibit what have been termed 'giant moments'. A comprehensive discussion of the dilute solid solutions of Pd and these transition metals is given by Nieuwenhuys[6.26].

Giant moments have also been observed in alloys such as PtCo. In the PdCo case the Co atoms exhibit magnetic moments of 10-12 μ_B, while in PtCo they are 3-4 μ_B. The Stoner enhancement factor of Pt is 1.8, considerably less than Pd, and this is thought to reflect the magnitude of the giant moments,

since those are believed to arise from polarisation of the local host atoms by the solute.

Rastogi and Coles[6.27] have suggested that YCo_2 is a Laves phase analogue of Palladium, strongly Stoner enhanced and not ferromagnetic. They further speculate that if the Y prisms in Y_9Co_7 were to behave similarly, then the presence of defects such as cobalt occupation of Y sites may have similar effects as cluster formation in PdCo solid solutions. Further, in all their samples they observe magnetic remanence at 4.2K, which persists to higher temperatures. The poorer the sample, the higher the temperature to which this magnetic remanence is observed. This implies the presence of magnetic behaviour above what has been proposed as a magnetic ordering temperature. A similar behaviour has been reported[6.26] in PdCo dilute solid solutions and has been attributed to cluster formation between solute atoms.

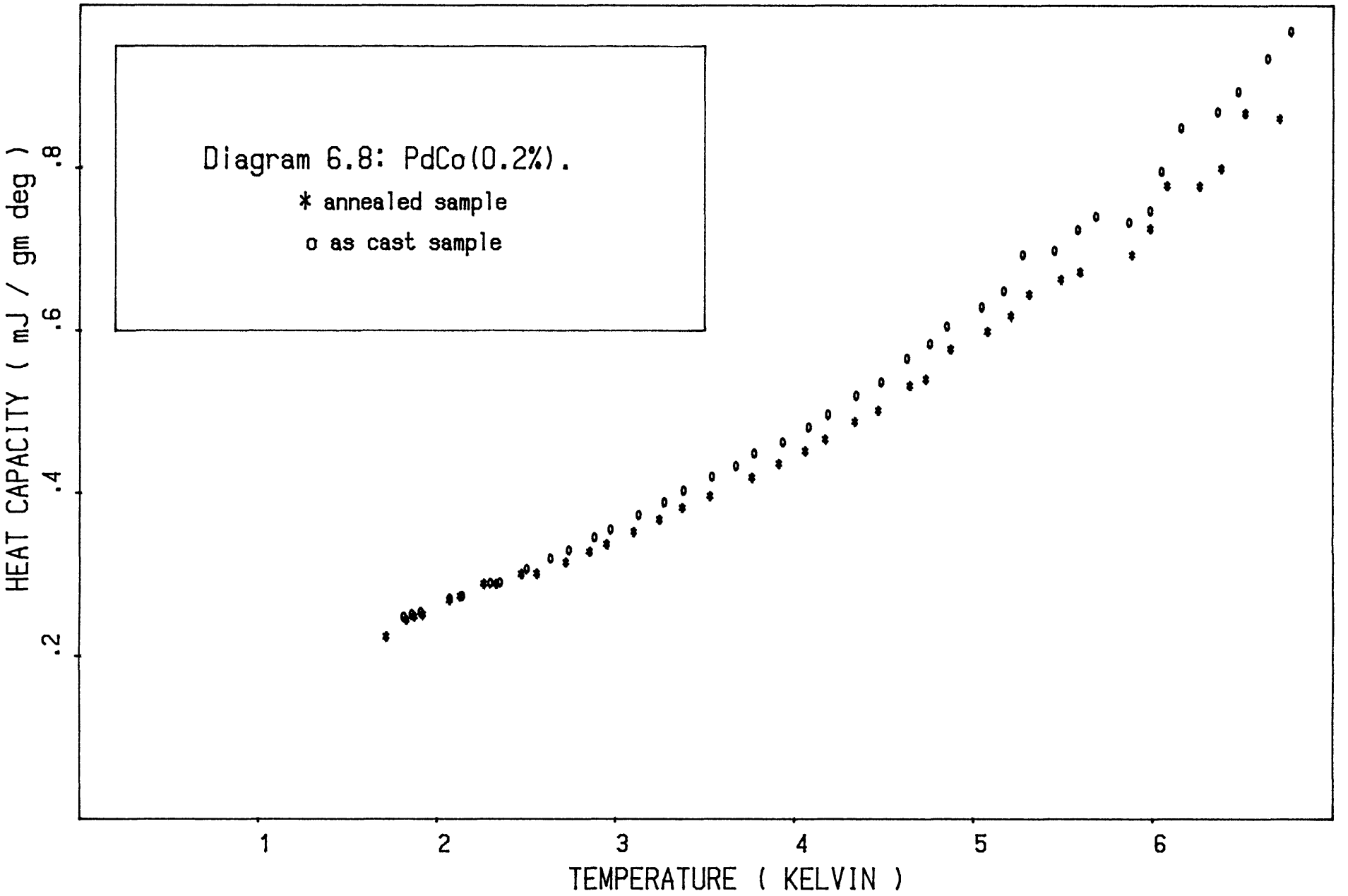
Such formation of clusters in materials such as PtCo and PdCo has been discussed by Ododo[6.28]. The treatment of magnetic impurities in non-magnetic or transition metal hosts is mainly within the framework of the Friedel-Anderson-Wolf[6.29] model or the spin fluctuation model[6.30]. However, recent opinion[6.31] has been that the predictions of both these models deviate strongly from empirical observations. It is thought that the process in which ferromagnetism occurs in materials such as PdCo is that for very dilute concentrations the solute atoms exhibit spin fluctuations, the statistical variation of concentration allows interaction between some solute atoms, which then stabilise their spins and begin to form clusters.

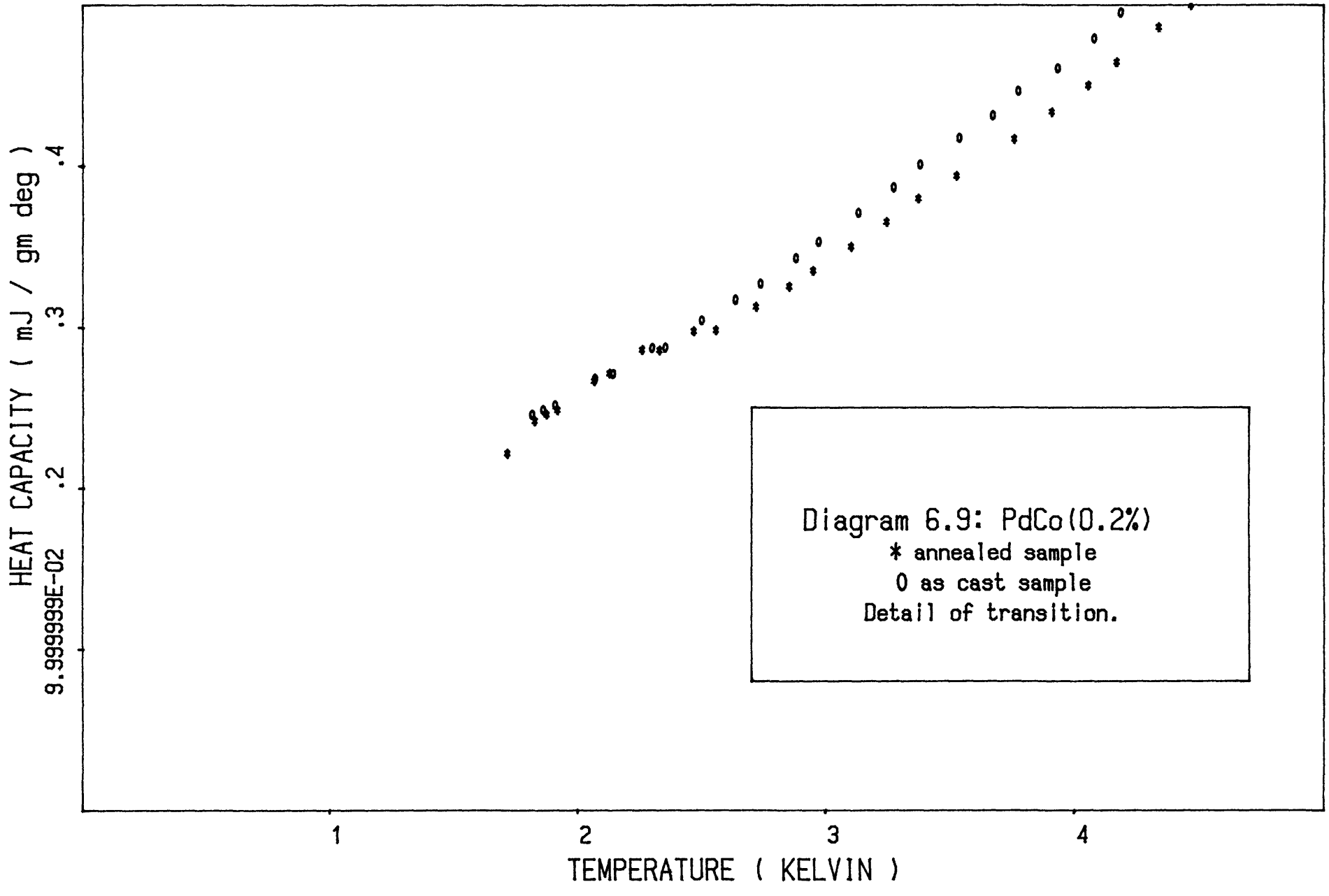
With increasing concentration the clusters become larger and begin to interact with each other, forming what has come

to be known as a 'cluster glass', until, close to a critical concentration, an infinite cluster is formed and ferromagnetic behaviour observed.

A model such as this predicts that the formation of clusters in the dilute limit is due to the statistical variation of the localised concentration. In completely ordered systems we would expect a transition to the ferromagnetic state at a temperature T_F, if the concentration is appropriate. If in the same system disorder were present, we would predict the formation of clusters due to localised variation of concentration at temperatures much higher than T_F. This would be observed both as magnetic remanence (if some spin freezing were present), above the transition temperature and an additional contribution to the specific heat.

A sample of Pd 0.2 at% Co was prepared in an argon atmosphere, by arc-melting together appropriate amounts of high purity Pd and Co. The resulting sample was spark-cut into two sections, one of which was enclosed in an evacuated quartz capsule and heat treated at 800°C for two weeks. The as cast sample constituted an inhomogeneous version of the alloy, while the annealed section was thought to be representative of a randomly ordered sample. The specific heat was measured and is presented in diagrams 6.8 and 6.9. The transition temperature was seen to be 2.2K, as expected from previous work[6.32], and a considerable excess specific heat is observable for the disordered alloy above the transition temperature for the entire temperature range of our experiment. Due to the limitation of this temperature range we are unable to carry out any quantitative analysis. We can only conclude that our experimental observations are in reasonable agreement with what we might expect from the above discussion.


Diagram 6.8: PdCo(0.2%).
* annealed sample
o as cast sample
HEAT CAPACITY (mJ / gm deg)
.2
.4
.6
.8
1
2
3
4
5
6
TEMPERATURE (KELVIN)


HEAT CAPACITY (mJ / gm deg)
9.999999E-02
.2
.3
.4
1
2
3
4
TEMPERATURE (KELVIN)
Diagram 6.9: PdCo(0.2%)
* annealed sample
0 as cast sample
Detail of transition.

6.7 Heat Capacity of Y_9Co_7

The physical properties of Y_9Co_7 as outlined in the Introduction lead to several controversial questions. Do magnetism and superconductivity co-exist? What is the nature of the superconductivity? What would be the properties of the ideal single crystal?

Rastogi and Coles[6.27] have shown that the physical properties are affected by the metallurgical character of the sample which is unlikely to be composition dependent since the Y_9Co_7 phase only exists over a comparatively short range (43.9 ± 0.2 at% Co). They observed with increasing quality of sample (purer yttrium, longer annealing times, etc.) a higher resistance ratio and a non-ferromagnetic nature to the Arrot plots. Although magnetic hysteresis was observed in all samples at 4.2, it was larger and persisted to higher temperatures in the poorer samples.

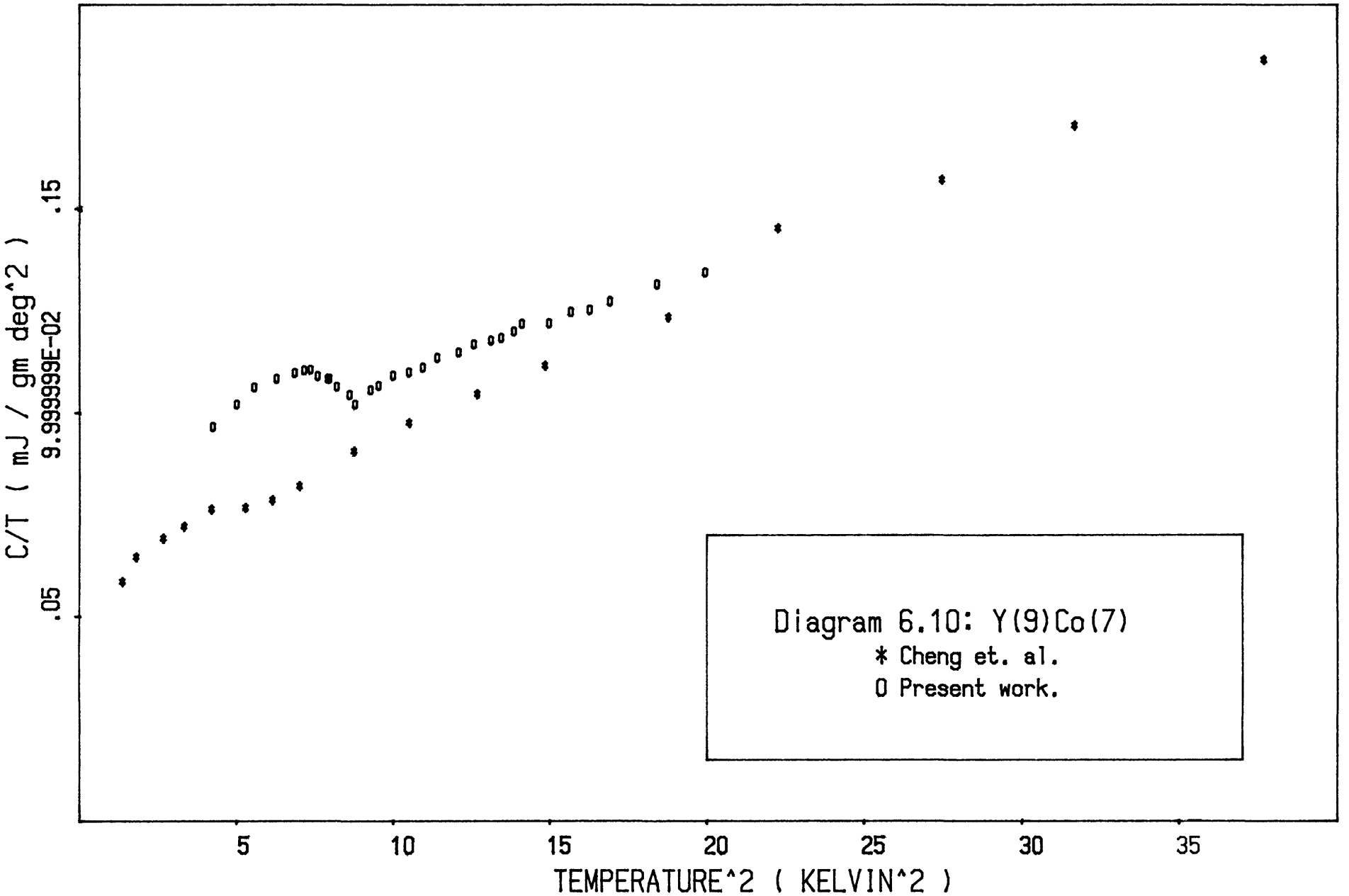
Cheng et al[6.33] have measured the specific heat of a sample of Y_9Co_7. They observed a broad superconducting transition at 2.5K and estimated that at least 20% of their sample was superconducting. Centered at 4K their data showed a specific heat bump which they attributed to weak magnetic ordering which they observed to begin on cooling at ~ 8K. The resistance ratio of their sample was 12, which places it around sample C of the Rastogi and Coles analysis. This sample C exhibited superconductivity at 2.5K, which agrees well with that seen in the Cheng et al sample, and a magnetic remanence of 10.2 x 10^{-2} e.m.u. g^{-1} at 4.2K, which persisted up to 18K. The difference in magnetic behaviour betwen the Cheng sample and the Rastogi and Coles sample C, implies that in the Cheng sample magnetic remanence may well persist above 8K; this would have an effect on their γ and Θ_D values, since they would no longer

be justified in the lattice contribution they proposed. Further, their entropy calculation, based on the magnetic contribution to the specific heat, would similarly suffer. Sample E of the Rastogi and Coles work has a resistance ratio of 23.5 and the observed remanence at 4.2 is 1×10^{-2} e.m.u. g^{-1} which persists to 7K, and no observable peak exists in the χ_{AC}. It is also superconducting at 2.65K. Specific heat observation on this sample should reflect the differences between it and sample C when compared to the Cheng et al data.

We have measured the sample E referred to in the Rastogi and Coles work, and in Figure 6.10 we show the results as compared to the Cheng et al data. The superconducting transition is considerably enhanced and no observable structure or bump exists at 4K to suggest any form of weak collective ferromagnetic behaviour. We know, however, that there is present from 4 to 7K a small magnetic remanence and consequently a contribution, C_M, to the specific heat; we suggest that it is small compared to that of the Cheng et al data and conclude from our results that the electronic specific heat coefficient $\gamma = 5.6$ mJ mol^{-1} k^{-2}. This is small when compared to the values of paramagnetic YCo_2 and superconducting Zr_2Co, which implies that any treatment of the Y prisms in Y_9Co_7 as enhanced paramagnetic units similar to YCo_2 and hence to Pd must suffer consequently.

We have further calculated from the BCS expression for the specific heat jump at T_c and γ, that 30% of the electrons that contribute to γ are participating in superconductivity, as compared to 20% in the Cheng et al sample.

Further analysis of the electronic states etc., would seem fruitless on the grounds of the 'a priori' knowledge of a magnetic contribution to our specific heat. In addition, the properties of Y_9Co_7 seem unlikely to be related purely to any


C/T (mJ / gm deg^2)
.15
9.999999E-02
.05
5
10
15
20
25
30
35
TEMPERATURE^2 (KELVIN^2)
Diagram 6.10: Y(9)Co(7)
* Cheng et. al.
0 Present work.

peculiarities in the density of states at the Fermi level, which may be reflected in γ.

We conclude, as other workers have done, that the strange structure of the Y_9Co_7 phase may well be responsible for the strange behaviour it exhibits. Yvon et al[6.34] detail this structure, which consists of Y prism enclosing cobalt atoms and forming channels, along which other cobalt atoms form chains. It is the latter Y channels and chains that are unique to the Y_9Co_7 structure. The cobalt separation inside the Y prisms is 2.35 Å[6.4], which, in our simple model, implies that these cobalt atoms do not have a tendency to collective magnetic behaviour. This is confirmed by the fact that the Co-Co distance in the non-magnetic Y_3Co_2 metastable phase is 2.37 Å[6.35] in a similar Y enclosing prism.

The cobalt separation in the chains is, however, undetermined but on average there are four cobalt atoms for each three sections of the hexagonal structure, each of which is 4.04 Å, implying an average Co-Co separation of 3.0 Å, a possible candidate for the magnetic behaviour. If this were the case the single crystal would display strong anisotropy.

We further propose that the Y atoms that form the channels into which the Co chains lie are the cause of the observed superconductivity of this system. Detailed analysis of the structure as depicted by Yvon et al implies that along the channel the Y-Y distance is 3.556 Å. Pure yttrium has a Y-Y separation of 3.638 Å, and, using Gschneidner's expression for the compressibility of Y as

$$\Delta V/V = - 26.79 \times 10^{-7} P + 4.484 \times 10^{-12} P^2 \qquad \text{Eq. 6.8}$$

where P is the pressure and once again assuming a wider

applicability (note: expression only quoted to 40 Kbar) we obtain a value for the pressure required to compress the Y atoms from 3.638 Å to 3.556 Å as 192 Kbar. Witting[6.36] has shown that at ~ 192 Kbar Y is superconducting at 2.88 K, which agrees well with the high quality sample E transition of 2.8K, as observed by Rastogi and Coles.

If this is the true cause of the superconductivity and the chains of cobalt atoms are responsible for the magnetic behaviour, we have an intriguing competition between magnetism and superconductivity, both arising from the same structure and hence interdependent.

The need for clarification of the origins of the magnetic behaviour is obviously important. It could seem, since the magnetic response decreases with increasing order, that the cobalt chains are,in fact , in the pure crystal at such a separation that they do not collectively interact magnetically and one would expect that the presence of cobalt occupation of Y sites destroys this delicate balance and hence is the cause of magnetism, as observed. The single crystal then would be superconducting at 3.0 K with only a fraction of the electrons co-operating in the condensation.

6.8 Conclusion

We have presented results on the yttrium-rich phases of the yttrium-cobalt phase diagram. No consistent behaviour due to systematic variation in the electronic density of states at the Fermi level was immediately obvious, and we have formulated, albeit a rudimentary but functional model. By empirical observations we have, with addition of qualitative arguments, explained the superconductivity of the $CeCo_2$ Laves phase and the Zr_2Co phase (which has a considerably higher transition

temperature than pure Zr). We have further extended the model to suggest the possible origin of the superconductivity is the Y_9Co_7 phase. In addition we have also been able to speculate as to the nature of the magnetic behaviour also observed in this compound.

In our model we have assumed in the qualitative arguments to support the empirical observations that the cobalt atoms with a separation less than a certain critical distance do not tend to magnetism, that is that variations in the parameter I, encountered in the Stoner criterion, are less important than band width effects. If this were not the case our simple picture as to the physical processes occurring as we compress the bands of the solid may require modification; however, this picture is an over-simplification in the case of chemical pressure anyway, but both these observations have no bearing on the empirical basis of our model.

We have further found it necessary to include the effects of electron transfer from one of the constituent elements to the other, a process known to occur, and hence a reasonable inclusion into the theory. This is an additional factor, controlling the loss of magnetism, and will also, of course, affect the superconducting behaviour.

It is well known that the d-d interaction in solids is not purely due to d wavefunction overlap; we have in fact discussed specific examples in which the separation of the d solute is large compared to the spatial extent of the d wavefunction. We would therefore note that our statement about the separation of cobalt atoms exceeding a critical value would cause a loss of magnetic tendency is too much an over-simplification. However, we have only applied it in one particular case, Zr_2Co, and also

noted that the respective electronegativity may well lead to sufficient electron transfer from Zr to Co to aid the loss of magnetism. However, we may still have a small tendency for the Co atoms to be magnetic and hence may have suppression of the superconductivity. This possibility is furthered by the observation of the transition temperature of the isomorphic compound Zr_2Rh, its T_c being $\sim 10K$[6.12]. The greater atomic volume of Rh may also be important in this higher T_c; however, the lattice parameter is slightly larger, i.e. 6.494 Å, as compared to 6.366 Å in Zr_2Co.

Another approximation we have made is the wider applicability of the compression data published by Gschneidner[6.9]. The majority of the data found in the tables of this reference are due to Bridgman, after being corrected for an erroneous value for Fe, relative to which the remaining data was calculated. Bridgman further presented his results as empirical fits to an $aP + bP^2 + cP^3$ type function, finding in general that the P^3 term was vanishingly small. The limitation on the range of his data is completely due to the range of his measured results, i.e. the pressures available to him at that time. Our assumptions that the expressions presented may be used to higher pressures is therefore not too much of an over-simplification.

We are currently waiting for the independent results on a $CeCo_2$ sample. It should be noted that, if due to defect occupation of Co sites by Ce atoms within the structure, the Ce rich resulting areas have Co-Co separations that are slightly larger than in the remainder of the sample, we may well, in our model, expect some form of magnetic behaviour. This would not be due to the presence of the $Ce_{24}Co_{11}$ phase, since this is not a cubic Laves phase and therefore not

contrary to our measurements.

Finally, we conclude that the superconducting and magnetic behaviour of Y_9Co_7 is due to the channels and the Co atom chains enclosed within, that are peculiar to this phase in the yttrium-cobalt phase diagram. The small separation of Y atoms in the channels themselves assists superconductivity and the weak ferromagnetism arises from the chains of Co atoms enclosed in them. As to the co-existence of the two, it would seem reasonable that the positions of the cobalt atoms in the chains are not unique and may have different separations throughout the structure. This would imply regions of magnetic and superconducting nature existing throughout the sample depending on the fortuitous position of cobalt atoms in the chains. Also, if the case were such that the chains were so occupied as to form a linear cluster, the appearance of a superconducting energy gap on a different sheet of the Fermi surface would not necessarily be prohibited, especially if the magnetic clusters wereboth weak and spatially small.

CHAPTER 7

INTERMEDIATE VALENCE MATERIALS

7.1 Introduction

This chapter is the second of two results chapters. In chapter 6 we have presented and discussed results on intermediate cobalt compounds, with particular emphasis on Y_9Co_7. In this chapter we present results on compounds believed to be intermediate valence (I.V.) materials.

Intermediate valence systems are generally encountered in compounds where the rare earth constituent is either Ce, Eu, Sm, Yb or Tm. Three of these in the pure metallic state are of anomalous valency with respect to the lanthanide series, namely Ce, Eu and Yb. The latter two are divalent in the metallic state and hence have a larger volume, consequently being offset in a volume vs. atomic number plot (as considered by Mattens[7.1]). Cerium exhibits two phases at room temperature, to a first approximation, at atmospheric pressure it is in a trivalent phase which is consistent with the volume vs. atomic number plot mentioned, but under pressure goes into a tetravalent state of reduced volume.

The valence volume correlation can easily be visualised as the promotion of an f electron to the conduction band, and a consequential increase in valence. This reduces the nucleus screening charge, causing a volume contraction.

With particular emphasis on Yb as a constituent of a metallic compound, both divalent ($YbAg$[7.2,7.3]) and trivalent (Yb_3Pd[7.4]) compounds are found. In addition, materials such as $YbAl_2$ and $YbAl_3$ are found to have what is termed as intermediate valence, that is for experiments such as the Mössbauer isomer shift, where the experimental time resolution is greater

than an interconfiguration fluctuation time constant $\tau_{v.f}$, a fractional valence is observed (2.45 for $YbAl_2$[7.5] and 2.7 for $YbAl_3$[7.6]. Experiments such as X-ray photoemission spectroscopy (X.P.S.), however, show both valencies (for example, Buschow on $YbAl_3$[7.7]) and their relative intensities can be interpreted as the probability of the occurrence of that valence in the ground state. These materials are what are referred to as rare earth intermediate valence compounds.

The unusual experimental behaviour of I.V. materials is often interpreted through the close proximity of a 4f level to the fermi energy which results in hybridization of the level with the conduction band. However, recent work[7.8,7.9, 7.10] has led to speculation that the feature at the fermi level responsible for such phenomena as very large electronic heat capacities is not the 4f level, but a many-body resonance, such as incorporated in the "Concentrated Kondo System" (C.K.S.) models. Brandt and Moshchalkov[7.11] suggest that I.V. materials are in fact concentrated Kondo systems with high Kondo temperatures. Both formulations are similar and are discussed in section 7.2. Section 7.3 presents results on $Yb_xLu_{(1-x)}Al_3$ and discusses the immediate features, while section 7.4 concludes with some final comments.

7.2 Valence Fluctuations

Intermediate valence materials (I.V. materials) are a class of rare earths in which the net valence is apparently non-integral. The condition for this to arise is that two bonding states, $4f^x(5d6s)^y$ and $4f^{x-1}(5d6s)^{y+1}$ are energetically almost degenerate and the number of 4f electrons can be considered to be fluctuating about a fractional mean value. The fluctuation

time scale between the two configurations is characterized by a quantity $\tau_{v.f}$, known as the valence fluctuation time (V.F.T.) or the interconfiguration fluctuation time (I.C.F.T.).

In a model with band structure considerations, hybridization between the two configurations involves the conduction band electrons. The process of particle conservation pins the f level to the bottom of the conduction band and, due to hybridization, it takes on a line width Δ , which can be related to the inter-configuration fluctuation time by $\Delta \sim 1/\tau$

Newns and Hewson[7.12] treated the I.V. problem with what they have termed as a "local fermi liquid theory", in which they have approximated the f atom as a classical non-interacting Friedel-Anderson impurity with an 1 = 3 phase shift. We follow their derivation of some useful quantities.

Assuming a lorentzian form to the resonance, we have for the phase shift ξ :

$$\xi(\varepsilon) = \tan^{-1} (\Delta/(\varepsilon_f - \varepsilon) \qquad \text{Eq. 7.1}$$

where ε_f is the effective position of the f level and Δ the width. If n_f is the mean number of electrons on the rare earth ion, then the Friedel sum rule gives

$$n_f = (2J + 1)\xi(\varepsilon_f)/\pi \qquad \text{Eq. 7.2}$$

Introducing a quantity v_f, such that in the case of electrons $n_f = v_f$, while for holes $\xi = \pi - \xi$ and $v_f = (2J+1) - n_f$, we have

$$v_f(t) = (-(2J+1)/\pi)\int_{-\infty}^{\infty}\xi(\varepsilon)\ (\varepsilon - \mu\ )f'(\varepsilon)\ d\varepsilon \qquad \text{Eq. 7.3}$$

where $f(\varepsilon)$ is the Fermi-Dirac distribution and the prime denotes a derivative with respect to energy.

We may further write an expression for the entropy, S,

$$S = (-(2J+1)/\pi T)\int_{-\infty}^{\infty} \xi(\varepsilon)(\varepsilon - \mu)f'(\varepsilon)\, d\varepsilon \qquad \text{Eq. 7.4}$$

where the quantity μ is the chemical potential. We can also write an expression for the impurity induced density of states per channel $\rho_f(\varepsilon)$:

$$\rho_f(\varepsilon) = \pi^{-1}\delta\xi/\delta t = \pi^{-1}\Delta/[(\varepsilon - \varepsilon_f)^2 + \Delta^2] \qquad \text{Eq. 7.5}$$

Approximating $v_f(T)$ as a constant (valid for $kT << \Delta$), we can, from equation 7.4, obtain the electronic specific heat,

$$C_v = \gamma T[1 + (\pi^2 k_B^2 T^2/3)\{(7/5)(\rho_f''/\rho_f) - (\rho_f'/\rho_f)^2\}]_{E=E_f} \qquad \text{Eq. 7.6a}$$

$$= \gamma T[1 + (2\pi k_B^2 T^2/15\Delta^2)(11\cos^2\xi - 7\sin^2\xi)\sin^2\xi] \qquad \text{Eq. 7.6b}$$

where

$$\gamma = (2J + 1)\pi k_B^2 \rho(\varepsilon_f)/3$$

A magnetic field splits the degeneracy of the f level into sub-levles $\varepsilon_f^m = \varepsilon_f + g\mu_B H_m$. If H is small we have a change $\delta v_f^{(m)}$ in $v_f^{(m)}$,

$$\delta v_f^m(T) = -\mu_B H_m \int_{-\infty}^{\infty} \rho_f(\varepsilon)\, f'(\varepsilon)\, d\varepsilon \qquad \text{Eq. 7.7}$$

enabling us to write:

$$\chi(T) = (g^2\mu_B^2 J(J+1)(2J+1)/3)\int_{-\infty}^{\infty} \rho_f(\varepsilon) f'(\varepsilon) d\varepsilon \qquad \text{Eq. 7.8}$$

again assuming $v_f(T)$ constant with respect to T,

$$\chi(T) = \chi(0)[1 + (\pi^2 k_B^2 T^2/6)\{(\rho_f''/\rho_f) - (\rho_f'/\rho_f)^2\}]$$

Eq. 7.9a

$$\chi(T) = \chi(0)[1 + (\pi^2 k_B^2 T^2/3\Delta^2)\cos 2\xi \sin^2\xi\ ]$$

Eq. 7.9b

We can combine, to first order, equations 7.6 and 7.9 to give us the following expression:

$$R = (\pi^2 k_B^2 \chi(0))/(g\mu_B^2\, J(J+1)\gamma) \qquad \text{Eq. 7.10}$$

In the Newns and Hewson model R~ 1.

Further, we can obtain Δ and $(\varepsilon_f - \varepsilon_F)$ from equations 7.5 and 7.1, i.e.

$$\Delta = \pi^2 k_B^2 (2J+1) \sin^2 (\pi\, v_f(0)/2J+1)\ /3\pi\gamma$$

Eq. 7.11

and hence

$$|(\varepsilon_f - \varepsilon_F)| = \Delta \cot [\pi v_f(0) (2J + 1)] \qquad \text{Eq. 7.12}$$

Newns and Hewson have taken previous data and applied their theory. For $YbAl_3$ they obtain R = 1.07, Δ = 17.7 meV and for $\varepsilon_f - \varepsilon_F$ = -42.7 meV. To obtain these values they have assumed $v_f(0)$ is constant and used γ = 45 mJ mol^{-1} K^{-1} (7.13).

The fermi liquid approach has met with considerable success in Mattens'(7.1= analysis of YbCuAl, where the observed specific heat and susceptibility were found to be in close agreement with that calculated by Newns and Hewson.

The formulation for concentrated Kondo systems arises from the framework of the Kondo model for antiferromagnetic exchange interaction J>0 of the s=½ magnetic impurity with conduction band electrons. The resulting hamiltonian can be deduced from the Anderson hamiltonian in the case of small hybridization. Expressions for C(t) and χ(t) have been calculated numerically and give Kondo compensation of the effective magnetic moment for s=½. The low temperature heat capacity C_v and magnetic susceptibility $\chi(0)$ can be expressed as

$$C_v(T \to 0)/T = \pi k_B/(6T_0) \qquad \text{Eq. 7.13}$$

$$\chi(0) = \mu_B^2 g^2 / (4\pi k_B T_0) \qquad \text{Eq. 7.14}$$

where g is the spectroscopic Lande factor

$$g = (1 + (J(J+1)+S(S+1)-L(l+1))/(2J(J+1))) \qquad \text{Eq. 7.15}$$

and T_o is related to the Kondo temperature through the Wilson

number,

$$T_k/T_0 = W = 0.1026.4\pi = 1.2909 \qquad \text{Eq. 7.16}$$

However, for the generalized case ($s>\frac{1}{2}$) the model does not give complete Kondo compensation of the localised magnetic moment. The Coqblin-Schrieffer model includes the process of conduction electrons hopping between angular momentum eigenstates by considering all spin projections and treating the conduction band as a sum of partial waves with non zero orbital momentum. The resulting expressions for the low temperature $C_v(T)$ and $\chi(0)$ are

$$\chi(0) = (\nu(\nu^2-1)\mu_B^2 g^2)/(24\pi k_B T_0) \qquad \text{Eq. 7.17}$$

and

$$C_v(T \to 0)/T = \gamma = ((\nu - 1)\pi k_B)/(6T_0) \qquad \text{Eq. 7.18}$$

where $\nu = (2J+1)$

which gives a χ/γ ratio:

$$\chi(0)/\gamma = (\nu(\nu+1)\mu_B^2 g^2)/(4\pi^2 k_B^2) = ((J+\tfrac{1}{2})(J+1)\mu_B^2 g^2)/(\pi^2 k_B^2)$$

which differs from the Newns and Hewson model only in that $(J + \frac{1}{2})$ replaces J.

In concentrated Kondo systems at low temperature in the non magnetic region, the electron clouds around the magnetic impurity are believed to give rise to a "mass" increase of the

electrons at the fermi level through the appearance of a many body resonance, referred to by Grüner and Zawadouski[7.14] as the Abrikosov-Suhl resonance (A.S.R.). The Gruner and Zawadouski phenomonological model can be shown to be in good agreement with the Coqblin-Schrieffer formulation[7.11]. The width of the ASR is believed to be ~ kT_k and its amplitude $(\pi\Delta)^{-1}$ per impurity.

The CKS approach has proven successful in application to heavy fermions such as $CeCu_2Si_2$ and $CeAl_3$. The T_k for these materials is believed to be low, $\sim$ 10K, and the exotic properties can be explained through the appearance of the ASR at the fermi level.

Brandt and Moshchalkov have speculated the possibility that I.V. materials are really high T_k CKS's and have in their paper attempted to show the equivalence of the fermi liquid approach to the CKS formulation. They suggest that the position of the ASR may well be dictated by the total magnetic moment j. If $j=\frac{1}{2}$, then E_R, the position of the ASR is E_F, the fermi energy. If $j>\frac{1}{2}$, then for Ce and Eu based materials $E_R > E_F$, while for Yb and Sm based $E_R < E_F$. This would mean that the lorentzian close to the fermi level is not the 4f level but the ASR.

7.3 Results and Discussion

The intermediate valence compound $YbAl_3$ has been discussed by Havinga et al[7.13]. Recent work by Murani[7.15] suggests an anomaly in the energy bands that can be interpreted as a hybridization gap near the fermi level. The structure of this compound is the cubic Cu_3Au type, which would suggest by comparison of lattice constants with the isomorphic compounds

$ErAl_3$ and $LuAl_3$ that Yb is trivalent in this compound. (At room temperature $ErAl_3$ has a lattice parameter a = 4.215 Å, $YbAl_3$ has a = 4.202 Å and $LuAl_3$ 4.191 Å). This valency would seem in contradiction to the observation that at 0.95K $YbAl_3$ becomes superconducting, since superconductivity is normally destroyed by local moments.

We present results in this section on the heat capacity and susceptibility of $YbAl_3$. In addition, the pseudobinary compounds $Yb_{.8}Lu_{.2}Al_{.3}$ and $Yb_{.5}Lu_{.5}Al_3$ have also been measured, along with $LuAl_3$. All the samples measured and reported in this chapter were produced in Grenoble. Appropriate amounts of pure Yb, Al and, where necessary, Lu, were sealed in tantalum crucibles in an argon atmosphere. The crucibles were heated to 1550°C, and the contents shaken while molten. Finally, the crucible was quenched in water and the samples extracted. An X-ray examination confirmed that the samples had less than 5-10% second phase present in the $YbAl_2$ type.

In table 7.1 we present our results for all four samples. The specific heat was measured and a first order least squares polynomial fit produced to the data in a C/T (T^2) format. The susceptibility was measured using an extraction and integration type magnetometer and was found to exhibit impurity effects as observed by other workers[7.1,7.13]. We have extrapolated our results to produce a value for $\chi(0)$.

Applying the fermi-liquid approach, the average occupancy of the f level and its degeneracy control the phase shift through the Friedel sum rule. Substitution of Yb by Lu should, due to the isolated impurity-type approach of the theory, simply dilute the system. We would expect, therefore, a scaling of the physical parameters with concentration, and no real change in the general behaviour. The results of the specific heat measure-

Sample	γ mJ/(mol deg^2)	β^* J/(mol deg^{-1})	χ e.m.u.	R
$YbAl_3$	50.88	2.517×10^{-4}	5.51×10^{-3}	1.10
$Yb_{.8}Lu_{.2}Al_3$	26.37	-1.212×10^{-4}	2.81×10^{-3}	1.09
$Yb_{.5}Lu_{.5}Al_3$	15.47	-3.15×10^{-5}	2.16×10^{-3}	1.42
$LuAl_3$	7.31	2.12×10^{-4}	-	-

Table 7.1 Results for $Yb_xLu_{1-x}Al_3$

R = Newns and Hewson parameter

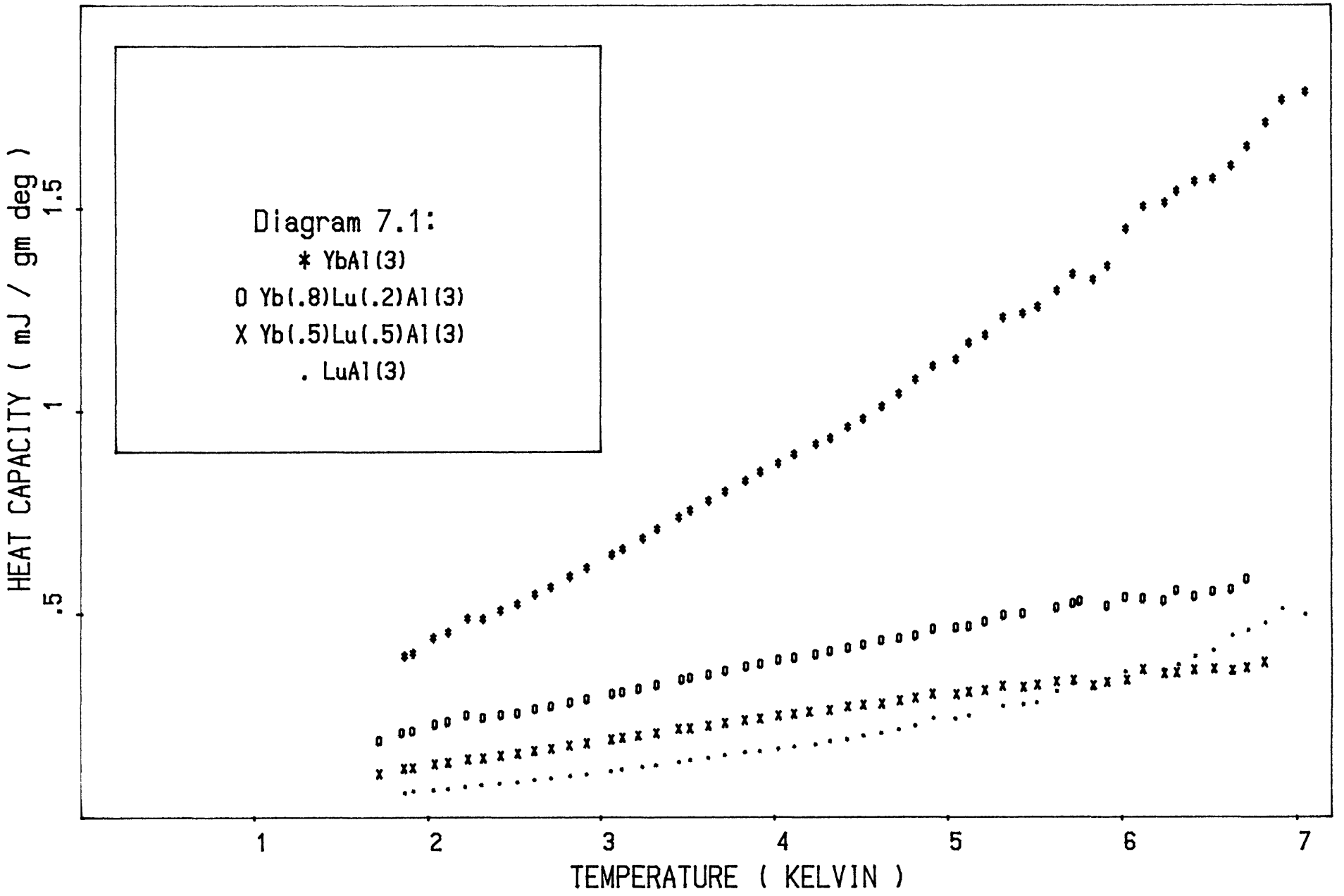
* assumes $C = \gamma T + \beta T^3$

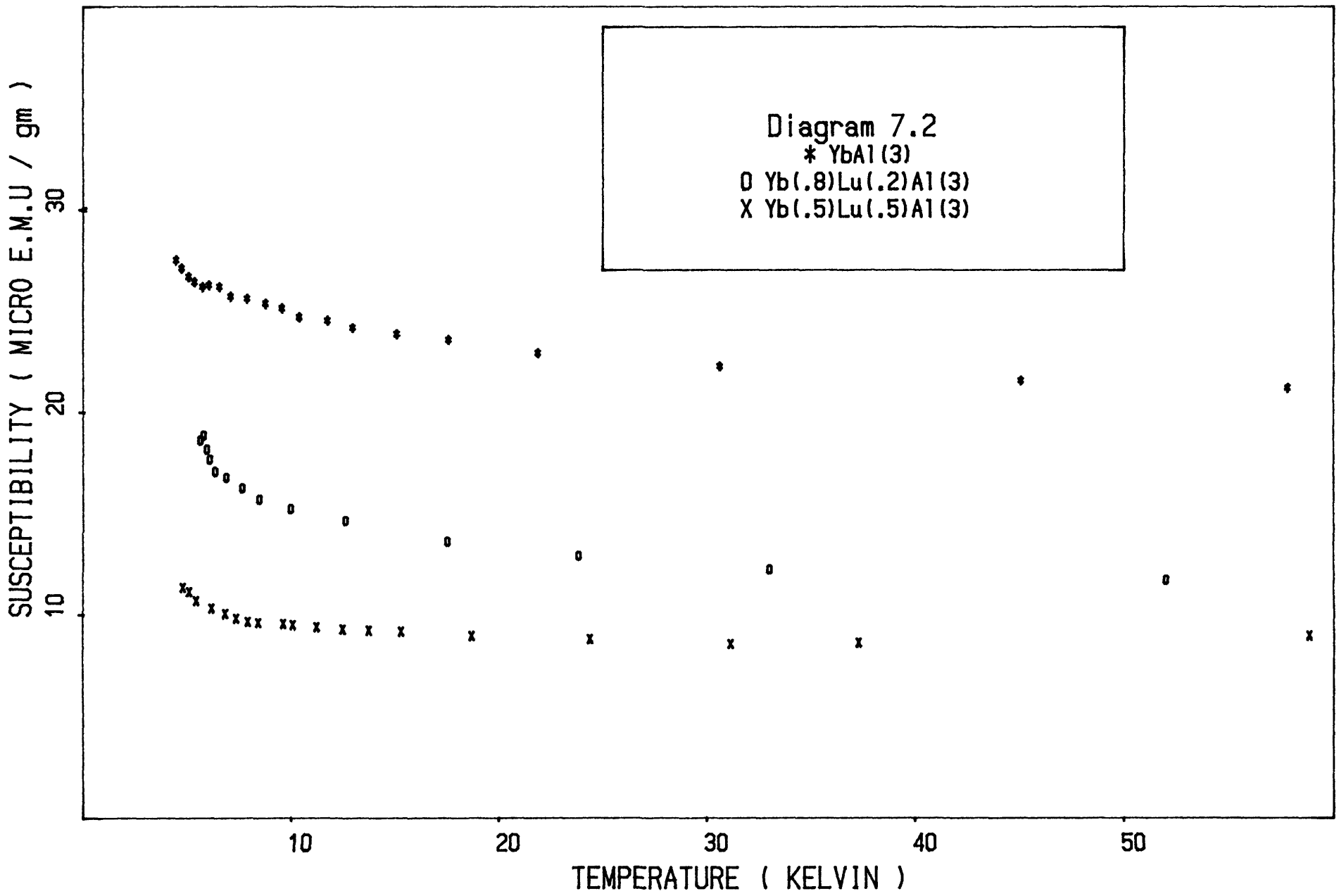
ments and the susceptibility as a function of temperature are shown in diagrams 7.1 and 7.2 respectively. The two intermediate pseudobinary compounds are known to exhibit no superconducting transition temperature[7.16], while $LuAl_3$ is superconducting at 1.05K.

We have also in table 7.1 calculated values for the Newns and Hewson parameter R for $YbAl_3$, $Yb_{.8}Lu_{.2}Al_3$ and $Yb_{.5}Lu_{.5}Al_3$. In all cases it was found to be close to unity. This forms a basis for the applicability of the fermi liquid theory.

Since the occupancy of the f level can have suffered no change on any remaining Yb atom by the introduction of Lu, we should simply observe a decrease of the γ and $\chi(0)$ values linearly with concentration. Diagrams 7.1 and 7.2 show this not to be the case. A considerably more important observation is the negative slope of $Yb_{.8}Lu_{.2}Al_3$ and $Yb_{.5}Lu_{.5}Al_3$. Although the theory allows negative T^3 terms to the electronic specific heat, it would not predict them for these compounds if they were not found in $YbAl_3$.

Taking the γ value of $YbAl_3$, we can calculate, using equations 7.11 and 7.12, that the width of the f level is 16.4 meV, and its position is -35meV, which is in reasonable agreement with the Newns and Hewson calculated values. Using equation 7.6b and knowing ξ from the Friedel sum rule, we obtain that the T^3 term due to the electronic specific heat is $6.47.10^{-7}$, which disagrees with the experimental value we have obtained of $3.924.10^{-5}$, in which we have subtracted a lattice term equal to that of $LuAl_3$. This implies that the shape of the density of states at the fermi surface and its evolution, with respect to temperature, is not as described by Newns and Hewson. Given we know experimentally the coefficient of the T^3 term, we can predict a value for the expression:


Diagram 7.1:
* YbAl(3)
O Yb(.8)Lu(.2)Al(3)
X Yb(.5)Lu(.5)Al(3)
. LuAl(3)
HEAT CAPACITY (mJ / gm deg)
.5
1
1.5
1
2
3
4
5
6
7
TEMPERATURE (KELVIN)


Diagram 7.2
* YbAl(3)
0 Yb(.8)Lu(.2)Al(3)
X Yb(.5)Lu(.5)Al(3)
SUSCEPTIBILITY (MICRO E.M.U / gm)
10
20
30
10
20
30
40
50
TEMPERATURE (KELVIN)

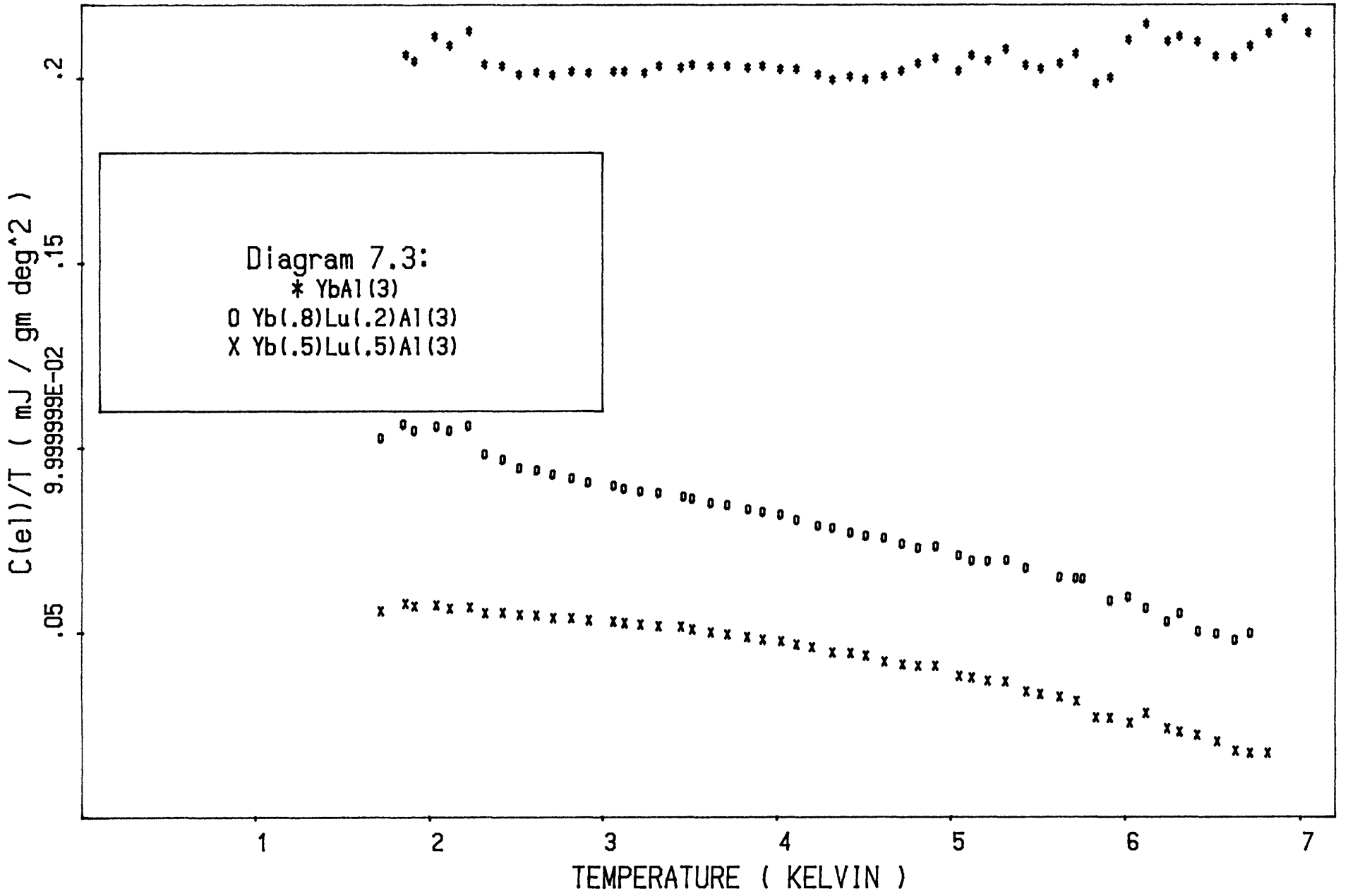
$$(7/5)[\ (\rho_f''/\rho_f)\ -\ (\rho_f'/\rho_f)^2\ ]$$

as equal to $1.23.10^{42}$, or, alternatively, we may use the information in equation 7.7b, i.e. $(11\cos^2\xi\ -\ 7\sin^2\xi\ )\ \sin^2\xi\ = 74.3$, which forms a quadratic in $\sin^2\xi$ whose roots are imaginary.

We therefore conclude that the fermi liquid theory does not predict the experimental behaviour as observed by us in the case of $YbAl_3$. We are unable to compare the T^3 variation of the electronic specific heat of $Yb_{.8}Lu_{.2}Al_3$ and $Yb_{.5}Lu_{.5}Al_3$ to theory, since both these exhibit negative slopes in the C/T (T^2) plots. As mentioned before, this behaviour is precluded on the grounds of there being no such trends in $YbAl_3$ within this theory[7.1].

In diagram 7.3 we show the observed variations of γ T vs. T. Although in the case of $YbAl_3$ the graph is, in fact, approximately constant, we have shown above that it is still in quantitative disagreement with the fermi liquid theory. The pseudobinary compounds show definite variation with temperature, decreasing with increasing temperature.

A qualitative argument that would explain our results would be the presence of a secondary peak which we calculate from our result to be at -5.1 meV with a width of 2.1 meV. Therefore, the $C(T \rightarrow 0)/T$ value would be dictated to by the broad feature at -35 meV, while the variation of the density of states with temperature would be mainly dependent on the secondary peak. Consequently, we would see a temperature variation of the T^3 term that would imply $\Delta \sim 2$ meV, while the value at T = 0 would imply a Δ of 16.4 meV.


Diagram 7.3:
* YbAl(3)
O Yb(.8)Lu(.2)Al(3)
X Yb(.5)Lu(.5)Al(3)
C(el)/T (mJ / gm deg^2)
.2
.15
9.999999E-02
.05
1
2
3
4
5
6
7
TEMPERATURE (KELVIN)

From our measured value for the electronic specific heat we have for $Yb_{.8}Lu_{.2}Al_{.3}$ that Δ = 31.6 meV and ($\varepsilon_f - \varepsilon_F$) = -76.2 meV, and for $Yb_{.5}Lu_{.5}Al_3$ Δ = 53.8 meV and ($\varepsilon_f - \varepsilon_F$) = -0.13 eV. These values completely oppose the possibility of a negative T^3 due to the electronic specific heat, since the condition for this would be that $|\varepsilon_f - \varepsilon_F| < \sqrt{7/11}\ \Delta$. The presence of a secondary feature would also explain these values. If the peak were somehow to remain at a constant position with respect to the fermi level, yet still undergo broadening due to dilution we may well expect the observed behaviour.

Our overall conclusion can only be that the fermi liquid model does not adequately describe the experimental behaviour as observed by us.

In the CKS approach to intermediate valence materials as outlined by Brandt and Moshchalkov, the position of the ASR is now dependent on the magnetic moment J. The amplitude and width of the resonance is related to T_k, the Kondo temperature. Since T_k in our system is large compared to the crystal field energy, we would in this approach expect the ASR to be positioned below E_F.

The effect of dilution is seen to increase T_k, since the electronic specific heat coefficient has decreased, but since the magnetic moment J is unaffected in our case, the resonance should not necessarily move down in energy with increasing Lu. This would also mean we would not expect simple dilution effects to the physical parameters as we decrease the Yb concentration.

The Kondo approach also reconciles the unfilled shell, i.e. the trivalent nature of Yb in $YbAl_3$ and the superconducting transition at 0.95K. The Kondo compensation of the local magnetic moment would imply that the unfilled shell need not

inhibit Cooper pairing. A similar argument has been used to discuss superconductivity in $CeCu_2Si_2$.

The general approach to concentrated Kondo systems does not include any effect due to the periodicity of the system. Although the 4f shells are spatially small, so any form of direct interaction is not possible, the clouds of electrons participating in the Kondo compensation process may well interact. It is this that is thought to be responsible for the formation of the ASR. Periodicity and its results in the non magnetic Kondo system have been discussed by Martin[7.17] and applied to experimental behaviour successfully by Bredl et al[7.18]. The presence of periodicity according to Martin causes the appearance of a dip in the ASR near the fermi level causing the resonance to have fine structure. This would explain the negative T^3 term in our electronic specific heat as the position of the fermi level close to a minimum in the ASR structure. Increasing temperature would then cause a decrease in the density of states and reproduce what we have observed.

7.4 Conclusion

We have measured the specific heat and susceptibility of $YbAl_3$ and studied the effect of dilution with Lu. The fermi liquid theory of Newns and Hewson is thought to be a good description of intermediate valence materials and we have attempted to apply it to our results. The theory develops a parameter R related to the susceptibility and electronic specific heat at zero temperature. By evaluating R for all our samples we have suggested that the criterion for applicability of the theory is fulfilled.

The properties of intermediate valence materials in this

theory are developed from the presence of the f level close to the fermi surface. The shape of the level is assumed lorentzian, and it is treated like the virtual bound state of a non-interacting Friedel-Anderson impurity. The resulting equations give analytical expressions for the electronic specific heat and its variation with temperature, as well as the susceptibility and its temperature dependence. We have used $LuAl_3$ as a dummy sample, since it has the same structure, to subtract the lattice contribution from our other data. The zero temperature electronic specific heat and its temperature dependence are inconsistent with the Newns and Hewson theory's predictions, requiring different widths and positions of the f shell in $YbAl_3$. A similar analysis of the susceptibility in the appropriate temperature range is impossible due to impurity effects. We conclude that $YbAl_3$ is not adequately described by the theory.

The pseudobinary alloys, $Yb_{.8}Lu_{.2}Al_3$ and $Yb_{.5}Lu_{.5}Al_3$ do not exhibit simple dilution with respect to $YbAl_3$, as would be expected from the fermi liquid model. In addition, they display negative T^3 terms in the electronic specific heat temperature dependence. Although possible within the theory, such negative coefficients are precluded in these samples due to the sum rule that forms the basis of the theory. We suggest this as further evidence for the failure of the theory to describe this system adequately.

An equivalent formulation, within certain limits, treats intermediate valence materials as concentrated Kondo systems, and the feature in the density of states at the fermi level is thought to be the Abrikosov-Suhl resonance. This is a many body resonance thought to arise not from the f levels, but from

the electron clouds around them which are participating in Kondo compensation of the local magnetic moment.

If we consider $YbAl_3$ as a concentrated Kondo system we instantly acquire an explanation to the seemingly inconsistent facts that the system has both unfilled f shells and is superconducting at 0.95K. We have suggested, due to the inequivalence of the zero and finite temperature behaviour of the system within the Newns and Hewson model, that we can explain the experimental results by introducing a secondary peak near the fermi level. This would be irreconcilable with the fermi liquid theory, but in the concentrated Kondo picture quite possible. Martin has shown that if the CKS is periodic a minimum appears in the ASR, resulting in a two peak structure at the fermi level. This would fit well our data on $YbAl_3$. One would expect features dependent on periodicity to be lost on random dilution; our results, however, suggest different. The specific heat measurements on the two pseudobinary alloys would seem to indicate that the twin peak structure is preserved on dilution, but the resonance broadens. Allowing the position of the fermi level to become such that the density of states would decrease with increasing temperature and result in a negative T^3 term in the electronic specific heat.

Finally, our model of a resonance at the fermi level in which there is structure would agree with the results obtained by Murani. The neutron scattering data reported by him can only be reconciled with the development of an energy gap in the energy surface of the material.

We could, therefore, conclude that the system we have investigated does not adhere quantitatively or qualitatively to the fermi liquid description of intermediate valence

materials. The theory ignores all crystal field effects and inter-f atom processes. The former, due to the high Kondo temperatures of these materials, would have negligible consequences; however, the latter we feel may well be the cause of the break down of the theory.

The concentrated Kondo approach would from a qualitative argument seem to explain the observed behaviour. Both the appearance of superconductivity in $YbAl_3$ and the negative slopes of the C/T (T^2) plots of the two pseudobinary compounds are accommodated by this theory. However, the loss of superconductivity by the introduction of Lu is not completely understandable. Considering both $YbAl_3$ and $LuAl_3$ are superconducting, it would seem reasonable to expect the pseudobinary alloys also to exhibit superconducting temperatures. Unless periodicity is a requirement for the superconductivity in $YbAl_3$, or loss of it makes the Kondo compensation locally less effective.

CONCLUSION

We have described the use of a Resistive SQUID, referred to as an RSQUID, as the basis of a sensitive calorimeter. In Chapter 6 we have used the RSQUID calorimeter to investigate some intermetallic cobalt compounds. The main reason for our work in this chapter is the properties of Y_9Co_7, believed to be a weak ferromagnet and a superconductor. We have initially followed the approach of Rastogi and Coles and conclude, as they did, that in a good quality sample (the higher the resistance ratio, the better the quality of the sample), the magnetic behaviour is decreased and the superconducting transition temperature increased. We have measured a good quality sample and found that the magnetic contribution to the specific heat is degraded, while the percentage of electrons participating in superconductivity is increased compared to that reported previously.

Buschow explains the observed magnetic moment and Curie temperature variation with composition of yttrium-nickel, yttrium-cobalt and yttrium-iron, using a simple rigid band model and the concept of electron transfer. In a similar fashion we have formulated a simple theory which fits our results quite successfully. Using simple arguments about 3d magnetism and superconductivity, we have explained the variation of the superconducting transition temperature of $CeCo_2$ with lattice parameter. Extending our ideas to zirconium-cobalt alloys, we have also been able to discuss within our model the observed superconducting transition temperatures of pure Zr, Zr_2Co and $ZrCo_2$. We have found that our model successfully explains our observation in these compounds. Finally, we have applied these ideas to the Y_9Co_7 phase and suggest that

the superconductivity is due to the yttrium channels within which lie the cobalt chains peculiar to this structure. In addition, we believe that the magnetic behaviour observed in this material is also due to the same structural feature. Depending on the separation of the cobalt atoms in the chains, which we believe is not unique throughout the phase, the cobalt atoms are able to form clusters and hence participate in magnetism. This would imply the presence of magnetic behaviour on a sheet of fermi surface and the appearance of a superconducting gap on another sheet, presenting a complex fermi surface.

In Chapter 7 we discuss intermediate valence materials, in particular $YbAl_3$ and its dilution with Lu. We have taken our results and attempted to apply the fermi liquid theory of Newns and Hewson. We found that we were unable to reconcile the zero temperature specific heat contribution with the finite temperature behaviour of the same. We have suggested a possible explanation for our results, based on the fermi liquid theory. That is, as postulated by the theory, there exists at the fermi level a lorentzian shaped feature which is believed to be the 4f level hybridized with the conduction band. We propose that in addition to this there may exist a narrower structure nearer the fermi surface, and the combination of the two would explain our results. We note that we could interpret our results within the framework of the concentrated Kondo approach. The narrower feature could be the many body Abrikosov-Suhl resonance, and the other the 4f level, as postulated by the fermi liquid theory. Alternatively, both peaks could be the ASR, which has developed due to the periodicity of the electron clouds participating in Kondo compensation, a dip in its structure near the fermi surface, as suggested by Martin.

The presence of Kondo compensation of the local moments in $YbAl_3$ would well aid the understanding of the observed superconductivity in this material. The loss of superconductivity by the addition of Lu would suggest a breakdown in this process; however, our results on the pseudobinary compounds would indicate the continued presence of the structure near the fermi level, as discussed before. This would seem to suggest that, not only the 4f level and the ASR are present, but in addition, in the case of $YbAl_3$, fine structure in the ASR is also seen. By the addition of Lu the periodicity is lost, causing the aforementioned structure to also be lost but the ASR to remain positioned such that with increasing temperature we have a decrease in the density of states. This type of argument would satisfy our observations in this system and is supported by the neutron scattering data of Murani, which can only be understood by the presence of a hybridization gap in the energy surface of $YbAl_3$, which is lost by the addition of Lu.

The temperature limitations of the RSQUID calorimeter leads us to suggest that the remeasurement of the specific heat of a good quality sample of Y_9Co_7 would enable the determining of the lattice contribution, and hence more precisely the electronic heat capacity. In addition, the total entropy due to the cobalt moments, if observable, could be determined. We have already suggested measuring the Y_3Co_2 sample to lower temperatures in order to search for a transition to the superconducting state, which, according to our data, should exist.

In the $YbAl_3$ based system, both the higher temperature and the lower temperature regions of the pseudobinary alloys would

seem worth further investigation. We would also suggest the measurement of $Yb_xLu_{1-x}Al_3$ for all values of x. However, we realize that the compositions are nominal due to the nature of the elements involved and all samples would have to be checked to determine true composition and fractional presence of $YbAl_2$ type second phase.

REFERENCES

(1.1) Park J.G. and Vaidya A.W.
J. Low Temp. Phys. 40 314 (1980)

(1.2) Vaidya A.W.
Thesis: University of London (1979)

(1.3) Pauthenet R., Lemaire R., Schweizer J.
Cobalt 39 97 (1968)

(1.4) Gratz E., Sechovsky V., Wohlfarth E.P.
J. Magn. magn. Mater. 21 191 (1980)

(1.5) Figiel , Gratz E. and Kapusta C.
J. Magn. magn. Mater. 23 123 (1981)

(1.6) Kolodziejczyk A. and Sarkissian B.V.B.
J. Phys. F: Met. Phys. 10 L333 (1980)

(1.7) Wohlfarth E.P.
Phys. Bulletin P235 33 (1982)

(1.8) Grover A.K., Coles B.R., Sarkissian B.V.B., Stone H.E.N.
J. Less Common Metals 86 29 (1982)

(1.9) Cheng W., Creuzet G., Garoche P., Campbell I.A. and Gratz E.
J. Phys. F: Met. Phys. 12 475 (1982)

(1.10) Huang C.V., Wolf S.A., Olsen C.E., Fuller W.W., Huang J.H. and Ting C.S.
Solid State Commun. 45 795 (1983)

(1.11) Sarkissian B.V.B.
J. Appl. Phys. 53 8070 (1982)

(1.12) Rastogi A.K., Coles B.R.
J. Phys. F: Met. Phys. 1165 (1985)

(1.13) Ishikawa M.
Contemp. Phys. 23 443 (1982)

(1.14) Ishikawa M., Fischer O.
Solid State Commun. 23 37 (1977)

(1.15) Fertig W.A., Johnson D.C., Delong L.E., McCallum R.W., Marple M.B., Matthias B.T.
Phys. Rev. Lett. 38 987 (1977)

(1.16) Newns D.M., Hewson A.C.
J. Phys. F10, 2429 (1980)

(2.1) Gopal E.S.R.
'Specific heats at low temperatures', Plenum Press, New York (1966)

(2.2) Phillips N.E.
CRC Cot. Rev. Solid State Sci. 2 467 (1977)

(2.3) Heiniger F., Bucher E. and Muller J.
Phys. Kondens. Materie 5 243 (1966)

(2.4) DeLaunay J.
Solid St. Phys. 2 219 (1956)

(2.5) Mcmillan W.L.
Phys. Rev. 167 331 (1968)

(2.6) Friedel J.
Nuovo Cimento Suppl. 7 287 (1958)

(2.7) Stewart G.R.
Rev. Mod. Phys. 56 755 (1984)

(2.8) Brandt N.B., Moshchalkov V.V.
Adv. Phys. 33 (1984) 373

(2.9) Bardeen J., Cooper L.N. and Schrieffer J.R.
Phys. Rev. 106 162 (1957)

(2.10) Parks R.D.
'Superconductivity', Marcel Dekker, New York (1969)

(3.1) Kittel C.
Introduction to Solid State Physics. J. Wiley & Sons

(3.2) Giffard R.P., Webb R.A. and Wheatley J.C.
(1972) J. Low Temp. Phys. 6 533-610

(3.3) Silver A.H., Zimmerman J.E.
Phys. Rev. 157 2 (1967) 317

(3.4) Park J.G.
J. Phys. F 3 (1973) 1144

(3.5) Park J.G., Cayless A.T., de Groot P.A.J.
J. Phys. D, under submission

(3.6) Park J.G.
J. Phys. F 4 (1974) 2239

(3.7) Harding J.T., Zimmerman J.E.
J. App. Phys. 41 4 (1970) 1581

(3.8) Park J.G., Vaidya A.
J. Low Temp. Phys. 40 314 1980

(3.9) Park J.G., Vaidya A.
IEEE transactions on magnetics Vol. Mag. 17 No. 1 1981

(3.10) Vaidya A.
Thesis, 1979

(3.11) Jackel L.D., Buhrman R.A.
J. Low Temp. Phys. 19 (1975) 201

(3.12) Kurkijarvi J.
J. Appl. Phys. 44 3729 (1973)

(3.13) Kurkijarvi J.
Phys. Rev. B 6 832 (1972)

(3.14) Bloch F.
Phys. Rev. Lett. 21 1241-43 (1968)

(3.15) Kurkijarvi J. and Webb W.W.
Proc. Appl. Superconductivity Conf. Annapolis IEEE
(1972)

(3.16) Kamper R.A.
Proc. Conf. Superconducting Devices, Charlottesville
(1967)

(3.17) Soulen R.J., Morshak H.
Proc. Appl. Superconductivity Conf. Annapolis IEEE (1972)

(3.18) Kamper, see ref. 10

(4.1) Joseph O., Moody D.E., Whiteheard J.P.
J. Phys. E 9 595 (1976)

(4.2) Martin D.L., Bradley L., Cazemir W.J., Snowdon R.L.
Rev. Sci. Inst. 44 675 (1973)

(4.3) Sullivan P.F. and Seidel G.
Phys. Rev. 173 679 (1968)

(4.4) Schwall R.E., Howard R.E., Stewart G.R.
Rev. Sci. Instr. 46 1054 (1975)

(4.5) Morin F.J., Maita J.P.
Phys. Rev. 129 1115 (1963)

(4.6) Holste J.C., Cetas T.C., Swenson C.A.
Rev. Sci. Instr. 43 670 (1972)

(5.1) Vaidya A.W.
Thesis: London University 1979

(5.2) Wun M. and Phillips N.E.
Cryogenics 15 36 (1975)

(6.1) Buschow K.H.J.
Rep. Prog. Phys. 40 1179 (1977)

(6.2) Wohlfarth J.E.P.
J. Appl. Phys. 39 1061 (1968)
J. Phys. C: Solid State 2 68 (1969)

(6.3) Cyrot M. and Lavagna M.
J. de Phys. 40 (1979) 763

(6.4) Grover A.K., Coles B.R., Sarkissian B.V.B. and Stone H.E.N.
J. Less Common Metals: 86 29 (1982)

(6.5) Singal C.M. and Das T.P.
Phys. Rev. B 16 5068 (1979)

(6.6) Luo H.L., Maple M.B., Harris I.R., Smith T.F.
Phys. Lett. (Netherlands) 27A 519 (1968)

(6.7) Hume-Rothery W. and Raynor G.C.
Institute of Metals (Monograph) (1962)

(6.8) Probst C. and Witting J.
Proc. Low Temp. 13 3 495 (1972)

(6.9) Gschneidner K.A.
Solid State Phys. 16 275 (1964)

(6.10) Lavanga M., Lacroix C., Cyrot M.
J. Phys. F: Met. Phys. 13 1007 (1983)

(6.11) Cooper J.R., Rizzuto C. and Olcese G.
Proc. Conf. R.E. and Actinides (Inst. Phys.) p.183 (1971)

(6.12) McCarthy S.L.
J. Low Temp. Phys. 4 489 (1971)

(6.13) McMillan W.L.
Phys. Rev. 167 331 (1968)

(6.14) Klein B.M., Pickett W.E., Papaconstantopoulos D.A. and Boyer L.L.
Phys. Rev. B. 27 6721 (1983)

(6.15) Bucher E., Muller J., Olsen J.L. and Palmy C.
Phys. Letters 15 303 (1965)

(6.16) Matthias B.T.
Phys. Rev. 100 626 (1955)

(6.17) Coles B.R.
Philos. Mag. Supp. 7 40 (1958)

(6.18) Webster P.J.

Contemp. Phys. 10 559 (1969)

(6.19) Gladysevkij E.I., Markiv V.J.A., Muz M.A.J.B.

Doplakad nauk Ukrain SR 10 1329 (1962)

(6.20) Webster P.J. and Ziebeck K.R.A.

J. Phys. Chem. Solid 34 1647 (1973)

(6.21) Kittel C.

'Introduction to Solid State Phys.' Wiley (1971)

(6.22) Pinski F.J., Allen P.B. and Butler W.H.

Phys. Rev. Lett. 41 431 (1978)

(6.23) Berk N.F. and Schrieffer J.R.

Phys. Rev. Lett. 17 433 (1970)

(6.24) Chen Z., Loram J.W., Mirza K.A.

J. Phys. F: Met. Phys. 14 L219 (1984)

(6.25) Loram J.W.

J. Phys. E: Sci. Instrum. 16 367 (1983)

(6.26) Nieuwenhuys G.J.

Thesis: University of Amsterdam (1946)

(6.27) Rastogi A.K., Coles B.R.

J. Phys. F: Met. Phys. 1165 (1985) 15

(6.28) Ododo J.C.

J. Phys. F: Met. Phys. 12 1821 (1982)

(6.29) Anderson P.W.

Phys. Rev. 124 41 (1961)

(6.30) Rivier N. and Zukermann M.J.

Phys. Rev. Lett. 21 904 (1968)

(6.31) Wohlleben D.K. and Coles B.R.

Magnetism Vol. 5 ed. H. Suhl (Academic Press)

(6.32) Rastogi and Coles

To be published

(6.33) Cheng W., Creuzet G., Garoche P., Campbell I.A., Gratz E.
J. Phys. F: Met. Phys. 12 475 (1982)

(6.34) Yvon K., Braun H.F., Gratz E.
J. Phys. F: Met. Phys. 13 L131 (1983)

(6.35) Moreau J.M., Parthe E. and Paccard D.
Acta Crystallogr. Sect. B31 747 (1975)

(6.36) Witting J.
Proc. Conf. Karlsruhe 321 (1982)

(6.37) Rastogi A.K.
To be published

(6.38) Muraoka Y., Shiga M., Nakamura Y.
J. Phys. Soc. Japan 42 2067 (1977)

(6.39) Morin F.J. and Maita J.P.
Phys. Rev. 129 1115 (1963)

(6.40) DeVries K.L., Baker G.S., Gibbs P.
WADC Tech. report p.59-341 (1960) Utah University

(6.41) Koskimaki D.C. and Gschneidner K.A.
Phys. Rev. B 11 4463 (1975)

(7.1) Matters W.
Ph.D. Thesis: Natuurkundig Laboratorium, University of Amsterdam 1980

(7.2) Buschow K.H.J.
J. Less Common Met. 26 (1972) 329

(7.3) Palenzona A.
J. Less Common Met. 21 (1970) 443

(7.4) Iandelli A. and Palenzona A.
Revue Chim. Min. 10 (1973) 303

(7.5) Bonville P., Imbert P., Jehanno G. and Gonzalez-Jiminez F.
J. Phys. Chem. Solids 39 (1978) 1273

(7.6) Ross J.W. and Tron E.

J. Phys. F 8 (1978) 983

(7.7) Buschow K.H.J., Campagna M. and Wertheim G.K.

Solid State Comm. 24 (1977) 253

(7.8) Peterman D.J., Weaver J.H., Croft M. and Peterson D.T.

Phys. Rev. B 27 (1983) 808

(7.9) Parks R.D., Reihl B., Martensson N. and Steglich F.

Phys. Rev. B 27 (1983) 6052

(7.10) Allen J.W., Oh S.J., Lindau I., Maple M.B. and

Hagström S.B.

Phys. Rev. Lett. 46 (1982) 1100

(7.11) Brandt N.B., Moshchalkov V.V.

Adv. Phys. 33 (1984) 373

(7.12) Newns D.M., Hewson A.C.

J. Phys. F 10 (1980) 2429

(7.13) Havinga E.E., Buschow K.S.T. and van Daal H.J.

Solid St. Comm. 13 (1973) 621

(7.14) Grüner G. and Zawadowski A.

Solid St. Comm. 11 (1972) 663

(7.15) Murani A.P.

Phys. Rev. Lett. 54 (1985) ¾444

(7.16) Murani A.P.

Private communication

(7.17) Martin R.M.

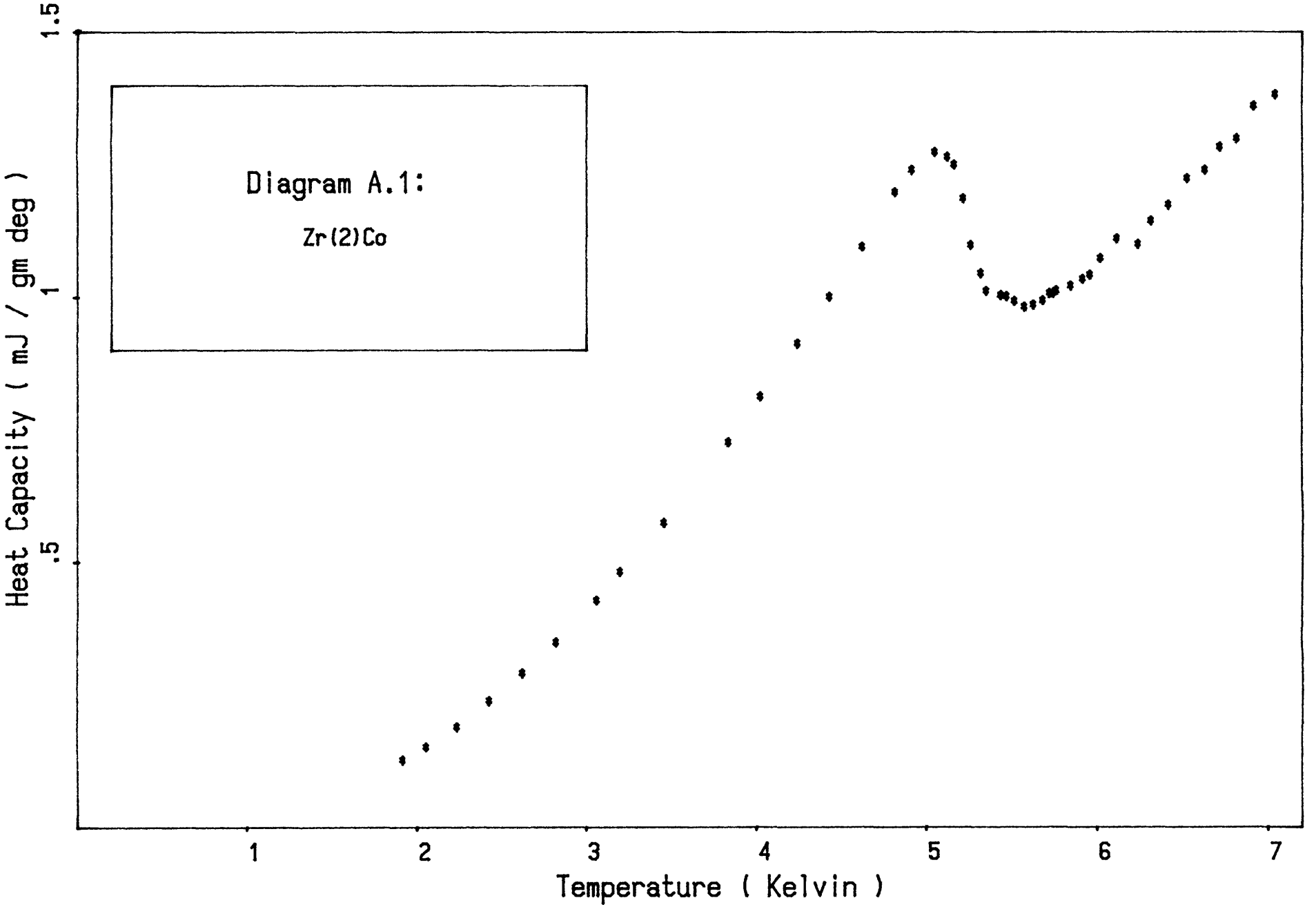
Phys. Rev. Lett. 48 (1982) 362

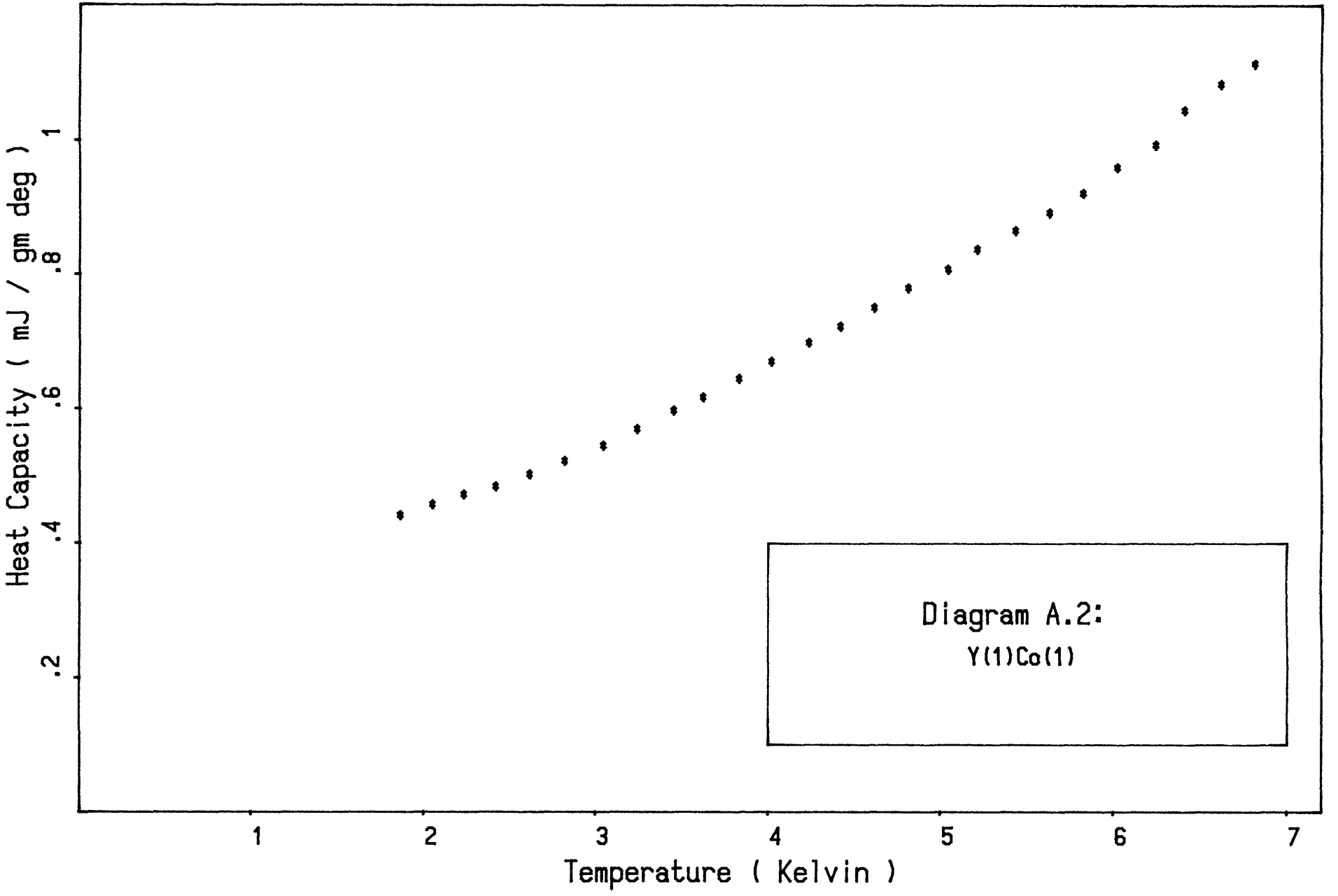
(7.18) Bredl C.D., Horn S., Steglich F., Lüthi B. and Martin R.M.

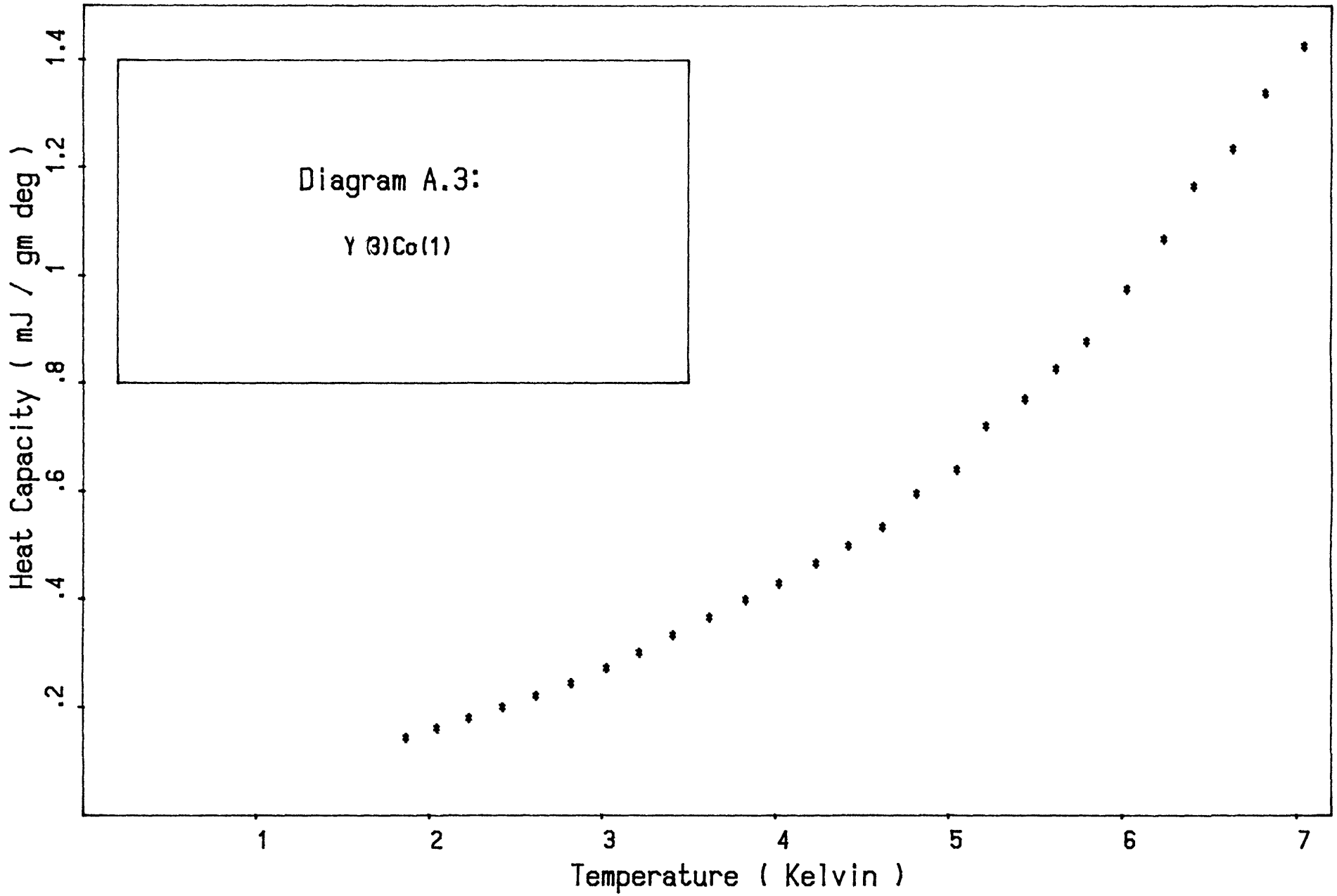
Phys. Rev. Lett. 52 (1984) 1982.

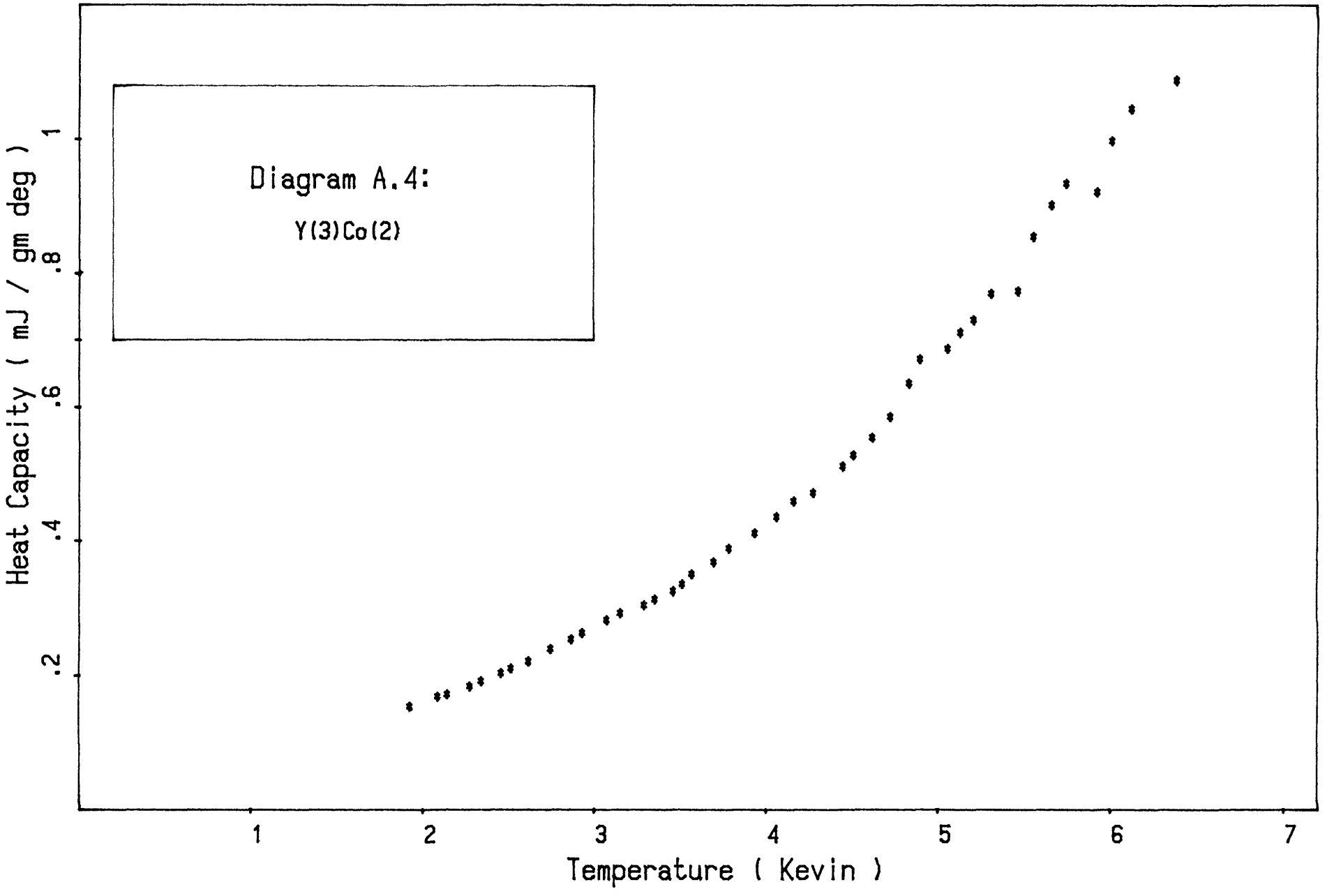
APPENDIX A

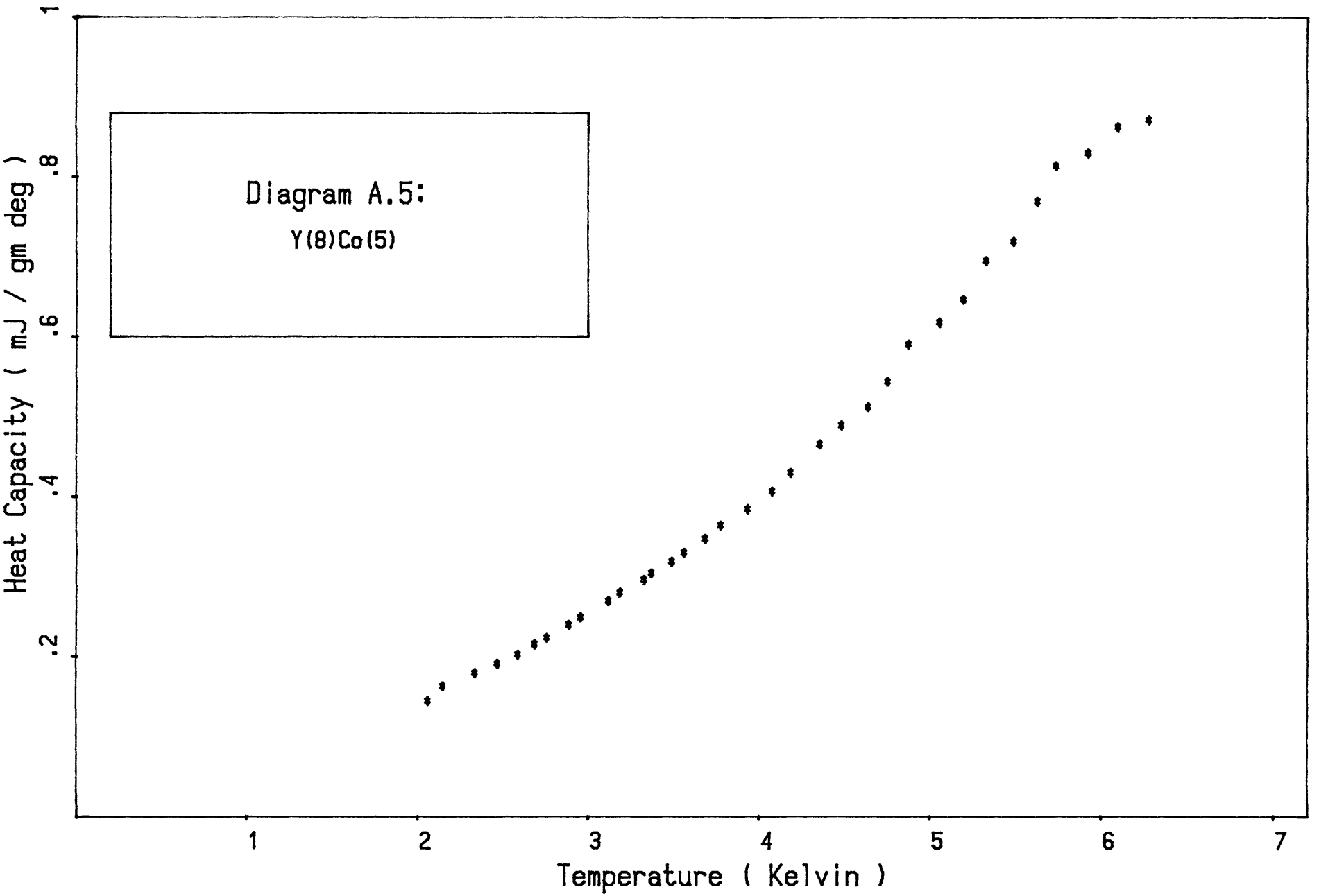
In this appendix we present all the specific heat data (in graphical form) taken in this project.

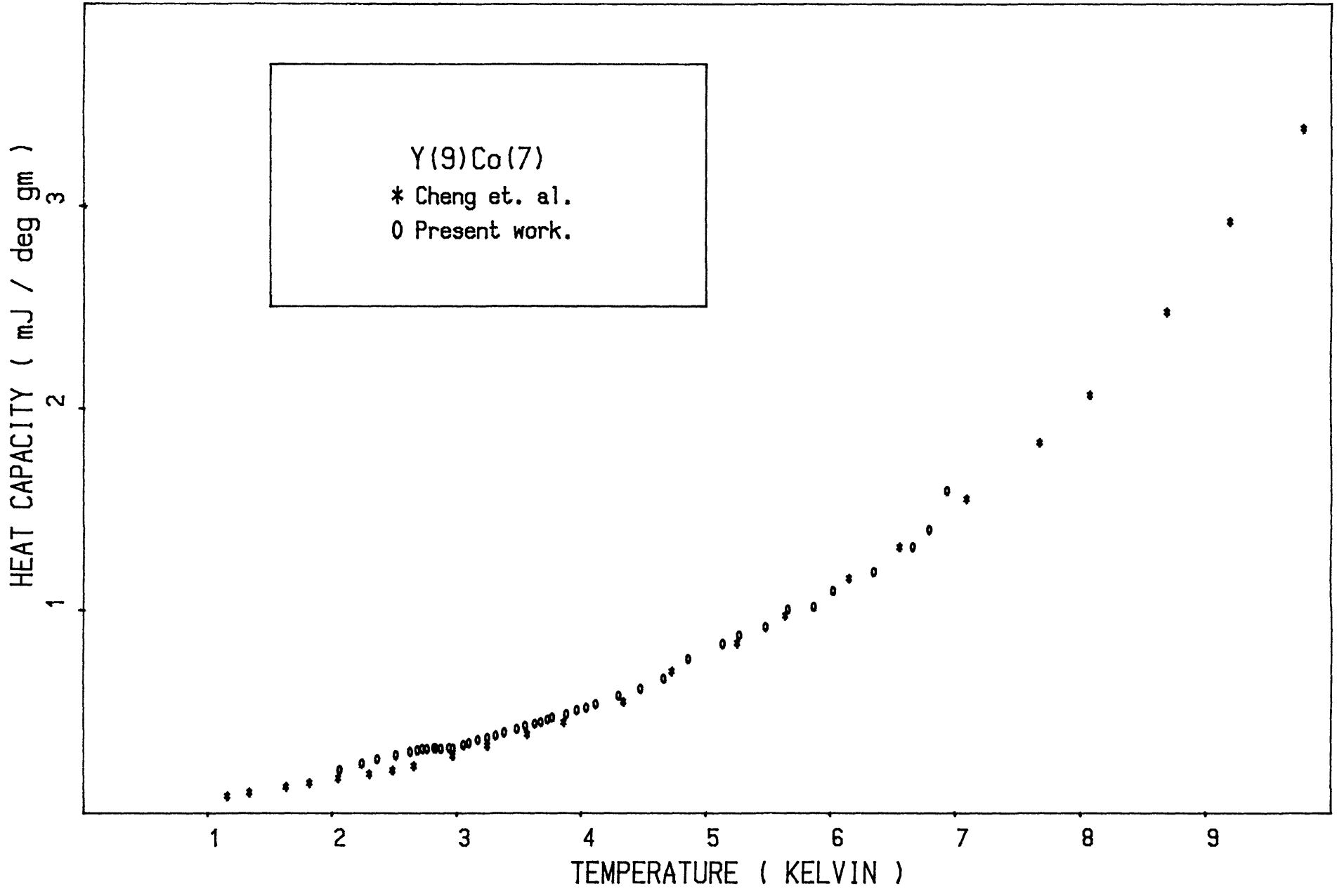

Diagram A.1:
Zr(2)Co
Heat Capacity (mJ / gm deg)
1.5
1
.5
1
2
3
4
5
6
7
Temperature (Kelvin)

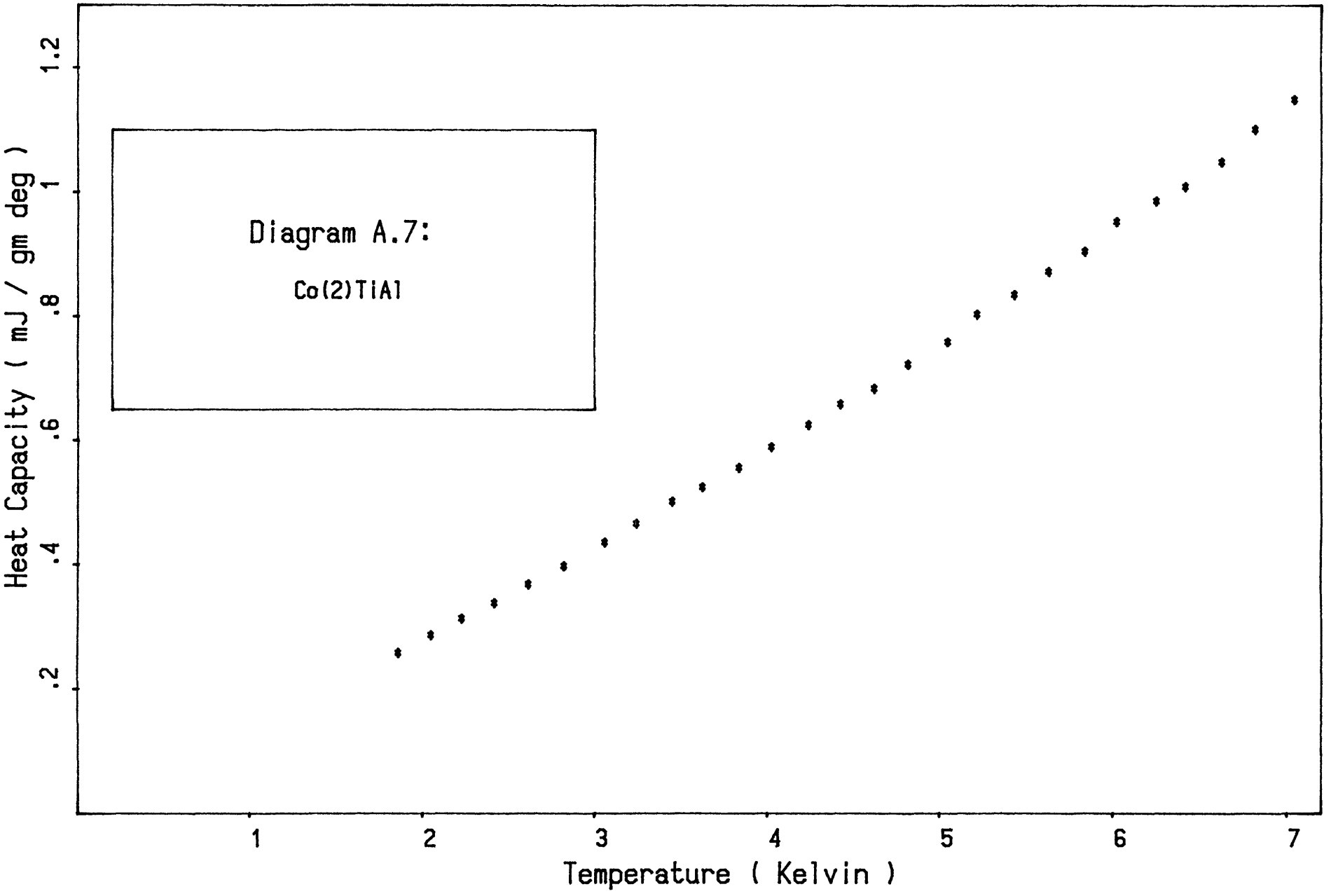

Heat Capacity (mJ / gm deg)
.2
.4
.6
.8
1
1
2
3
4
5
6
7
Temperature (Kelvin)
Diagram A.2:
Y(1)Co(1)

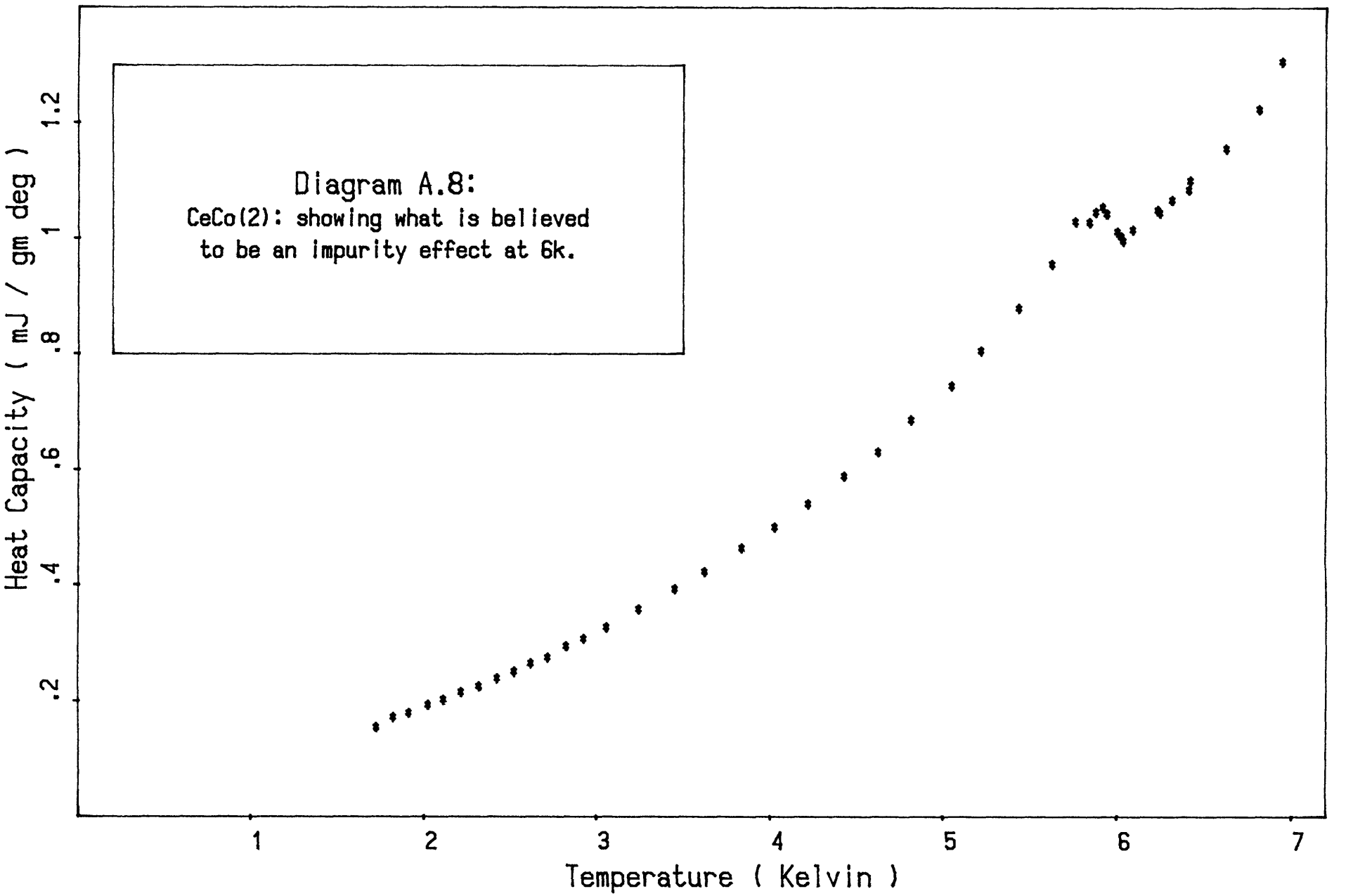

Diagram A.3:
Y (3)Co(1)
Heat Capacity (mJ / gm deg)
.2
.4
.6
.8
1
1.2
1.4
1
2
3
4
5
6
7
Temperature (Kelvin)

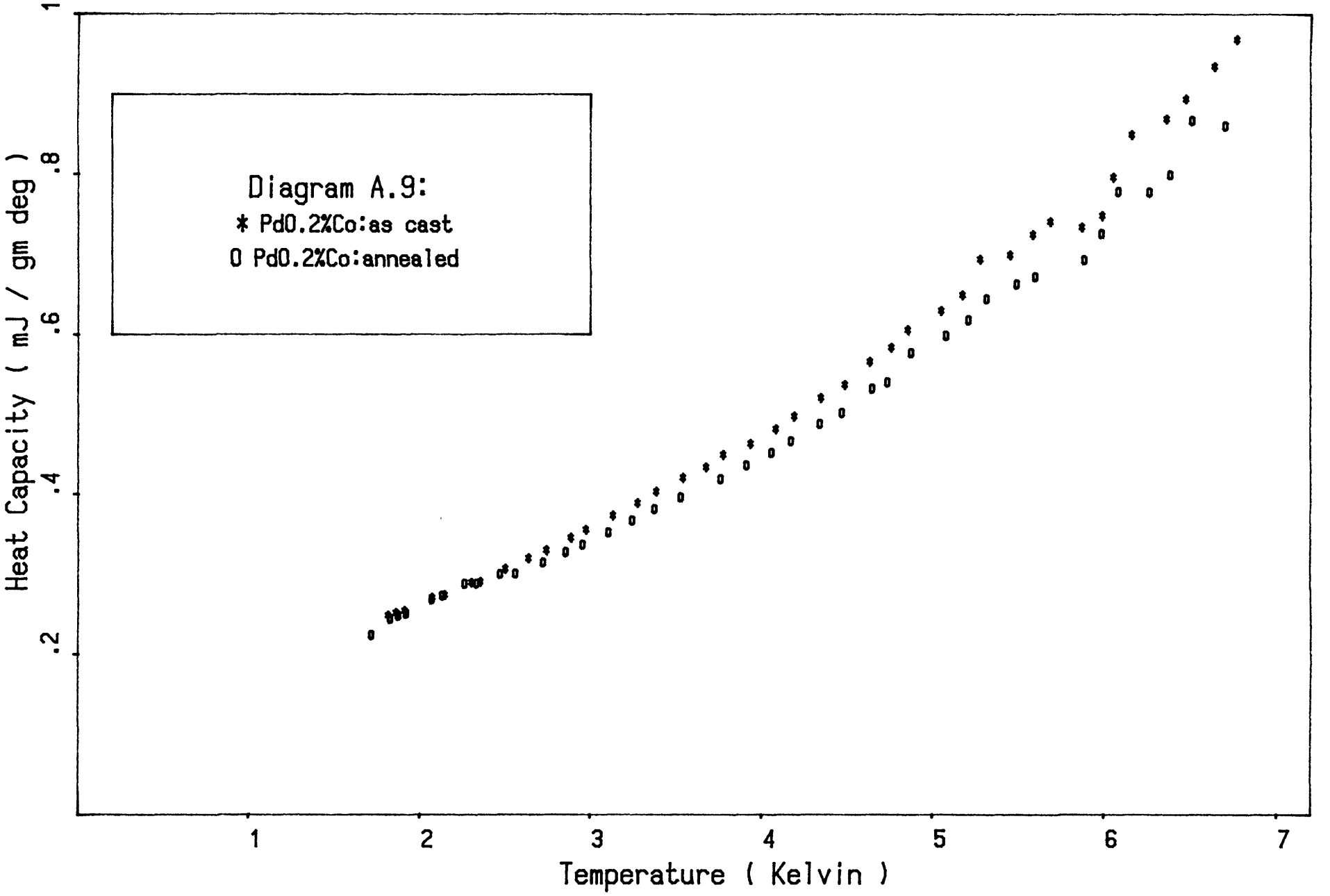

Diagram A.4:
Y(3)Co(2)
Heat Capacity (mJ / gm deg)
.2
.4
.6
.8
1
1
2
3
4
5
6
7
Temperature (Kevin)

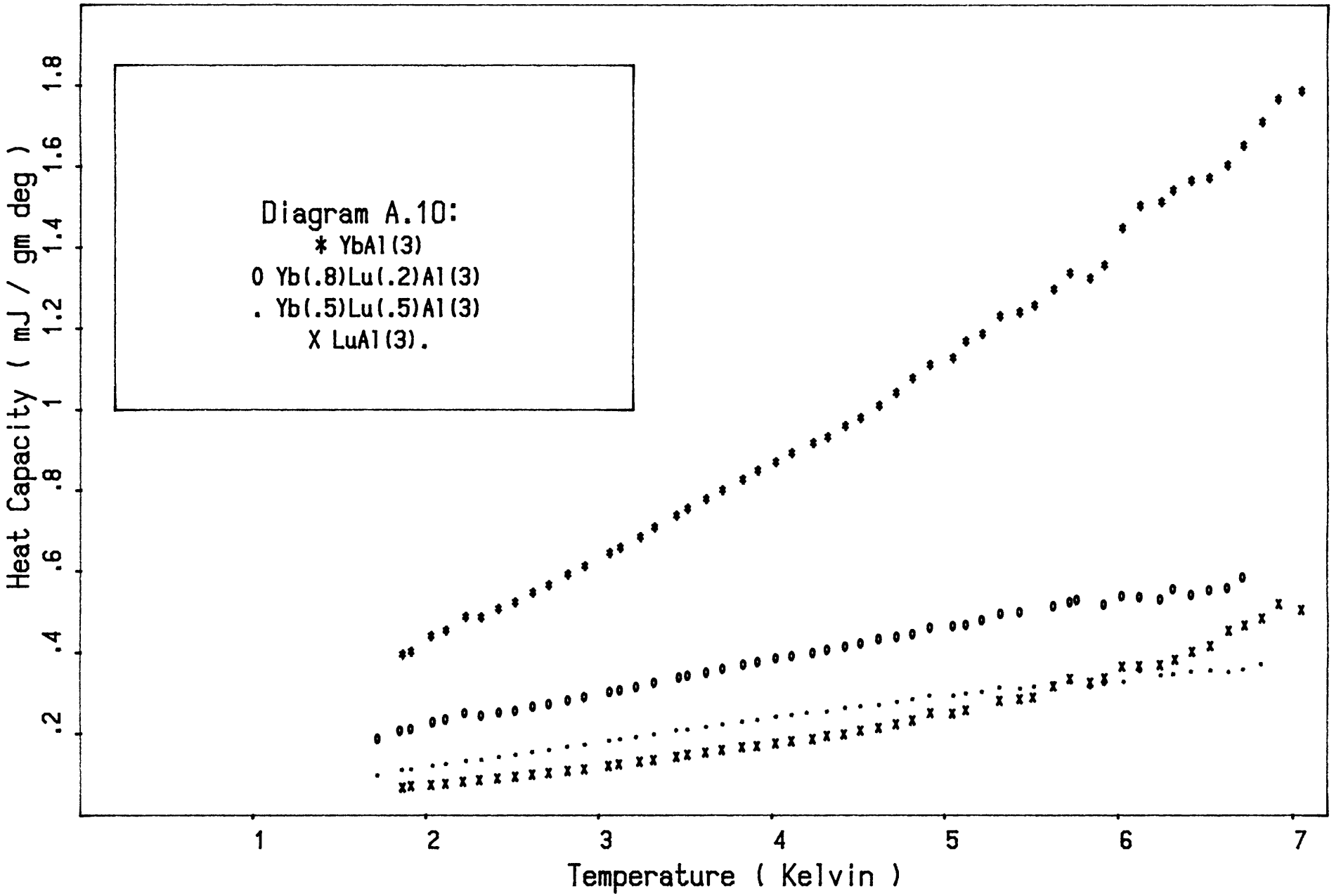

Diagram A.5:
Y(8)Co(5)
Heat Capacity (mJ / gm deg)
.2
.4
.6
.8
1
1
2
3
4
5
6
7
Temperature (Kelvin)


Y(9)Co(7)
* Cheng et. al.
0 Present work.
HEAT CAPACITY (mJ / deg gm)
1
2
3
1
2
3
4
5
6
7
8
9
TEMPERATURE (KELVIN)


Diagram A.7:
Co(2)TiAl
Heat Capacity (mJ / gm deg)
.2
.4
.6
.8
1
1.2
1
2
3
4
5
6
7
Temperature (Kelvin)


Diagram A.8:
CeCo(2): showing what is believed
to be an impurity effect at 6k.
Heat Capacity (mJ / gm deg)
.2
.4
.6
.8
1
1.2
1
2
3
4
5
6
7
Temperature (Kelvin)


Diagram A.9:
* Pd0.2%Co:as cast
0 Pd0.2%Co:annealed
Heat Capacity (mJ / gm deg)
.2
.4
.6
.8
1
1
2
3
4
5
6
7
Temperature (Kelvin)


Diagram A.10:
* YbAl(3)
0 Yb(.8)Lu(.2)Al(3)
. Yb(.5)Lu(.5)Al(3)
X LuAl(3).
Heat Capacity (mJ / gm deg)
.2
.4
.6
.8
1
1.2
1.4
1.6
1.8
1
2
3
4
5
6
7
Temperature (Kelvin)

APPENDIX B

In this appendix we list all the programs which were used directly in the collection or manipulation of our data. This includes the main data-taking program and a polynomial fitting program. All these programs were written by the author.

Program B.1 :

```
READY.
 1 INPUT"FROM";H1
 2 INPUT"TO";H2
 3 DIMF(150,2),A(H2,4),P(H2+1,H2+1)
 4 INPUT"FILE NAME";Z$:INPUT"DRIVE  NUMBER";Z
 5 FORM=H1TOH2
 10 REM**************************************
 20 REM**************************************
 25 REM**                                  **
 30 REM**      LEAST  SQUARE               **
 32 REM**                                  **
 35 REM**      APPROXIMATION               **
 37 REM**                                  **
 40 REM**            BY                    **
 42 REM**                                  **
 50 REM**       A.K.CHHABRA                **
 55 REM**                                  **
 60 REM**************************************
 70 REM**************************************
 100 N=26
 110 GOSUB2590
 170 PRINT"ORDER IS";M
 180 FORI=0TOH2+1:FORJ=0TOH2+1:P(I,J)=0:NEXTJ:NEXTI
 190 FORI=0TOH2:FORJ=0TO4:A(I,J)=0:NEXTJ:NEXTI
 200 REM**************************************
 201 REM********                   *********
 202 REM********   CURVE FIT       *********
 203 REM********                   *********
 204 REM**************************************
 210 P(0,0)=1
 215 A(0,1)=0:FORJ=1TON:A(0,1)=A(0,1)+1:NEXTJ
 220 A(0,2)=0:FORI=1TON:A(0,2)=A(0,2)+F(I,1)/A(0,1):NEXTI
 230 P(0,1)=-1*A(0,2):P(1,1)=1
 240 FORI=1TOM:A(I,1)=0
 250 FORJ=1TON:GOSUB800:A(I,1)=A(I,1)+(SUM)↑2:NEXTJ
 260 A(I,2)=0:FORJ=1TON:GOSUB800:A(I,2)=A(I,2)+(F(J,1)*(SUM)↑2)/A(I,1):NEXTJ
 270 A(I,3)=0:A(I,3)=A(I,1)/A(I-1,1)
 275 P(0,I+1)=P(0,I+1)-P(0,I-1)*A(I,3)-A(I,2)*P(0,I)
 280 FORK=1TOI:P(K,I+1)=P(K,I+1)-P(K,I-1)*A(I,3)-A(I,2)*P(K,I)+P(K-1,I):NEXTK
 285 P(I+1,I+1)=1
 290 NEXTI
 295 FORI=0TOM:A(I,4)=0:FORJ=1TON
 296 GOSUB800:A(I,4)=A(I,4)+F(J,2)*SUM/A(I,1):NEXTJ:NEXTI
 300 FORI=0TOM:FORJ=0TOM:A(I,0)=A(I,0)+P(I,J)*A(J,4):NEXTJ:NEXTI
 320 PRINT"▒▒▒▒▒▒▒▒▒▒YOUR FIT IS:"
 330 PRINT"▒▒▒▒▒ORDER▒▒▒▒▒▒▒▒▒A(0)"
 340 FORI=0TOM
 350 PRINT"▒▒▒▒▒";I;"▒▒▒▒▒▒▒▒▒▒";A(I,0)
 360 NEXTI
 440 OPEN4,4
 450 PRINT#4,"ORDER                    FIT"
 460 FORI=0TOM
 470 PRINT#4,"   ";I;"              ";A(I,0)
 480 NEXTI
 500 GOTO1000
```

B.1. contd.

```
READY.

 800 REM***     ORTH GENERATE     ***
 810 SUM=0:FORK=0TOI
 820 SUM=SUM+(P(K,I)*F(J,1)↑K):NEXTK
 830 RETURN
 1000 REM*********************************
 1005 REM*******                 *********
 1010 REM*******   CHECK FIT     *********
 1020 REM*******                 *********
 1030 REM*********************************
 1100 DY=0:Y1=0:FORI=1TON
 1110 Y=0:FORJ=0TOM:Y=Y+A(J,0)*F(I,1)↑J:NEXTJ:Y1=F(I,2)-Y:DY=DY+SQR(Y1↑2)
 1120 PRINT" X=";F(I,1);"  SET Y";F(I,2);"  FIT=";Y;"DIFF";Y1
 1125 PRINT#4," X=";F(I,1);"  SET Y";F(I,2);"  FIT=";Y;"  DIFFERENCE=";Y1
 1130 NEXTI
 1135 PRINT"TOTAL ERROR=";DY
 1136 PRINT#4,"SUM OF DIFF:";DY
 1140 CLOSE4
 2000 NEXTM
 2010 END
 2500 REM*********************************
 2505 REM*******                 *********
 2510 REM*******   INPUT DATA    *********
 2520 REM*******                 *********
 2530 REM*********************************
 2580 REM
 2590 REM
 2592 DOPEN#1,(Z$),D(Z),R:I=1
 2593 INPUT#1,F(I,1),F(I,2)
 2594 IFST=64THENN=I-1:GOTO2596
 2595 I=I+1:GOTO2593
 2596 DCLOSE#1
 2598 FORL=1TO1000:NEXTL
 2599 RETURN

READY.
```

READY.

Program B.2:

Main data program.

READY.

```
 10 REM ******* DATA PROGRAM 1 *******
 20 REM *** CALL SET UP ROUTINE ***
 30 GOSUB 1000
 100 REM ***  MAIN LOOP  ***
 110 PRINT"■■■■■■PRESS:"
 120 PRINT"■■■■■■■T. FOR TEMP CONVERTION"
 130 PRINT"■■■■■D. FOR DATA POINT"
 140 PRINT"■■■■■P. FOR SELF ENTRY PAGE"
 150 PRINT"■■■■■A. FOR ABORT"
 160 GETA$:IFA$="T"GOTO2000
 170 IFA$="D"GOTO2300
 180 IFA$="P"GOTO3000
 190 IFA$="A"GOTO300
 200 GOTO160
 300 REM *** TERMINATE ***
 310 DCLOSE#3:CLOSE4:CLOSE5:CLOSE6
 320 END
 1000 REM *** SET UP ROUTINE ***
 1010 DIMNUP(30,4),C(40,5),B(3,4),RC(30,2),D(9),E(8),F(9)
 1020 POKE59459,48:POKE59468,PEEK(59468)AND254:POKE59464,16:POKE59471,16
 1030 POKE59467,PEEK(59467)AND227OR20
 1040 REM *** CALL INITILISE INPUTS ***
 1050 GOSUB1500
 1060 DOPEN#1,"TABATHA",D1:FORI=1TO40
 1070 INPUT#1,A$,B$,C$,D$,E$:C(I,1)=VAL(A$):C(I,2)=VAL(B$):C(I,3)=VAL(C$)
 1080 C(I,4)=VAL(D$):C(I,5)=VAL(E$):NEXTI
 1090 DCLOSE#1
 1100 OPEN4,4,1:OPEN5,4,2:OPEN6,4,0
 1110 DOPEN#3,(Z$),D1,W
 1120 PRINT#6,Y$CHR$(1)" "CHR$(1)X$CHR$(1)"MASS=";MS
 1130 B$=" 9999999  9999999  9999999  9999999"
 1140 C$="    AAAAAAA AAAAAAAAAAAAAAAA    AAA AAAAAAAAAAAAAAAAAA"
 1150 D$="   AA AAAAA    AAAAAAAAA  AAAAAAAAAAAAAAAAAAA      AAA AAAAA"
 1160 E$="    AAAAAAAAAAAAAAA      AAAAAAA      AAAAAAA    AAAAAAAAAAAAAA"
 1170 F$="           A             AAAAA        AAAA          AAAAA"
 1190 RETURN
 1200 REM *** PRINT ROUTINES ***
 1210 REM PRINT ROUTINE 1
 1220 PRINT#5,B$
 1230 FORJ=1TO4:PRINT#4,NUP(I,J);:NEXTJ
 1240 PRINT#6,"  RC(B)=";RC(I,1);"  RC(D)=";RC(I,2):RETURN
 1250 REM PRINT ROUTINE 2
 1260 PRINT#5,"AAA AAAAA"
 1270 PRINT#4,"T="CHR$(29)T:RETURN
 1280 REM PRINT ROUTINE 3
 1290 PRINT#5,C$
 1300 PRINT#4,"#RC(B)="CHR$(29)B(3,1)CHR$(29)"ER="CHR$(29)B(3,3)
 1305 PRINTB(3,1),B(3,3)
 1306 PRINTB(3,2),B(3,4)
 1310 PRINT#4,"#RC(D)="CHR$(29)B(3,2)CHR$(29)"ER="CHR$(29)B(3,4)
 1320 PRINTRC,T
 1330 PRINT#5,D$
 1340 PRINT#4,"T="CHR$(29)TCHR$(29)"RC(MEAN)="CHR$(29)RCCHR$(29)"TG="CHR$(29)TG
 1350 RETURN
```

B.2 contd.

```
READY.
 1400 REM PRINT ROUTINE 4
 1410 PRINT#5,F$
 1420 PRINT#4,"C"CHR$(29)"RESIS"CHR$(29)"ADDE"CHR$(29)"C(G)"
 1450 PRINT#5,E$
 1460 PRINT#4,CHCHR$(29)RRCHR$(29)FFCHR$(29)EE
 1470 PRINT#6,"TEMP STEP=";TS
 1480 RETURN
 1500 REM *** INITILISE INPUTS ***
 1510 INPUT"■■■■■NAME FOR DATA FILE";Z$
 1520 INPUT"■■■■■■DATE";Y$
 1530 INPUT"■■■■■■SAMPLE";X$
 1540 INPUT"■■■■■■MASS OF SAMPLE (GM)";MS
 1550 INPUT"■■■■■■MASS OF GREASE (MG)";MG
 1560 FORI=0TO9:READD:D(I)=D:NEXTI
 1570 FORI=1TO8:READD:E(I)=D:NEXTI
 1580 FORI=0TO9:READD:F(I)=D:NEXTI
 1600 RETURN
 2000 REM *** MAIN TEMP ROUTINES ***
 2010 PRINT"■■■■■■■TEMPERATURE PAGE"
 2020 INPUT"■■■■CONDUCTANCE";K:R=1/(K*1E-3)
 2030 GOSUB2200
 2040 PRINT"■■■■■■■■■■ **********************************************"
 2050 PRINT"■■■■■■■■TEMP=";T
 2060 PRINT"■■■■■■■AGAIN...Y/N"
 2070 GETA$:IFA$="Y"GOTO2010
 2080 IFA$="N"GOTO100
 2090 GOTO2070
 2200 REM *** TEMP CONVERSION ***
 2210 FORI=1TO40:IFR<C(I,1)GOTO2230
 2220 NEXTI:PRINT"ERROR..1":RETURN
 2230 IFR>C(I+1,1)GOTO2250
 2240 GOTO2220
 2250 V=R-C(I,1):T=C(I,2)+C(I,3)*V+C(I,4)*(V↑2)+C(I,5)*(V↑3)
 2260 RETURN
 2300 REM *** DATA POINT PAGE ***
 2310 INPUT"■■■NO. OF CYCLES";N
 2320 INPUT"■■■■■■ATE TIME";TG
 2330 INPUT"■■CONDUCTANCE AT START";K:R=1/(K*1E-3):GOSUB2200:TI(1)=T:GOSUB1250
 2360 FORI=0TON:FORJ=1TO4
 2370 GOSUB2500:NUP(I,J)=A:NEXTJ
 2380 FORK=1TO4:B(1,K)=NUP(I,K):NEXTK
 2390 GOSUB2540:NEXTI
 2400 INPUT"■CONDUCTANCE AT END";K:R=1/(K*1E-3):GOSUB2200:TI(2)=T:GOSUB1250
 2410 PRINT"■CALCULATE MEAN SUM..Y/N"
 2420 GETA$:IFA$="Y"THENGOSUB2700:GOTO100
 2430 IFA$="N"GOTO100
 2440 GOTO2420
 2500 REM *** GET A NUMBER ***
 2510 WAIT59469,2:A=0
 2520 FORL=0TO6:POKE59466,2↑L:A=A+((PEEK(59457)AND15)*10↑L):NEXTL
 2530 RETURN
```

B.2 contd.

```
READY.

 2540 REM *** CALCULATE RC ***
 2550 AA=B(1,1):IFAA<B(1,2)THENAA=B(1,2)
 2560 IFAA<B(1,3)THENAA=B(1,3)
 2570 IFAA<B(1,4)THENAA=B(1,4)
 2580 IFAA=B(1,1)THENFORK=1TO4:B(2,K)=B(1,K):NEXTK
 2590 IFAA=B(1,2)THENFORK=1TO3:B(2,K)=B(1,K+1):NEXTK:B(2,4)=B(1,1)
 2600 IFAA=B(1,3)THENFORK=1TO2:B(2,K)=B(1,K+2):B(2,K+2)=B(1,K):NEXTK
 2610 IFAA=B(1,4)THENFORK=2TO4:B(2,K)=B(1,K-1):NEXTK:B(2,1)=B(1,4)
 2620 DENOM=((B(2,1)+B(2,2))-(B(2,3)-B(2,4)))
 2630 RC(I,1)=B(2,2)*TG/DENOM
 2640 RC(I,2)=B(2,4)*TG/DENOM
 2650 GOSUB1200:RETURN
 2700 REM *** CALCULATE MEAN/SUM ***
 2710 B(3,1)=0:B(3,2)=0
 2720 FORI=1TON:B(3,1)=B(3,1)+RC(I,1)
 2730 B(3,2)=B(3,2)+RC(I,2)
 2740 NEXTI:B(3,1)=B(3,1)/N:B(3,2)=B(3,2)/N
 2750 B(3,3)=0:B(3,4)=0
 2760 FORI=1TON
 2770 B(3,3)=B(3,3)+(RC(I,1)-B(3,1))↑2
 2780 B(3,4)=B(3,4)+(RC(I,2)-B(3,2))↑2:NEXTI
 2790 B(3,3)=SQR(B(3,3)/N):B(3,4)=SQR(B(3,4)/N)
 2800 T=(TI(1)+TI(2))/2:RC=(B(3,1)+B(3,2))/2
 2810 GOSUB1280:GOSUB4100:GOSUB4500:GOSUB4600:GOSUB4700:GOSUB4800:GOSUB1400
 2820 PRINT"DISC COPY...Y/N"
 2830 GETA$:IFA$="Y"GOTO2900
 2840 IFA$="N"THENRETURN
 2850 GOTO2830
 2900 REM *** STORE DATA ON DISC ***
 2910 PRINT#3,TCHR$(44)CHCHR$(13):RETURN
 3000 REM **** EXTRA FUNCTIONS ****
 3010 PRINT"■■■■■■■■PRESS:"
 3020 PRINT"■■■■■■■■1.FOR THERMAL RESISTANCE."
 3030 PRINT"■■■■■■■■2.FOR SAMPLE HEATER RECORDING."
 3040 PRINT"■■■■■■■■3.FOR D HEATER RECORDING."
 3045 PRINT"■■■■■■■■4.FOR RETURN TO MAIN PAGE."
 3050 GETA$:IFA$="1"GOTO3100
 3060 IFA$="2"GOTO3200
 3070 IFA$="3"GOTO3300
 3075 IFA$="4"GOTO100
 3080 GOTO3050
 3100 REM *** THERMAL RESISTANCE ***
 3110 INPUT"■■■■■■■TEMPERATURE";T
 3120 GOSUB4100
 3130 PRINT"■■■■■■THERMAL RESISTANCE=";RR
 3140 PRINT"■■■■■■■■AGAIN....Y/N?"
 3150 GETA$:IFA$="Y"GOTO3100
 3160 IFA$="N"GOTO3000
 3170 GOTO3150
 3200 REM *** SAMPLE HEATER ***
```

B.2 contd.

```
READY.

3200 REM *** SAMPLE HEATER ***
3205 PRINT"■■■■■■■ENSURE DEVICE 89 ON .2 VOLT"
3210 GOSUB4200:GOSUB4300:GOSUB4400
3220 V=V2*V1*1E-8:E(0)=V
3230 PRINT"■■■■■■■SAMPLE HEATER POWER=";V
3240 PRINT"■■■■■■■PRESS:"
3241 PRINT"■■■■■■■■■1.REDO."
3242 PRINT"■■■■■■■■■2.HARDCOPY."
3243 PRINT"■■■■■■■■■3.RETURN TO OPTIONS."
3244 GETA$:IFA$="1"GOTO3200
3245 IFA$="2"GOTO3250
3246 IFA$="3"GOTO3000
3247 GOTO3244
3250 PRINT#6,"    SAMPLE HEATER POWER:";V
3260 GOTO3230
3300 REM *** D HEATER ***
3305 PRINT"■■■■■■■ENSURE DEVICE 89 ON 2 VOLT"
3310 GOSUB4200:GOSUB4300:GOSUB4400
3320 V=V2*V1*1E-4/(99.79)
3330 PRINT"■■■■■■■D HEATER POWER=";V
3340 PRINT"■■■■■■■PRESS:"
3341 PRINT"■■■■■■■■■1.REDO."
3342 PRINT"■■■■■■■■■2.HARDCOPY."
3343 PRINT"■■■■■■■■■3.RETURN TO OPTIONS."
3344 GETA$:IFA$="1"GOTO3300
3345 IFA$="2"GOTO3350
3346 IFA$="3"GOTO3000
3347 GOTO3344
3350 PRINT#6,"    D HEATER POWER:";V
3360 GOTO3330
4000 DATA16680.9539,-6452.53005,-8949.26113,10316.7869,-4876.09349,1310.92568
4010 DATA-214.617578,21.1745732,-1.15618885,.02677008824
4020 DATA2.80019E-2,-4.87887E-3,3.81486E-3,-9.072917E-4,9.76703E-5
4030 DATA-5.23844E-6,1.21072E-7,-3.12038E-11
4040 DATA2.3317564,-4.78499257,4.06911583,-1.75818193,.370369019,-.0117046355
4050 DATA-.0117515993,2.62268448E-3,-2.35953426E-4,8.0649705E-6
4100 RR=0:FORJ=0TO9:RR=RR+D(J)*T↑(J):NEXTJ:RETURN
4200 OPEN10,18:OPEN11,89:RETURN
4300 INPUT#10,V1$:IFST=2GOTO4300
4310 INPUT#11,V2$:IFST=2GOTO4300
4340 V2=VAL(V2$):V1=VAL(RIGHT$(V1$,12)):IFV1<.01GOTO4300
4350 RETURN
4400 CLOSE11:CLOSE10:RETURN
4500 EE=0:FORJ=3TO9:EE=EE+E(J-2)*T↑(J):NEXTJ:EE=EE+E(8)*T↑11
4510 EE=EE*MG*1E-6
4520 RETURN
4600 FF=0:FORJ=0TO9:FF=FF+F(J)*T↑(J):NEXTJ:RETURN
4700 CH=((RC-FF)/RR)-EE):RETURN
4800 TS=E(0)*RR:RETURN
READY.
```

Program B.3.
Plotter software.

```
READY.

 1 DIM AX(500),AY(500),G(20,2)
 10 XS=1:YS=1:XO=0:YO=0
 20 POKE59459,240:POKE59467,PEEK(59467)AND227OR20
 100 DEF FNX(X)=INT(XS*(X-XO) +4.5)
 110 DEF FNY(Y)=INT(YS*(Y-YO)+4.5)
 200 PRINT"■■■■■■■■PRESS:"
 210 PRINT"■■■■■■■1.DATA FROM DISC."
 220 PRINT"■■■■■■■2.DATA IN BY HAND."
 240 PRINT"■■■■■■■3.PLOT PAGE"
 250 GETA$:IFA$="1"GOTO3000
 260 IFA$="2"GOTO3100
 280 IFA$="3"GOTO500
 290 GOTO250
 500 REM PLOT
 510 PRINT"■■■■■■■■PRESS:"
 520 PRINT"■■■■■■■1.AUTO PLOT."
 530 PRINT"■■■■■■■2.PLOT FROM KEY BOARD."
 540 PRINT"■■■■■■■3.RESTRICTED PLOT."
 550 GETA$:IFA$="1"GOTO600
 560 IFA$="2"GOTO700
 570 IFA$="3"GOTO800
 580 GOTO550
 600 REM
 610 GOSUB1000:GOSUB9000
 620 GOTO200
 700 REM
 701 PRINT"■■■■■■■■NOT READY!!"
 702 FORI=1TO1000:NEXTI
 710 GOTO510
 800 GOSUB1000
 801 INPUT"■■■■■■■■■MAX X";XL
 802 INPUT"■■■■■■■■■MIN X";XS
 803 INPUT"■■■■■■■■■MAX Y";YL
 804 INPUT"■■■■■■■■■MIN Y";YS
 810 GOSUB8100:GOSUB9020
 820 GOTO200
 1000 GOSUB5000:XL=0:YL=0:X=0:Y=249
 1005 GOSUB6000
 1010 GOSUB5000:XL=0:YL=0:Y=0:X=249
 1100 GOSUB6000:RETURN
 1500 PRINT"■■■■X MAX";XL;
 1510 PRINT"■■■■X MIN";XO
 1520 PRINT"■■■■Y MAX";YL;
 1530 PRINT"■■■■Y MIN";YO
 1540 RETURN
 1600 PRINT"■■■■■■ZITS ON AXIS....Y/N?"
```

B.3 contd.

```
READY.

 1600 PRINT"■■■■■ZITS ON AXIS....Y/N?"
 1610 GETA$:IFA$="N"THENRETURN
 1620 IFA$="Y"GOTO1640
 1630 GOTO1610
 1640 INPUT"■■■■■NUMBER ON X AXIS";W1
 1650 FORI=1TOW1
 1660 INPUT"X";G(I,1)
 1670 NEXTI
 1680 INPUT"■■■■■NUMBER ON Y AXIS";W2
 1690 FORI=1TOW2
 1700 INPUT"Y";G(I,2)
 1710 NEXTI
 1720 FORI=1TOW1:Y=Y0:X=G(I,1):X1=FNX(X):Y1=FNY(Y):Y0=Y1:X0=X1
 1730 GOSUB5000:GOSUB7000:GOSUB5100:Y0=Y0+3:GOSUB7000:NEXTI
 1740 FORI=1TOW2:X=X0:Y=G(I,2):X1=FNX(X):Y1=FNY(Y):Y0=Y1:X0=X1
 1750 GOSUB5000:GOSUB7000:GOSUB5100:X0=X0+3:GOSUB7000:NEXTI
 1760 RETURN
 2999 END
 3000 REM READ IN FROM DISC
 3010 INPUT"■■■■■DRIVE NUMBER";Z
 3020 INPUT"■■■■FILE NAME";Z$
 3040 DOPEN#1,(Z$),D(Z),R:I=1
 3050 INPUT#1,A,B:AX(I)=A:AY(I)=B
 3060 IFST=64GOTO3080
 3070 I=I+1:GOTO3050
 3080 NP=I-1:DCLOSE#1
 3090 GOTO200
 3100 REM MANUAL INPUT
 3110 INPUT"■■■■■NUMBER OF POINTS";N
 3120 FORI=1TON
 3130 INPUT"X,Y";AX(I),AY(I)
 3140 NEXTI
 3150 PRINT"■■■■■CHECK...Y/N?"
 3160 GETA$:IFA$="N"GOTO3300
 3170 IFA$="Y"GOTO3190
 3180 GOTO3160
 3190 FORI=1TON:PRINTAX(I),AY(I)
 3200 PRINT"O.K....Y/N?"
 3210 GETA$:IFA$="Y"THENGOTO3235
 3220 IFA$="Y"GOTO3400
 3230 GOTO3210
 3235 NEXTI
 3300 PRINT"■■■■■WOULD YOU LIKE A DISC COPY.....Y/N"
 3310 GETA$:IFA$="N"GOTO3390
 3320 IFA$="Y"GOTO3340
 3330 GOTO3310
 3340 INPUT"■■■■■FILE NAME";Z$
 3350 INPUT"■■■■■DRIVE NUMBER";Z
 3360 DOPEN#1,(Z$),D(Z),W
 3370 FORI=1TON:PRINT#1,AX(I)CHR$(44)AY(I)CHR$(13)
 3380 NEXTI:DCLOSE#1
 3390 NP=N:GOTO200
 3400 INPUT"X,Y";AX(I),AY(I)
 3410 GOTO3235
```

B.3 contd.

```
READY.

5000 REM PEN UP            ††
5010 POKE59471,255-64:POKE59466,0
5015 FORQQ=1TO 90:NEXTQQ
5020 RETURN
5100 REM PEN DOWN
5105 FORQQ=1TO 90:NEXTQQ
5110 POKE59471,255-64:POKE59466,150
5120 RETURN
6000 REM LINE (XL,YL) TO (X,Y)
6010 X1=FNX(XL):X2=FNX(X):Y1=FNY(YL):Y2=FNY(Y):DX=X1-X2:DY=Y1-Y2:XQ=X1:YQ=Y1
6014 IF DX=0 THEN DX=1E-20
6015 G=DY/DX:GOSUB 7000:GOSUB 5100
6020 IF ABS(DX)<ABS(DY) THEN 6100
6030 FOR XQ=X1 TO X2 STEP -SGN(DX)
6040 YQ=INT(Y1+G*(XQ-X1)+0.5)
6050 GOSUB 7000
6060 NEXT XQ
6070 GOTO 6200
6100 REM
6130 FOR YQ=Y1 TO Y2 STEP -SGN(DY)
6140 XQ=INT(X1+1/ G*(YQ-Y1)+0.5)
6150 GOSUB 7000
6160 NEXT YQ
6200 XL=X:YL=Y
6210 RETURN
7000 REM MOVE PEN TO (XQ,YQ) REAL COORDS
7005 IFXQ<0ORXQ>250THENRETURN
7006 IFYQ<0ORYQ>250THENRETURN
7010 POKE59471,255-128:POKE59466,XQ:POKE59471,255-16:POKE59466,YQ
7020 FOR QQ=1 TO 10  :NEXT QQ
7030 RETURN
7500 REM MOVE PEN TO (X,Y)     PEN UP FIRST
7510 GOSUB 5000:FOR QQ=1 TO 100:NEXT QQ:GOTO 7600
7515 REM MOVE PEN TO (X,Y)     PEN DOWN   FIRST
7520 GOSUB 5100:FOR QQ=1 TO 100:NEXY QQ:GOTO 7600
7600 REM MOVE PEN TO (X,Y) NO CHANGE FOR PEN
7610 XQ=FNX(X):YQ=FNY(Y):GOSUB 7000
7615 XL=X:YL=Y
7620 RETURN
```

B.3 contd.

```
READY.
 8000 REM SCALE AX(),AY()
 8005 XS=AX(1):YS=AY(1):XL=AX(1):YL=AY(1)
 8010 FOR J=1 TO NP
 8020 IF XS>AX(J) THEN XS=AX(J)
 8030 IF XL<AX(J) THEN XL=AX(J)
 8040 IF YS>AY(J) THEN YS=AY(J)
 8060 IF YL<AY(J) THEN YL=AY(J)
 8070 NEXT J
 8100 X0=XS:Y0=YS
 8110 XS=245/(XL-XS):YS=245/(YL-YS)
 8120 RETURN
 8500 REM CROSS AT (X,Y)
 8505 GOSUB 7500
 8510 X1=FNX(X):Y1=FNY(Y)
 8520 X0=X1-2:Y0=Y1:GOSUB5100  :GOSUB 7000:X0=X0+2:GOSUB 7000:X0=X0+2:GOSUB 700
 8530 GOSUB 5000
 8540 X0=X1:Y0=Y1-2:GOSUB7000:GOSUB 5100:Y0=Y0+2:GOSUB 7000:Y0=Y0+2:GOSUB 7000
 8550 GOSUB 5000
 8560 XL=X:YL=Y
 8570 RETURN
 9000 REM DRAW A SET OF DATA
 9010 XL=AX(1):YL=AY(1):GOSUB 8000
 9020 GOSUB1500:GOSUB1600:FOR K=1 TO NP  STEP 1
 9025 X=AX(K):Y=AY(K)
 9030 GOSUB 8500
 9040 NEXT K
READY.
```

APPENDIX C

The circuits described in this appendix were used to interface the PET. The parallel user port available on the PET is basically a VIA 6520 chip. We intended to use the serial port as our main data line, i.e. all data would be outputted or inputted on this line, with the bi-directional parallel data lines being for selecting the relevant 'boards' into or out of which the data would go.

However, owing to the internal architecture of the PET, something not specified in the available literature, the serial port can only be used to output data. It was then decided to use the serial port to specify the digit of our data and then use four of the parallel lines to receive it. The following circuits were used to achieve this.

The circuit in diagram C1 is the main selector circuit for the 32 BCD data lines which form the data output from the counting system. By sending one of eight lines high the respective digit appears in the output. This is simply achieved through the use of a SN 74LS368 chip.

Diagram C2 shows the Pet-Count/temp interface. The temperature interface was never completely connected to the PCB conductance bridge, so will not be described here. The counting systems interface consists of an enable line which activates the board, a 74LS164 - a serial to parallel converter chip, into which the user port sends serially the digit of the data to be read. This is then connected to the selector circuit of diagram C1. The BCD data are read through the interface board, back to the PET.

Diagram C3 shows the Plotter-PET interface board. This

consists of three identical circuits. An enable selects the board, and a further selection is necessary to determine which of the three circuits is being addressed. These circuits are a 74LS$\frac{3}{4}$64, serial to parallel converter, which feeds a D to A converter which outputs through a small amplifier. Two of these circuits constitute the X and Y channels, while the third was used for a pen up and pen down line. However, with an additional current buffer on the pen up/pen down channel, this could also be used as the power supply for the D-heater.

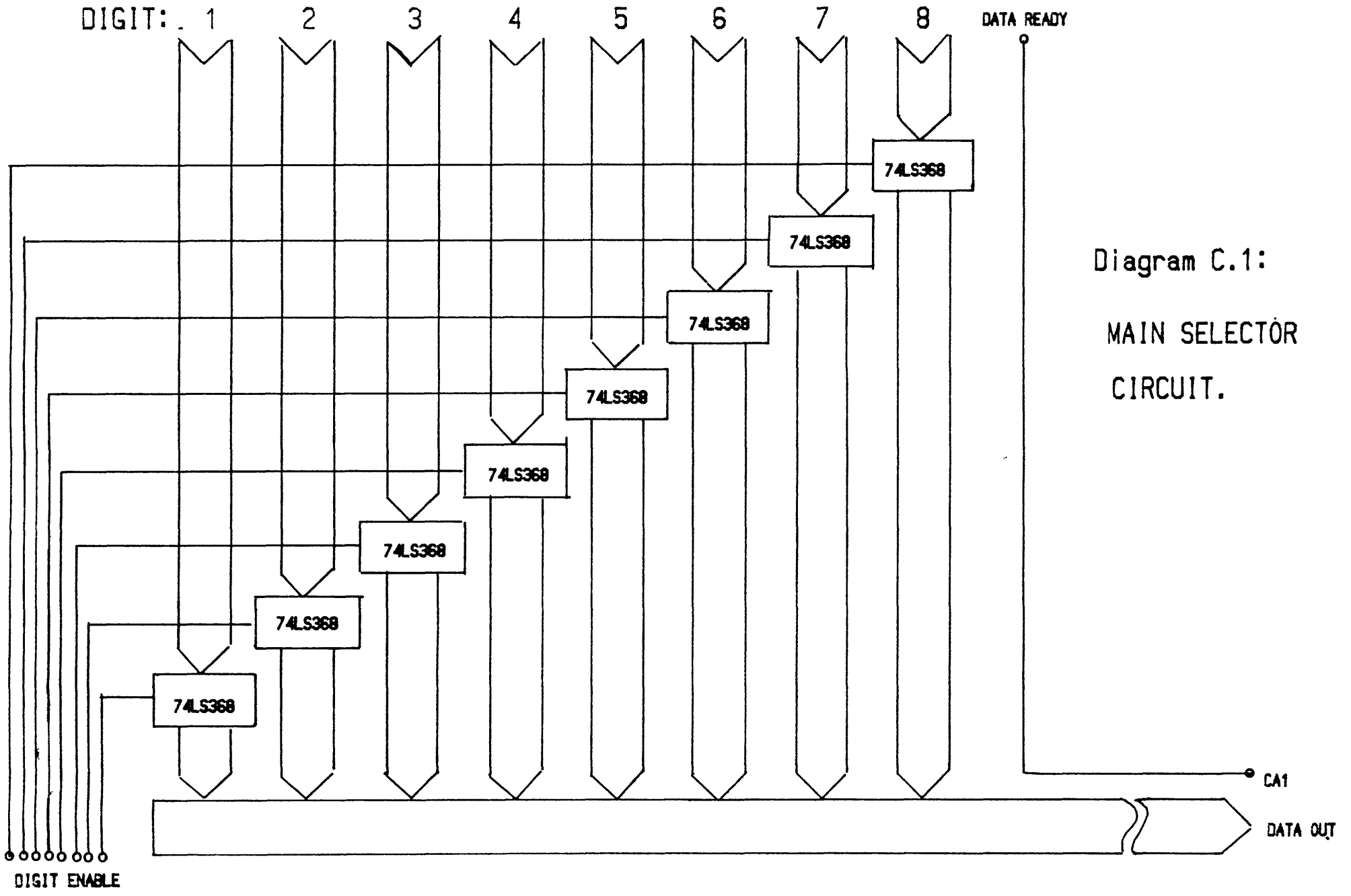


Diagram C.1:

MAIN SELECTOR CIRCUIT.

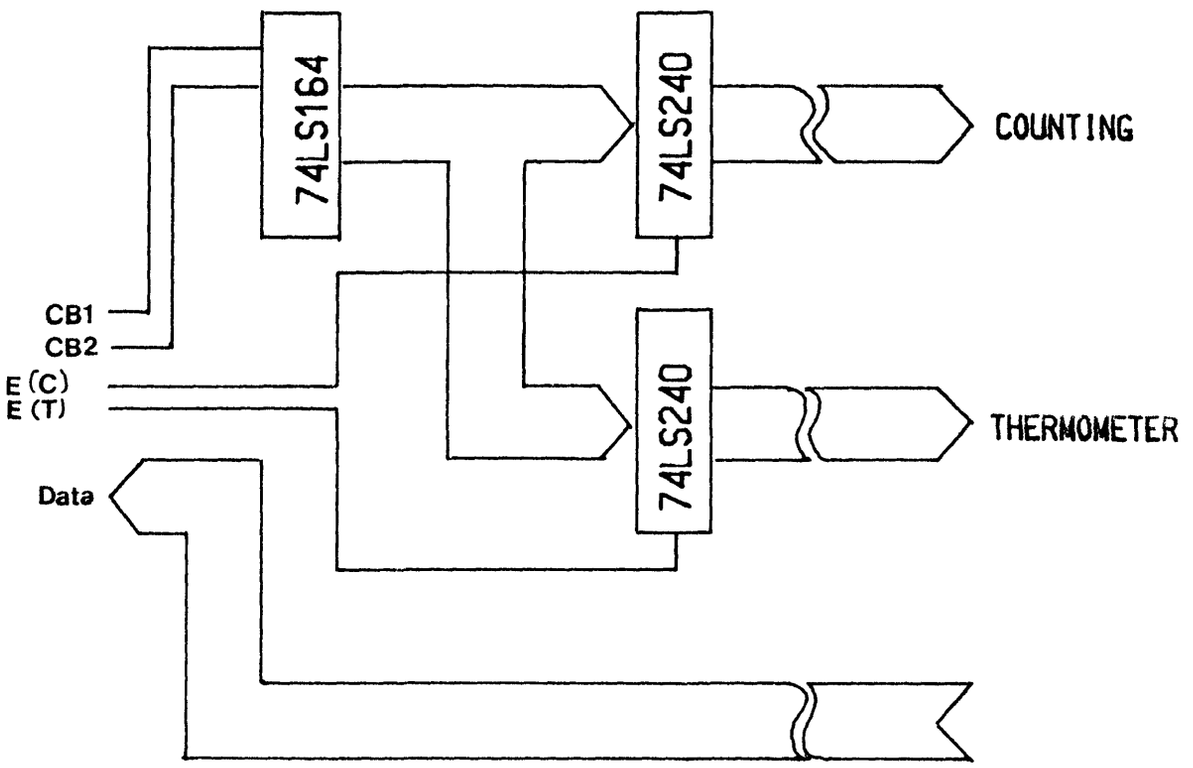


Diagram C.2:

PET - COUNT/TEMP INTERFACE.

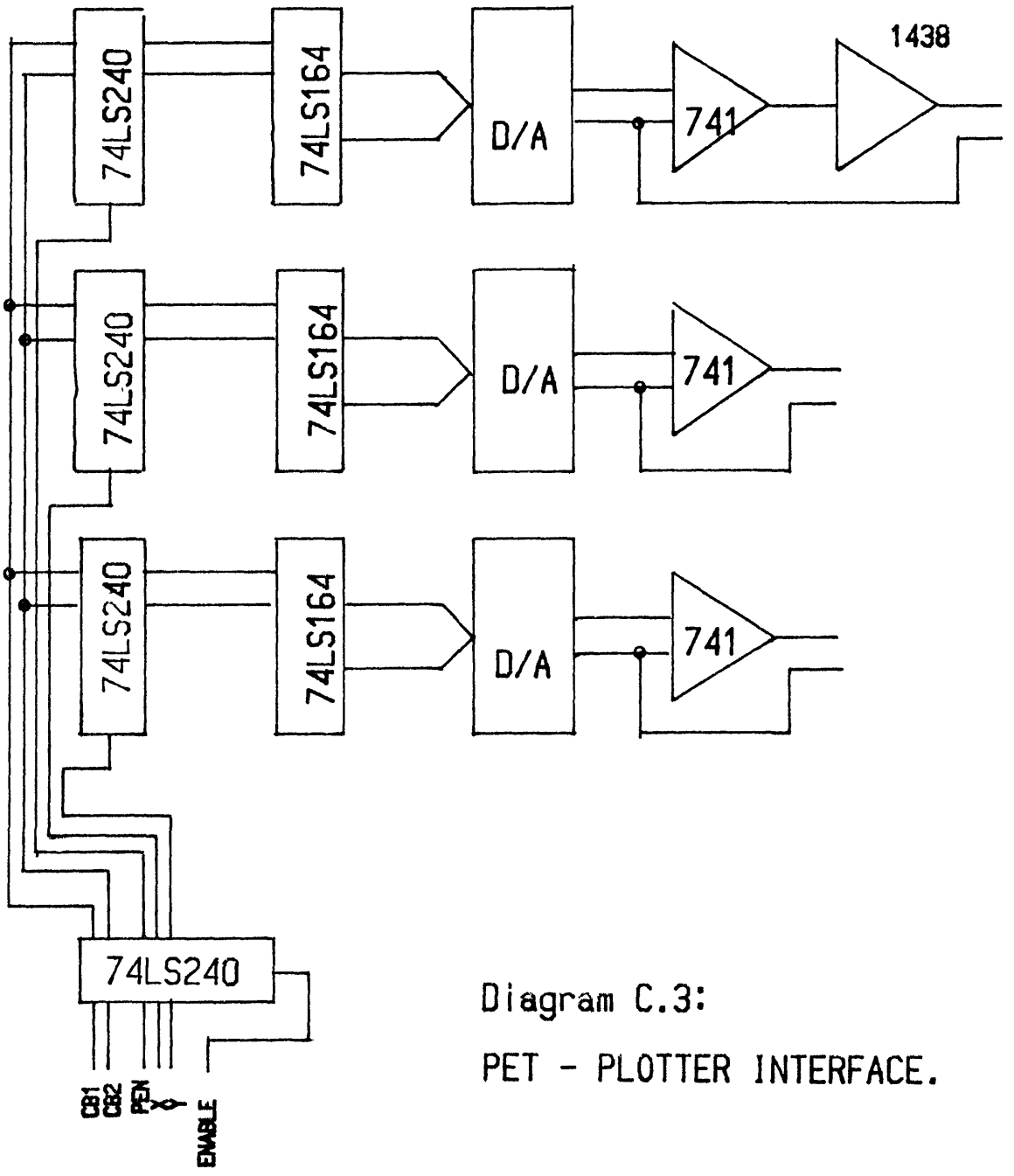


Diagram C.3:

PET - PLOTTER INTERFACE.